

國立臺灣大學醫學院醫學系

學士班學生論文

Department of Medicine

School of Medicine

National Taiwan University

Bachelor Degree Thesis



PPAR- δ 促效劑 GW501516 對疫苗反應之篩選生發中心

B 細胞和抗體製造之影響

The effects of a PPAR- δ agonist GW501516 on the
selection of germinal center B cells and antibody
production in vaccination

懷穎

Haw Hwai

指導教授：曾賢忠 博士

Advisor: Shiang-Jong Tzeng, M.D., Ph.D.

中華民國 108 年 5 月

May, 2019



國立臺灣大學學士班學生論文

口試委員會審定書

PPAR- δ 促效劑 GW501516 對免疫反應之篩選
生發中心 B 細胞和抗體製造之影響

The effects of a PPAR- δ agonist GW501516 on the
selection of germinal center B cells and antibody
production in vaccination

本論文係懷顥君（學號 B01401004）在國立臺灣大學醫學系完成之學士班學生論文，於民國 107 年 04 月 26 日承下列考試委員審查通過及口試及格，特此證明

口試委員(3 位)：

曾賢忠

(簽名)

(指導教授)

吳青鸞

林琬琬

系主任： 林琬琬 (簽名)

(是否須簽章依各院系規定)



致謝

時光飛逝，七年的大學生涯已經接近尾聲，當初大五進實驗室原本只是抱持著嘗試的心態，沒想到最後居然能發表論文，真的出乎預期。

大七實習忙碌，完全無法做實驗，但最後能夠依靠前兩年的資料完成論文，最感謝的無疑是指導教授 曾賢忠老師，從大四的藥理討論課中受到學習的啟發，到真的進入實驗室裡面，老師對於細節的要求、實驗的大膽假設、教學的態度、報告上的協助以及鼓勵我參加各種獎項等，讓學生看見醫學除了記憶、考試以外，是一個遠比我想得更深更廣的宇宙。這三年跟隨曾老師的腳步，獲益匪淺。

再來要感謝琮智學長，學長在碩二要完成許多實驗與畢業論文的壓力下，依然盡力帶我熟悉各種動物實驗，在畢業後也留下許多珍貴的資料，讓我得以順利完成後續實驗。另外，也感謝健翔常常會在提供實驗上的協助跟討論，以及留下精美的實驗筆記本供我參考。感謝峻需學長，雖然不常回實驗室，但是學長的論文絕對是我從剛入門了解實驗流程到最後撰寫論文重要的參照。感謝家銘、竺君在實驗、跑行政流程上面的協助，沒有你們，我一個人一定忙不過來，帶你們的同時也刺激我不斷學習。感謝呂醫師、黃博士在知識以及技術上的討論。感謝動物中心、流氏細胞儀、所辦、系辦的成員提供實驗需要的資源與行政上的協助。

也要感謝 林琬琬教授、 吳青錫助理教授，願意在百忙之中撥空擔任口試委員，並且在口試過程中給予許多研究思路跟未來臨床應用上的建議，也包容許多學生不夠嚴謹的地方。

當然更要感謝的是家人與女友無怨無悔的愛、關懷與支持，體諒我的忙碌，在我疲累的時候給我避風港跟鼓勵，讓我總能充滿動能、沒有後顧之憂地完成本學士論文。謹將此學士論文獻給我的家人與女友。


懷顯

2019.4 月於台大醫學系

中文摘要



Fc γ RIIB 是 IgG 免疫球蛋白的抑制型受體，它也是 B 細胞最重要的負調節分子。B 細胞針對遇到同源或非同源之抗原和抗體形成之免疫複合體，抗體的 Fc 區域與 Fc γ RIIB 結合，會分別傳遞只以 SHIP 或者只以 c-Abl 為主的訊息路徑去進行抑制。Fc γ RIIB 在 B 細胞的重要性可由其基因剔除鼠獲得明證。小鼠缺乏 Fc γ RIIB 時，在疫苗注射會產生比正常鼠更高量的抗體。更重要的是，Fc γ RIIB 基因剔除鼠會自發類紅斑性狼瘡，導因於不受抑制之過度漿細胞增生和其製造過量之免疫複合體，並沉積在身體組織及引起腎絲球腎炎和腎衰竭。因此，Fc γ RIIB 被認為是 B 細胞的免疫檢查點分子，調節漿細胞在體內數量，而漿細胞為終分化之 B 細胞。由於漿細胞源自在脾臟和淋巴組織之生發中心 B 細胞，我的論文研究在探討在疫苗反應時，Fc γ RIIB 在篩選生發中心 B 細胞以進行分化為漿細胞之角色，以及採用一種 PPAR- δ 促效劑 GW501516 去改變 Fc γ RIIB 表達量，對生發中心 B 細胞篩選結果與產生高效價抗原專一性抗體之影響。由於 Fc γ RIIB 經 c-Abl 傳遞細胞凋亡訊息，而生發中心 B 細胞表達之 BCR 若對抗原具低親合性，將會因無法競爭到抗原而凋亡。因此，我們推論當 Fc γ RIIB/c-Abl 訊息傳遞受到抑制時，將會影響生發中心 B 細胞篩選結果及產生抗體之抗原親合性。為了驗證我們的假說，我們對正常野生型 C57BL/6 小鼠採用實驗常用之模式抗原 NP(4-hydroxy-3-nitrophenylacetyl)- CGG (chicken gamma globulin) 當疫苗，在第二次疫苗接種後第七至九天投予 c-Abl 抑制劑 nilotinib (2 毫克/公斤/天)，此時正逢篩選生發中心 B 細胞最旺盛時期。如我們所預測，我們測得小鼠血清之對 NP 抗原低親合性之 IgG 抗體濃度上升，並伴隨脾臟分泌對 NP 抗原低親合性 IgG 抗體之漿細胞數目增加，顯示生發中心反應未能有



致使低親合性生發中心 B 細胞凋亡，而致殘留並分化成漿細胞。另一方面，前人研究發現 GW501516 可使 FcγRIIB 表達下降。於是我們在相同小鼠疫苗實驗及相同時間點自腹腔給予 GW501516 (3 或 6 毫克/公斤/天)，發現與給予 nilotinib 類似之篩選生發中心 B 細胞缺陷及抗體親合性變化。總結，根據我們的研究結果提出 FcγRIIB 在去除低親合性生發中心 B 細胞，以確保製造出對抗原具高親合性之抗體，扮演免疫檢查點角色。此外，我們初步的研究顯示 NP 低親合性抗體對同源抗原具交叉免疫反應，未來將探討是否可藉藥物調控 FcγRIIB/c-Abl 活性，應用於促進季節性流感疫苗產生對 A 型流感病毒產生交叉保護效果。

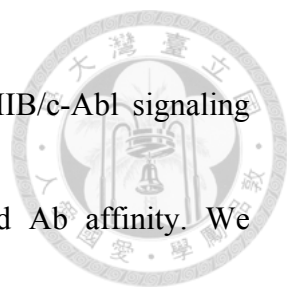
關鍵詞：

FcγRIIB、生發中心、PPAR-δ、GW501516、nilotinib、交叉保護效果

ABSTRACT



Fc γ RIIB is an inhibitory Fc receptor of IgG and an essential negative regulator of B cells. In response to cognate and non-cognate immune complexes (ICs), Fc γ RIIB can transduce SHIP-dependent and c-Abl-dependent signaling pathways, respectively, in a mutually exclusive manner. Mice deficient in Fc γ RIIB display an enhanced humoral immune response after immunization. Moreover, Fc γ RIIB knockout mice spontaneously develop a lupus-like disease as a result of uncontrolled expansion of plasma cells (PCs) and thereby excess generation of ICs that accumulate in tissues, leading to glomerulonephritis. Thus, Fc γ RIIB is considered to play a checkpoint role in regulating the homeostasis of PC numbers. Because PCs are terminally differentiated B cells and they originate from germinal center (GC) B cells, we investigate the functional role of Fc γ RIIB in the selection of GC B cells for further differentiation into PCs after secondary immunization, and pharmacological modulation with GW501516, a PPAR- δ agonist, on this selection process, known as affinity maturation to generate antibody (Ab) of high affinity to antigen (Ag). Because Fc γ RIIB/c-Abl signals for apoptosis of B cells and GC B cells of which B-cell receptor (BCR) binds to the Ag with low affinity will be



eliminated by apoptosis, we hypothesized that inhibition of FcγRIIB/c-Abl signaling during affinity maturation could alter the selection outcome and Ab affinity. We immunized C57BL/6 mice with a model Ag NP-CGG (4-hydroxy-3-nitrophenylacetyl hapten-chicken gamma globulin) and treated mice with nilotinib (2 mg/kg/day), a clinically used c-Abl inhibitor, during the seventh to ninth days when GC B cells undergo apoptosis for selection. Indeed, we found an increase of serum NP⁺ IgGs accompanied by an increased number of low-affinity NP⁺IgG⁺ PCs, indicating reduced affinity maturation. Previously, GW501516 was shown to down-regulate the expression level of FcγRIIB. When GW501516 (3,6 mg/kg/day) was administered intraperitoneally to mice during the peak of selection of GC B cells, we found a similar phenotype of affinity maturation. Taken together, we propose that FcγRIIB plays a checkpoint role in the negative selection of low-affinity GC B cells to ensure the production of high-affinity Abs for humoral host protection. Moreover, our preliminary data showed cross-reactivity of low-affinity Abs to cognate Ags. Thus, it will be of interest to examine whether modulation of inhibitory activity of FcγRIIB could enhance cross-protection against distinct influenza A virus by seasonal influenza vaccination.

Key words: FcγRIIB, germinal center, PPRA-δ, GW501516, nilotinib, cross-protection

CONTENTS

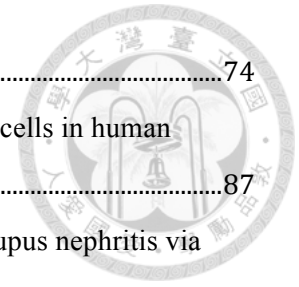


口試委員會審定書	i
致謝	ii
中文摘要	iii
ABSTRACT	v
LIST of FIGURES.....	x
LIST of ABBREVIATION	xi
Chapter 1 Introduction	1
1.1 Germinal center (GC) reaction	2
1.1.1 Anatomy and function of germinal center.....	2
1.1.2 Somatic Hypermutation.....	3
1.1.3 Affinity maturation	4
1.1.4 Class switch recombination.....	6
1.2 Hapten carrier system as a model for vaccination response	6
1.3 Fcγ Receptors.....	8
1.4 Fcγ receptor IIB (FcγRIIB, a.k.a. CD32B).....	10
1.4.1 General Properties	10
1.4.2 Physiological function and signal transduction of Fc γ RIIB.....	11
1.4.3 Fc γ RIIB-I232T polymorphism.....	12
1.5 Peroxisome proliferator activated receptors (PPARs)	14
1.6 PPARδ	15
1.7 GW501516	16
1.8 Nilotinib	17
1.9 Motivation	19
Chapter 2 Materials and Methods.....	20
2.1 Mice.....	21
2.2 Enzyme Linked Immunosorbent spot (ELISPOT) assay	21
2.3 Enzyme Linked Immunosorbent assay (ELISA).....	22
2.4 Confocal microscopy	23

Chapter 3 Results	25
3.1 FcγRIIB^{232T/T} mice show persistent impaired affinity maturation over time	26
3.2 Association of FcγRIIB and BCR with the lipid raft after coligation was impaired in FcγRIIB^{232T/T} mutant mice	27
3.3 Nilotinib administration during GC reaction has a negative impact on affinity maturation	29
3.4 GW501516 increases respective total and low-affinity Ag-specific IgG PCs at the dose of 3 and 6 mg/kg/day during GC reaction	30
3.5 GW501516 increases the serum levels of total and low-affinity Ag-specific IgG at the dose of 3 and 6 mg/kg/day in wild-type mice	32
3.6 GW501516 increases total Ag-specific IgM secreting PCs at the dose of 6 mg/kg/day during GC reaction	33
3.7 GW501516 increases the serum levels of high-affinity Ag-specific IgM at the dose of 3 and 6 mg/kg/day and total Ag-specific IgM at 6 mg/kg/day	35
Chapter 4 Discussion	36
4.1 FcγRIIB^{232T/T} mutant mice as a model for investigating the functional role of FcγRIIB in GC reaction	37
4.2 Difference between FcγRIIB^{232T/T} mutant mice and wild type mice treated with nilotinib or GW501516	38
4.3 Summary of the overall effect of GW501516 on GC reaction	39
4.4 Could GW501516 affect GC reaction other than FcγRIIB down-regulation induced by PPAR-δ activation?	40
4.5 Pharmacological modulation of FcγRIIB activity is an applicable method for novel manipulation of immune response	43
4.6 Potential role of macrophages in the GC reaction to influence the generation of Ag-specific Abs	44
Figures	47
References	65
Appendix	71
Publication List	72
Publications	73

The lupus-associated FcγRIIB-I232T polymorphism results in impairment in the negative

selection of low-affinity germinal center B cells via c-Abl in mice.....	74
B-cell ELISpot assay to quantify antigen-specific antibody-secreting cells in human peripheral blood mononuclear cells.....	87
Dual immuno-renal targeting of 7-benzylidenenaltrexone alleviates lupus nephritis via Fc γ RIIB and HO-1	96



LIST of FIGURES

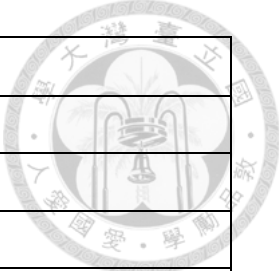


Figure 1 Mouse immunization schedules.	48
Figure 2 Analysis of the differences of affinity maturation status between wild-type and FcγRIIB ^{232T/T} mice over time.	50
Figure 3 Analysis of the differences of affinity maturation status between wild-type and FcγRIIB ^{232T/T} mice over time.	51
Figure 4 Analysis of the effect of nilotinib on the affinity maturation of female wild-type mice.	53
Figure 5 Analyzing IgG-secreting PCs in the spleen of female C57BL/6 mice immunized with two different GW501516 doses by ELISPOT assay.....	55
Figure 6 Measurement of serum IgG levels of female C57BL/6 mice immunized with two different GW501516 doses by ELISA assay.	58
Figure 7 Analyzing IgM-secreting PCs in the spleen of female C57BL/6 mice immunized with two different GW501516 doses by ELISPOT assay.....	60
Figure 8 Measurement of the serum IgM levels of female C57BL/6 mice immunized with two different GW501516 doses by ELISA assay.....	63

LIST of ABBREVIATION



15-HETE	15-hydroxyeicosatetraenoic acid
4-HNE	4-hydroxynonenal
Ab	Antibody
AEC	3-amino-9-ethylcarbazole
AF-1	Activation function-1
Ag	Antigen
AID	Activation-induced cytidine deaminase
AMPK	AMP-activated protein kinase
Bcl-6	B-cell lymphoma 6
BCR	B-cell receptor
BCR-Abl	Breakpoint cluster region-Abelson tyrosine kinase
Blimp-1	B lymphocyte-induced maturation protein-1
CML	Chronic myelogenous leukemia
CSR	Class switch recombination
CXCL12	C-X-C motif chemokine 12
CXCL13	C-X-C motif chemokine 13
CXCR4	C-X-C chemokine receptor 4
CXCR5	C-X-C chemokine receptor 5
DMSO	Dimethyl sulfoxide
DZ	Dark zone
ELISA	Enzyme Linked Immunosorbent assay
ELISPOT	Enzyme Linked Immunosorbent spot assay
FACS	Fluorescence-assisted cell sorting
FDA	Food and Drug Administration
GC	Germinal center
GPI	Glycosylphosphatidyl inositol
HBV	Hepatitis B virus



HODE	9-hydroxyoctadecadienoic acid
HRP	Horseradish peroxidase
ICAM-1	Intercellular adhesion molecule 1
Ics	Immune complexes
Ig	Immunoglobulin
IRF-4	Interferon regulatory protein-4
ITAMs	Immunoreceptor tyrosine-based activating motifs
ITIM	Immunoreceptor tyrosine-based inhibitory motif
LZ	Light zone
MMM	Marginal metallophilic macrophage
MZM	Marginal zone macrophage
NIP	4-Hydroxy-5-iodo-3-nitrophenylacetic acid
NP	4-hydroxy-3 nitrophenylacetic acid
NP-CGG	4-hydroxy-3-nitrophenylacetyl hapten-chicken gamma globulin
PBS-T	Phosphate buffered saline with 0.05% Tween 20
PCs	Plasma cells
Ph+	Philadelphia chromosome positive
PPARs	Peroxisome proliferator activated receptors
PPAR- δ	Peroxisome proliferator activated receptor delta
PPRE	PPAR response element
RBCs	Red blood cells
RXR	Retinoid X receptor
SHIP	SH2-containing inositol 5'-Phosphatase
SHM	Somatic hypermutation
SLAM	Signaling lymphocyte activation molecule
SNP	Single nucleotide polymorphism
TBM	Tingible body macrophage



Chapter 1

Introduction

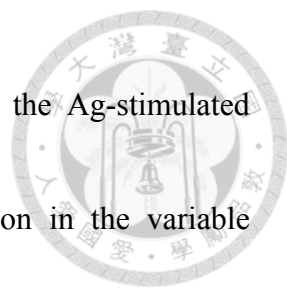
Chapter 1 Introduction



1.1 Germinal center (GC) reaction

1.1.1 Anatomy and function of germinal center

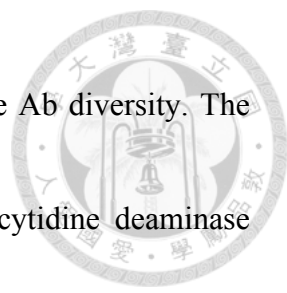
The primary follicle is a B cell-rich structure, which locates in the secondary lymphoid organs, including, the spleen, lymph nodes, Peyer's patches of the intestine and tonsils. In response to antigen (Ag) stimulation, B cells in the primary follicle proliferate and form the secondary follicle, which comprises of the marginal zone, the mantle zone and the germinal center (GC). The GC localizes in the central portion of the secondary follicle and contacts with the T cell zone (Victoria and Nussenzweig, 2012). In the GC, Ag-stimulated B cells sequentially undergo somatic hypermutation, affinity maturation and class switching. Based on the hematoxylin-eosin staining of nuclear contents, it was well established that the GC comprises the dark zone (DZ) and the light zone (LZ), both of which are filled with GC B cells differentiated in different stages, and also called centroblasts and centrocytes, respectively. Histologically, the DZ is densely packed with proliferating centroblasts (Allen, *et al.*, 2015). In contrast, the LZ is mostly composed of centrocytes and follicular dendritic cells that can trap



immune complexes (ICs) for presentation to B cells. In the DZ, the Ag-stimulated centroblasts rapidly proliferate and undergo somatic hypermutation in the variable region of immunoglobulin (Ig) gene to increase the repertoire of mutated B-cell receptor (BCR) on GC B cells for selection. The centroblasts later cease proliferation and migrate to the LZ to differentiate into centrocytes for affinity maturation for selection, followed by class switching of Ig isotypes (Zhang, *et al.*, 2016).

1.1.2 Somatic Hypermutation

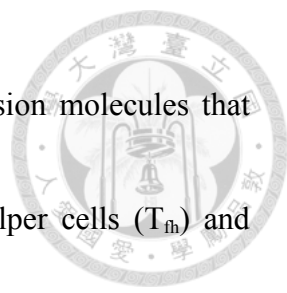
The immature B cells undergo the V(D)J gene recombination to diversify the surface B cell receptor and further mature into naïve B cell. It is process completed in the bone marrow. Somatic hypermutation (SHM) occurs to the rapid proliferating GC B cells, derived from antigen-stimulated naïve B cells. It is a tightly regulated mechanism that the genes of the B-cell receptor (BCR) acquire a higher-than-usual mutation rate during proliferation to expand its repertoire. The mutation rate is estimated about 10^3 to 10^5 per base pair, about 10^6 folds greater than other somatic cells' proliferation (Martin, *et al.*, 2015). The mutations of BCR are mostly point mutations and are left unaltered to



accumulate in the variable region of the Ig genes for increasing the Ab diversity. The key enzymes that contribute to SHM include activation-induced cytidine deaminase (AID), uracil N-glycosylase, and error-prone DNA-polymerase. Since SHM is a random process, the majority of the mutations will lead to decreased Ab affinity (Kanyavuz, *et al.*, 2019). Only a small portion of the centroblasts that acquire higher Ag binding affinity after SHM will survive owing to BCR signals.

1.1.3 Affinity maturation

The affinity maturation is a process to select high-affinity centrocytes as a result of success in competing limited Ag on follicular dendritic cells for survival and proliferation (Zhang, *et al.*, 2016). High-affinity GC B cells induce stronger CD40 and BCR signals that enhance c-Myc, interferon regulatory protein-4 (IRF-4) expression levels. IRF-4 upregulates the expression of B lymphocyte-induced maturation protein-1 (Blimp-1), a transcriptional factor that ceases proliferation, induces plasma cell differentiation, and increases antibody synthesis and secretion. CD40 activation leads to higher expression levels of intercellular adhesion molecule 1 (ICAM-1) and signaling



lymphocyte activation molecule (SLAM), both of which are adhesion molecules that can enhance interaction and adhesion between the T follicular helper cells (T_{fh}) and centrocytes during affinity maturation and class switching (Shulman, *et al*, 2013). The current paradigm is that centrocytes with high affinity BCRs promote more signal help from the T_{fh} for survival and plasma cell (PC) differentiation. In contrast, low-affinity centrocytes that cannot receive Ag-triggered survival signals are doomed to be eliminated by apoptosis or survive as memory B cells (Wataru and Tomohiro, 2018). The organization and migration between the DZ and the LZ are highly dynamic and require chemokine receptor expression and chemokine gradients to direct the destination of GC B cells in the GC. Namely, the centroblasts express higher C-X-C chemokine receptor type 4 (CXCR4) levels and respond to C-X-C motif chemokine ligand 12 (CXCL12) produced in the DZ, while the centrocytes express abundant CXCR5 and migrate to CXCL13 gradients established in the LZ. Recent studies have shown that some positively selected centrocytes with intermediate Ag binding affinity will reenter the DZ for further proliferation and SHM in order to obtain higher affinity to Ag (De Silva and Klein, 2015).




1.1.4 Class switch recombination

The variable region of an antibody determines its Ag binding affinity. On the other hand, the constant region defines the class (isotype) of the antibody, and its distinct function and distribution. The naïve B cells that express IgM or IgD on the surface will undergo class switch recombination (CSR) to transform into IgG, IgA or IgE (Stavnezer, *et al.*, 2008). It is a process that determine by the type of helper T cells and cytokines, with which the B cells interact. In the GC, T_h interact with the GC B cells at the interface of the GC and T cell zone for CSR. Nevertheless, triggered by Th1 and Th2 cells, CSR can also take place in extrafollicular regions. In addition to the involvement in SHM, AID is the major enzyme of initiation of CSR (Chua, *et al.*, 2002).


1.2 Hapten carrier system as a model for vaccination response

Vaccination is a clinical procedure and active immunity aimed to enhance host immunity by artificially exposing antigens of target pathogens. The vaccine antigen (Ag) can be live attenuated, inactivated or subunits of pathogens. It is a cost-effective method



for individuals to generate effective and protective immune responses prepared for encountering the target pathogens (WHO, 2017). When pathogens invade the host, the primary humoral response is slow, inefficient and less in scale. Nevertheless, after the primary response fades away the pathogen-specific memory B and T cells will be generated and stay long term. Because of the presence of memory cells, a quicker and greater secondary immune response can occur as the individual encounters the original or similar pathogens (Kurosaki, *et al.*, 2015). Taking advantage of the memory response of the adaptive immunity, we can generate specific immune memory for better protection by vaccination.


Hapten carrier system is a widely used model for research on T-cell-dependent response of vaccination. T-cell-dependent response occurs in the GC. Haptens are small molecules that do not elicit immune response alone but they become immunogenic when they are conjugated with a carrier protein to increase molecular weight. The valence of the hapten-carrier protein is defined as the average number of the haptens that are able to bind to the carrier protein (Oda, *et al.*, 2004). Commonly used carrier proteins include albumin, ovalbumin, gamma globulin, etc. The haptens modulate the



amino acid epitopes and trigger T-cell-dependent adaptive immunity against the hapten, hapten-carrier epitopes or the carrier after immunization (Gefen, *et al.*, 2015). The GCs induced by immunization undergo the affinity maturation to select GC B cells that carry B-cell receptors with higher Ag affinity, meaning that cells are able to bind against hapten-carrier protein with lower valence. As a result, by detecting the percentage of antibodies that can bind against the hapten-carrier protein with lower or higher valence than the immunogen, researchers can trace the affinity maturation status of vaccination. The fundamental goal of vaccination is to generate antibodies with higher affinity to target Ag for humoral host protection.

1.3 Fc γ Receptors

Fc γ receptors are a class of Fc receptors that bind the constant region of immunoglobulin G (IgG) to function. Different types of Fc γ receptors show different affinity to IgG isotypes, and express on different immune cells. Among the Fc γ receptors, only the Fc γ RI, an activating receptor, binds the monomeric form of IgGs. Fc γ RIIB is the only inhibitory receptor in the Fc γ receptor family and it possesses weak



affinity to IgG in mice and humans. In humans, the other Fc γ receptors are classified into Fc γ RIIA, Fc γ RIIC, Fc γ RIIIA, and Fc γ RIIIB. In mice, other activating Fc γ receptors are Fc γ RIII and Fc γ RIV. With the exception of Fc γ RI, which have three Ig-like domains in the extracellular part, all the Fc γ receptors have only two Ig-like domains, resulting in weak to medium affinity for IgG and only binding to IgG immune complex (IC). Activating Fc γ receptors of humans contain immunoreceptor tyrosine-based activating motifs (ITAMs) on either the intracellular domain itself, like Fc γ RIIA, Fc γ RIIC or on the adaptor protein Fc γ subunit, such as Fc γ RIIIA. Human Fc γ RIIIB is a glycosylphosphatidyl inositol (GPI)-anchored protein without ITAMs that activate intracellular signaling by lipid raft-mediated activation (Yang, *et al.*, 2018). All the activating Fc γ receptors of mice, including Fc γ RI, Fc γ RIII and Fc γ RIV, have their ITAMs on the adaptor protein Fc γ subunit. Aside from the Fc γ receptor subtypes, the IgG isotypes also show difference between mice and human. For example, the human IgG1 with high effector function and affinity toward Fc γ receptors is more similar to the characteristics of mouse IgG2a, instead of the mouse IgG1 (Steward, *et al.*, 2014).


1.4 Fcγ receptor IIB (FcγRIIB, a.k.a. CD32B)



1.4.1 General Properties

Both FcγRIIB (a.k.a. CD32B) of mice and humans are low-affinity Fcγ receptors and the only inhibitory Fcγ receptors, which contains an immunoreceptor tyrosine-based inhibitory motif (ITIM) (Moldta and Hesselb, 2014). Except for T cells and NK cells, immune cells express certain isoforms of FcγRIIB. FcγRIIB demonstrate highest binding affinity toward IgG1 or IgG3 in humans, whereas IgG2a and IgG2b in mice. FcγRIIB can be further classified into FcγRIIB1, FcγRIIB2 and FcγRIIB3 isoforms, based on alternative splicing of the mRNA. FcγRIIB1 is expressed in B cells and is usually prevented from endocytosis function. FcγRIIB2 is generated by alternative splicing of mRNA, giving rise to a 47-amino acid deletion at the upstream of the ITIM. FcγRIIB2 is mainly expressed on the surface of myeloid cells, including macrophages, monocytes and dendritic cells, and function as an endocytosis mediator. FcγRIIB3 is a soluble isoform without the transmembrane region and signal transduction domain, which can inhibit forming of ICs (Li and Kimberley, 2015).

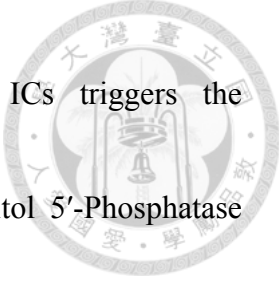
FcγRIIB deficiency is found be correlated with autoimmune diseases, such as



systemic lupus erythematosus, multiple sclerosis, etc. Clinically, FcγRIIB is expressed on malignant B cells enhance the internalization rate of monoclonal antibody and thus, contribute to the resistance of B-cell immunotherapy (Roghalian, *et al.*, 2015). Mice deficient in FcγRIIB spontaneously develop splenomegaly due to uncontrolled expansion of B cells. These mice gradually develop a lupus-like disease resulting from massive IC deposition in the kidney after 6 months of age (Bolland, *et al.*, 2002). Consistent with these results, the surface expression level of wild-type FcγRIIB in memory B cells and PCs is down-regulated, thereby reducing inhibitory activity in patients with SLE (Mackay, *et al.*, 2006). Likewise, lupus-prone mice fail to up-regulate FcγRIIB expression on GC B cells, regardless of their genetic backgrounds, suggesting a role of FcγRIIB in the GC (Rahman, *et al.*, 2005).

1.4.2 Physiological function and signal transduction of FcγRIIB

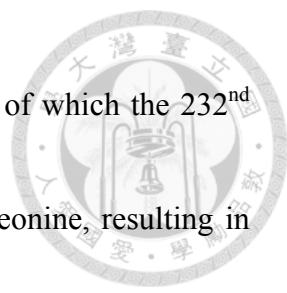
The main physiological function of FcγRIIB is to serve as a negative regulator by feedback inhibition of humoral response via cognate ICs that co-ligate BCR (via Ag) and FcγRIIB (via IgG Ab), resulting in inhibition on proliferation and differentiation of



B cells. Coengagement of BCR and Fc γ RIIB by the IgG ICs triggers the phosphorylation of ITIM and recruitment of SH2-containing inositol 5'-Phosphatase (SHIP) to transduce inhibitory signals (Ambrosio, *et al.*, 1996). On the other hand, non-cognate IgG ICs can mediate Fc γ RIIB aggregation when BCR is not recognized or has low affinity to the Ag and induce apoptosis of B cells through c-Abl tyrosine kinase in mice (Zheng, *et al.*, 2005). We have recently shown that this pathway mediated by Fc γ RIIB alone is crucial for the deletion of low-affinity GC B cells in that a human polymorphic allele of Fc γ RIIB-I232T defective in inhibition leads to retention of low-affinity GC B cells, a major source of autoreactive B cells (Jhou, *et al.*, 2018).

1.4.3 Fc γ RIIB-I232T polymorphism

Compared to wild-type mice, deficiency in Fc γ RIIB results in higher antibody titers after immunization (Ono, *et al.*, 1996). This result suggests Fc γ RIIB as a potential target of immunomodulation for vaccine-elicited antibody response. On the other hand, Fc γ RIIB-deficient mice are prone to produce self-reactive B cells that secrete anti-nuclear antibodies and ultimately lead to a lupus-like disease (Li and Kimberley,



2014). Recently, we have shown that FcγRIIB-I232T variant mice, of which the 232nd amino acid of FcγRIIB protein was mutated from isoleucine to threonine, resulting in reduced inhibition as previously reported (Kono, *et al.*, 2005). We demonstrated that these mutant mice display impairment in the elimination of low-affinity GC B that should have been deleted during affinity maturation. As a result, immunized FcγRIIB^{232T/T} mice exhibit higher levels of both high- and low-affinity IgGs after immunization and also expansion of LZ B cells in the GC due to a failure in the elimination of low-affinity GC B cells (Jhou, *et al.*, 2018).

In addition, our preliminary data showed cross-reactivity of 4-hydroxy-3-nitrophenylacetyl (NP) Ag-specific IgGs to 4-hydroxy-5-iodo-3-nitrophenylacetyl (NIP), a cognate Ag. This finding suggests the repertoire of low-affinity IgGs is diverse and potentially cross-reactive. Based on these findings, we reasoned that pharmacological down-regulation of FcγRIIB levels during the affinity maturation in the GC might be able to safely generate higher levels of both Ag-specific and cross-reactive Abs without long-term side effects for ongoing affinity maturation can clear low-affinity B cells after a period of time. Such modulation via FcγRIIB might be able to alter vaccine responses

for better efficacy and cross-protection, e.g. influenza, HBV, etc.



1.5 Peroxisome proliferator activated receptors (PPARs)

PPARs are nuclear receptors that are activated with ligand binding and they function as transcription factors. Various PPARs share similar structures that contain the N-terminal domain, the DNA-binding domain, the hinge and the ligand-binding domain. The activation function-1 (AF-1) domain that can control the activation of PPARs independently of the ligand binding lies in the N-terminal region. The DNA-binding domains are highly conservative with zinc fingers among PPARs (Higashiyama, *et al.*, 2007). During activation, the PPARs heterodimerize with the retinoid X receptor (RXR) and bind to the PPAR response element (PPRE) with DNA sequences of “AGGTCA_nAGGTCA” (Zhang and Young, 2008).


PPARs are classified into PPAR- α , PPAR- β/δ , PPAR- γ . PPAR- α regulates fatty acid oxygenation and ketogenesis, and is mainly expressed on cardiac muscle, hepatocytes and brown adipose tissue. PPAR- γ is mainly expressed on brown and white adipose tissues and controls adipogenesis and lipid storage (Poulsen, *et al.*, 2012).

PPARs affect cell metabolism and energy usage, making them potential targets for regulating immune response, cell differentiation and development.



1.6 PPAR δ

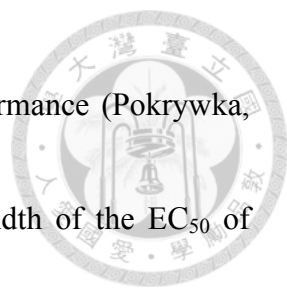
PPAR- δ is localized in the nucleus in most tissues with exception of cytoplasmic localization in the islet of Langerhans, nervous system and macrophages. PPAR- δ regulates gene expression and mediates cell differentiation, metabolism, tumorigenesis and immune reaction. Thiazolidinediones (TZD) is a PPAR γ , another subtype of PPAR receptor, agonist and it has therapeutic effects on type 2 diabetes mellitus (Quinn, *et al*, 2008). However, no drugs of PPAR- δ have been approved for clinical use so far. The natural ligands of PPAR- δ are intracellular fatty acids and metabolites, including 9-hydroxyoctadecadienoic acid (HODE), 4-hydroxynonenal (4-HNE), and 15-hydroxyeicosatetraenoic acid (15-HETE). Synthetic compounds of PPAR- δ have been developed, based on the ligand binding site structural design (Wu, 2017). With the co-repressor B-cell lymphoma 6 (Bcl-6) binding to the PPAR- δ and RXR, conformational change blocks access of the ligand binding sites for PPAR- δ and RXR



and thereby inactivates gene transcription. Whereas through ligand and coactivator binding, activated PPAR- δ forms a stable complex with RXR and activates transcription (Cox, 2017). Whether PPAR- δ is involved in the regulation of humoral response by influence the gene expression of Fc γ RIIB has not been determined. Interestingly, PPAR- δ agonists have been shown to enhance macrophage survival under hypoxic stress and down-regulate gene transcription of Fc γ RIIB in macrophages (Adhikary, *et al.*, 2015).

1.7 GW501516

GW501516, also known as cardarine, is a synthetic and specific PPAR- δ agonist, which was designed from the structure of the ligand binding site, and therefore it is highly specific. GW501516 has been shown to confer striking effects on improving serum lipid profile in obese rhesus monkeys at the dose of 3 mg/kg/day (Luo, 2012). However, carcinogenesis was observed in mice by daily oral administration of greater than 10 mg/kg/day (Newsholme, *et al.*, 2012). The tumor promoting effect is considered through PPAR- δ activation rather than genotoxicity. On the other hand, GW501516 is a



selective androgen receptor modulator that enhances athletic performance (Pokrywka, 2014). The EC_{50} of GW501516 to PPAR- δ is less than a thousandth of the EC_{50} of PPAR- α and PPAR- γ , respectively. *In vitro* study of GW501516 further reveals peak activity at the concentration above 10 nM (Oliver, *et al.*, 2001).

1.8 Nilotinib

Nilotinib is a Food and Drug Administration (FDA) approved medication for treating chronic myelogenous leukemia (CML). It is a small molecule that acts as a tyrosine kinase inhibitor (TKI) that blocks the activity of breakpoint cluster region-Abelson tyrosine kinase (BCR-Abl), discoidin domain receptors, platelet-derived growth factor receptors, etc. Nilotinib can bind to either wild-type or imatinib-resistant BCR-Abl due to its rational design from the protein binding pocket. Nilotinib is effective for most identified imatinib-resistant related mutations of BCR-Abl, with an IC_{50} below 2000 nM (Manley, *et al.*, 2010). The elimination half-life of nilotinib is 17 hours. The recommended dose for Philadelphia chromosome positive (Ph+) CML pediatric patients is 230 mg/m² twice daily orally based on two clinical trials:

CAMN107A2120, CAMN107A2203. For newly diagnosed Ph+ adult CML patients,

300 mg orally twice daily is recommended (Prod Info Tassigna, 2007).



1.9 Motivation



A recent study of human monocyte-macrophage has identified a paradoxical phenomenon that both anti-inflammatory and pro-inflammatory genes were activated by GW501516 (Adhikary, *et al.*, 2015). The FCGR2B gene expression is suppressed during hypoxic stress based on fluorescence-assisted cell sorting (FACS) analysis. Interestingly, the LZ of the GCs is a hypoxic environment (Cho, 2016). Taken together, we hypothesized that by activation of PPAR- δ during the stage of affinity maturation in the LZ, the surface expression level of Fc γ RIIB on macrophages and/or B cells could be down-regulated. If our hypothesis is correct, the number of PCs will increase substantially and so do the titers of the low-affinity Abs owing to a reduced inhibition by Fc γ RIIB.

In this study, we use the commonly used hapten 4-hydroxy-3-nitrophenyl acetic acid conjugated with chicken gamma globulin (NP-CGG) as the immunogen to investigate the Ab titers and distinguish their affinity to the NP Ag. We performed ELISA and ELISPOT assays for detecting serum Ag-specific Abs and splenic PC numbers as a functional readout of the stringency of selection of GC B cells in the LZ.



Chapter 2

Materials and Methods

Chapter 2 Materials and Methods



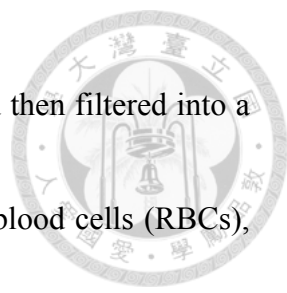
2.1 Mice

Female C57BL/6 mice were obtained from the Laboratory Animal Center of National Taiwan University College of Medicine. We immunized 7 to 10-week-old mice intraperitoneally with 50 μ g nitrophenyl-chicken gamma globulin (NP-CGG, ratio 20, 1 mg/ml, Bioresearch Technology) admixed with equal volume alum precipitate (Alhydrogel® adjuvant 2%). The same antigen was immunized a second time 28 days later. GW501516 was administered intraperitoneally on the 6th day to 9th day after the second booster of immunization. Nilotinib was administered intraperitoneally on the 7th day to 9th day after the second booster of immunization. Mice were then sacrificed on the next day of the last injection. The animal protocol and schedule are illustrated in

Figure 1.

2.2 Enzyme Linked Immunosorbent spot (ELISPOT) assay


PVDF-based ELISPOT plates were pretreated with 30% ethanol to increase hydrophobicity. After PBS wash twice, NP7-BSA and NP30-BSA were coated with 50 μ l/well at the concentration of 10 μ g/ml in PBS at 4°C overnight. Splenocytes were



harvested by crushing the spleen with two pieces of microslides and then filtered into a 15 ml centrifuge tube containing sterile PBS. To eliminate the red blood cells (RBCs), RBC lysis buffer was added and incubated for 5 min. Cells were centrifuged and resuspended in RPMI 1640 containing 10% fetal bovine serum. Splenocytes were seeded at about 3×10^5 /well for detection of Ag-specific IgG and IgM secreting PCs and incubated at 37°C, 5% CO₂ overnight. Horseradish peroxidase (HRP) conjugated rabbit anti-mouse IgG and goat anti-mouse IgM Abs were incubated at room temperature for detection of PCs for 2 hours. The 3-amino-9-ethylcarbazole (AEC substrate, BD Bioscience) of 50 µl was added as the substrate of HRP to develop spots resulting from PCs. To quench the reaction, plates were washed with ddH₂O. The spots were counted after completely air dry by C.T.L. S6 universal analyzer (Cellular Technology Limited, Cleveland, OH, USA).

2.3 Enzyme Linked Immunosorbent assay (ELISA)

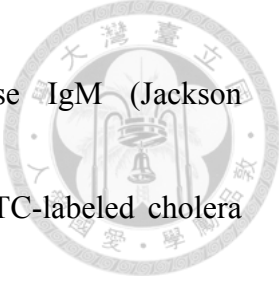
High binding 96-well microplates (Corning® 96 Well EIA/RIA Assay Microplate) were coated with anti-mouse IgG + IgM Abs, NP2-BSA, NP7-BSA, and NP30-BSA



with 10 $\mu\text{g/ml}$ in 50 μl at 4°C overnight, respectively. Plates were blocked with BlockPRO™ blocking buffer in room temperature for 2 hours. Serum samples collected from submandibular vein puncture of the mice were diluted in blocking buffer with 1: 40000 or 20000 dilutions for measuring IgG and IgM levels, respectively. Mouse reference serum (mouse reference serum, RS10-101, Bethyl Laboratories) in 2-fold serial dilution was used for generation of standard curves for quantification. Samples and diluted reference serum were incubated at room temperature for 2 hours. HRP conjugated rabbit anti-mouse IgG and goat anti-mouse IgM were incubated at room temperature for detection for 2 hours. After washing with PBS-T (phosphate buffered saline with 0.05% Tween 20), tetramethylbenzidine substrate was added for development. The reaction was terminated with 2N H₂SO₄. The absorbance OD_{450 nm} and OD_{570 nm} was read by an ELISA plate reader (BioTek, Winooski, VT, USA).

2.4 Confocal microscopy

Mouse splenic B cells were isolated from wild-type and FcγRIIB^{232T/T} mice of 8 weeks of age using the mouse B cell isolation kit (BD Pharmingen) to more than 95%



purity. Cells were treated with 10 μg of rabbit anti-mouse IgM (Jackson Immunoresearch) for 15 min on ice. After a brief wash, either FITC-labeled cholera toxin B (Sigma) or Cy3-labeled anti-rabbit IgGs (Jackson Immunoresearch) were added for 15 min on ice, followed by additional incubation for 5-60 min at room temperature. Cells were washed by PBS, fixed by 4% paraformaldehyde and then mounted. Metamorph software was applied to quantify colocalization of Fc γ RIIB with lipid raft.



Chapter 3


Results

Chapter 3 Results



3.1 FcγRIIB^{232T/T} mice show persistent impaired affinity maturation over time

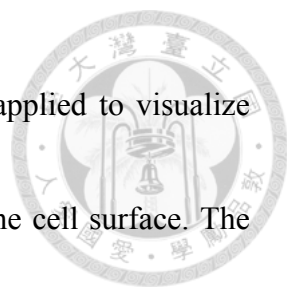
To investigate whether reduced inhibitory function of FcγRIIB could affect the selection of GC B cells, we have generated FcγRIIB^{232T/T} mice to test our concept. We have recently shown that the FcγRIIB-I232T polymorphism, of which the 232th amino acid was substituted from isoleucine to threonine, in mice results in impairment in the negative selection of GC B cells during GC reaction (Jhou, *et al.*, 2018). To evaluate the long-term effect of FcγRIIB^{232T/T} on affinity maturation, we immunized female wild-type and FcγRIIB^{232T/T} mice with 50 μg of NP-CGG admixed with an equal volume of alum adjuvant. Serum samples were collected on days 14, 28 and 35. Serum levels of high-affinity NP-specific IgG and total NP-specific IgG were measured with ELISA plates coated with NP7-BSA and NP30-BSA proteins, respectively. The affinity maturation status was measured by dividing high-affinity NP-specific IgG by total NP-specific IgG from ELISA readings. We found that on day 14, the serum levels of NP-specific IgG of FcγRIIB^{232T/T} mice showed significantly lower affinity maturation



($P < 0.05$, **Figure 2**) than those of wild-type mice. By day 35, the affinity maturation status of serum NP-specific IgGs of wild-type mice was close to 1, indicative of nearly total elimination of the low-affinity NP-specific GC B cells to produce mostly high-affinity NP-specific IgGs. In contrast, $Fc\gamma RIIB^{232T/T}$ mice revealed continued retention of low-affinity NP-specific IgGs and a slower affinity maturation kinetic toward maturation to high-affinity NP-specific IgGs over time. These data from $Fc\gamma RIIB^{232T/T}$ mice suggest that pharmacological down-regulation of $Fc\gamma RIIB$ expression might induce a similar Ab phenotype resulting from reduced inhibitory activity of $Fc\gamma RIIB$.

3.2 Association of $Fc\gamma RIIB$ and BCR with the lipid raft after coligation was impaired in $Fc\gamma RIIB^{232T/T}$ mutant mice

The I232T polymorphism is a single nucleotide polymorphism (SNP) in the transmembrane domain of $Fc\gamma RIIB$ proteins. Coligation of $Fc\gamma RIIB$ with immune complex results in apoptosis of the centrocytes. We hypothesized that the mouse $Fc\gamma RIIB$ -I232T would alter its stability in the association with lipid raft as observed in



human counterpart. To investigate this, confocal microscopy was applied to visualize the effect of FcγRIIB-I232T on BCR in the lipid microdomain at the cell surface. The ganglioside GM1, a lipid raft marker that binds to the subunit B of cholera toxin, and FcγRIIB were respectively labeled as green with FITC and red with Cy3-conjugated Abs. As shown in **Figure 3A**, the wild-type B lymphocytes showed remarkable yellow cap structure at 30 to 60 min, indicating that the FcγRIIB were stably coligated within the lipid raft with BCR in response to whole anti-Ig crosslinking. In contrast, B lymphocytes from FcγRIIB^{232T/T} mice showed discrete FcγRIIB and lipid raft co-localization. Metamorph analysis tool was applied to quantify the percentage of FcγRIIB localized in the lipid raft. From 15 to 60 min, we found that a significantly lower co-localization in isolated FcγRIIB-232T B cells in comparison with the wild-type B cells in a time-dependent fashion (**Figure 3B**). Our findings FcγRIIB-232T B cells are consistent with those observed in human peripheral mononuclear cells isolated from FcγRIIB-232T carriers (Kono, *et al.*, 2005).

3.3 Nilotinib administration during GC reaction has a negative impact on affinity maturation



To assess whether it is applicable to manipulate affinity maturation with Fc γ RIIB targeting agent, we examine the effects of nilotinib, a specific c-Abl inhibitor. As reviewed in the introduction, c-Abl is the key downstream signal protein involved in the apoptosis pathway induced by aggregation of Fc γ RIIB via non-cognate ICs. Mice were immunized twice with NP-CGG 50 ug admix with equal volume of alum on day 1 and day 28 (**Figure 1**).


After the second booster of NP-CGG, we administered the wild-type female mice with nilotinib with the dose of 2 mg/kg/day daily from the sixth day (day 35) to the ninth day (day 37), which was the most active time of GC reaction, clonal selection and apoptosis of low-affinity GC B cells. Immunized mice were sacrificed on day 38, the following day after last treatment of nilotinib. Sera and splenocytes were collected. NP-specific IgG secreting PCs and IgG levels were detected and quantified with ELISPOT and ELISA assays, respectively. Low-affinity NP-specific IgG secreting PCs were measured with subtracting the NP7-specific IgG-secreting PC count from

NP30-specific IgG-secreting PC count. In nilotinib-treated group, the low-affinity NP-specific IgG secreting cell count was significantly higher ($P < 0.05$, **Figure 4A**).

Correspondingly, the affinity maturation status of the circulating NP-specific IgGs was significantly reduced ($P < 0.05$, **Figure 4B**).

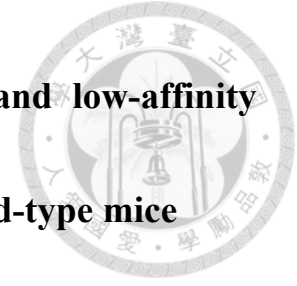
3.4 GW501516 increases respective total and low-affinity Ag-specific IgG PCs at the dose of 3 and 6 mg/kg/day during GC reaction

To observe the effects of GW501516 on the selection process of GC reaction, we gave each wild-type female mouse with either 3 or 6 mg/kg/day on the sixth to the ninth day after the secondary immunization when IgG ICs were abundantly present. The choice of doses was based on a study of obese rhesus monkey, of which lipid-lowering effect by GW501516 was dramatically observed at 3 mg/kg/day given for 1 month. More importantly, the dosage of 3 mg/kg/day was safe and not reported to induce carcinogenesis in mice in previous studies. Due to the short-term treatment of GW501516 for 4 days, a higher dose of 6 mg/kg/day of GW501516 was also included in our study to observe a potential dose-dependent effect. The control group was given

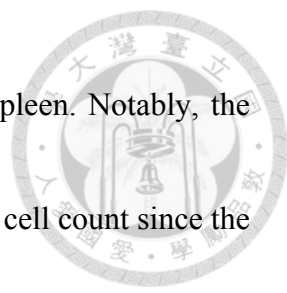


an equal volume of diluted dimethyl sulfoxide (DMSO) in PBS, which is the vehicle of GW501516. We performed ELISPOT assay to assess Ag-specific IgG secreting PCs in spleen. We found that mice respectively given 3 and 6 mg/kg/day of GW501516 could generate more NP30-specific IgG secreting PCs than those of control mice. Moreover, the increase in the both groups of 3 and 6 mg/kg/day was statistically significant ($P < 0.05$, **Figure 5B**). The total Ag-specific IgG secreting cells show increment in each dose but no dose dependent effect was observed. The number of NP7-specific IgG secreting cells, considered as high affinity NP-specific IgG secreting cells, did not show a significant change (**Figure 5A**). The low-affinity Ag-specific IgG secreting PC count, defined as the numbers of NP30-specific IgG secreting PC numbers minus NP7-specific IgG secreting PC numbers, increased at the dose of 3 and 6 mg/kg/day in a dose-dependent fashion ($P < 0.05$, **Figure 5C**). The effect was apparent on 6 mg/kg/day probably because of no significant increase and also mild decrease in some of the mice in the numbers of high-affinity NP⁺ PCs.

3.5 GW501516 increases the serum levels of total and low-affinity Ag-specific IgG at the dose of 3 and 6 mg/kg/day in wild-type mice



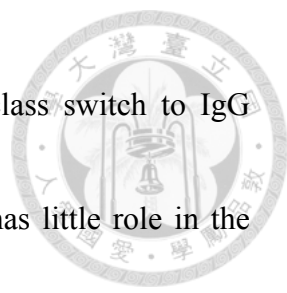
In order to assess whether the serum IgG level was associated with the numbers of IgG secreting PCs, we performed indirect ELISA with either NP2-BSA (1 BSA conjugated with 2 NPs) or NP30-BSA as the Ag coated onto 96-well plates. Serum samples were diluted with PBS in a factor of 4×10^4 . The relative NP Ag-specific IgG concentrations expressed in arbitrary units per ml (AU/ml) were calculated from semilog regression of the OD₄₅₀ levels of standard serum. The average of total antigen-specific (NP30-specific) IgGs increased approximately 2 folds in both 3 and 6 mg/kg/day groups but the results did not show a dose-dependent pattern ($P < 0.05$, **Figure 6B**). The level of high-affinity IgGs (NP2-specific) did not show significant differences (**Figure 6A**). We divided the high-affinity Ag-specific IgG level over total Ag-specific IgGs as the antibody avidity index as a functional readout of affinity maturation. The higher the ratio, the better the affinity maturation in terms of high-affinity IgG production. The results showed a significant decrease in the affinity maturation in 3 mg/kg/day but not in 6 mg/kg/day. As a result, the circulating IgG



levels were highly relevant to the IgG secreting cell count in the spleen. Notably, the interpretation of IgG levels is slightly distinct from antigen secreting cell count since the affinity maturation terminates and the germinal centers diminished in the spleen after the primary immunization. But the circulating IgGs continue to increase affinity till day 35 as shown in **Figure 2**. The average ratio was about 0.8 in 3 mg/kg/day (**Figure 6C**) compared with 1 in control group, which indicating complete affinity maturation on day10 after the second booster. The results were consistent with the prediction that GW501516 can increase low-affinity antibody production and impair negative selection during the GC reaction. On average, high-affinity antibody levels were not affected, but the GW501516-treated mice presented a greater variation than the control group. Namely, the GW501516 treatment has an ambiguous effect on high-affinity Abs.

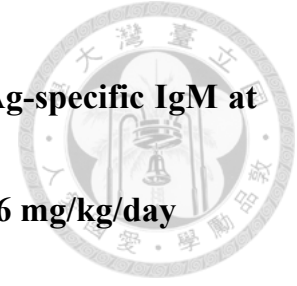
3.6 GW501516 increases total Ag-specific IgM secreting PCs at the dose of 6 mg/kg/day during GC reaction

Our results had shown effects of GW501516 on the GC reaction and humoral response of repeated immunization. Traditionally, IgM is not considered as the main



component of affinity maturation since the centrocytes undergo class switch to IgG secreting PCs. Especially after the secondary immunization, IgM has little role in the humoral immunity. Circulating IgMs are produced from extrafollicular PCs that do not participated in the GC reaction. To evaluate whether GW501516 had effects on extrafollicular IgM secreting PCs, we performed ELISPOT assay to determine the numbers of IgM secreting PCs in the spleen. GW501516 administration increased the levels of NP30-specific (total NP-specific) IgM at the dose of 6 mg/kg/day ($P < 0.05$, **Figure 7B**) but not 3 mg/kg/day. In the group of mice treated with 3 mg/kg/day, the effect of GW501516 varies that some of the mice decreased but some increased in total numbers of NP-specific PCs (**Figure 7A**). When the numbers of high-affinity IgM PCs were analyzed, no significant difference was observed in each dose. However, the numbers of low-affinity IgM NP⁺ PCs (total IgM PCs minus high-affinity IgM PCs) increased significantly in mice treated with 6 mg/kg/day for 4 days ($P < 0.05$, **Figure 7C**). The avidity index was 0.5 in control group but the GW501516-treated group display an average 0.6 and up to 0.8 in some mice.

3.7 GW501516 increases the serum levels of high-affinity Ag-specific IgM at the dose of 3 and 6 mg/kg/day and total Ag-specific IgM at 6 mg/kg/day



To assess whether the result of Ag-specific IgM PCs is associated with serum levels of Ag-specific IgMs, we performed ELISAs. The serum samples were diluted in a factor of 2×10^4 . The serum Ab levels were displayed in arbitrary units per ml. Consistent with the findings in NP30-specific (total NP-specific) IgM secreting PCs, the serum total Ag-specific IgM levels increased in mice treated with 6 mg/kg/day ($P < 0.05$, **Figure 8B**) but not in 3 mg/kg/day. On the other hand, the NP2-specific (high affinity NP-specific) IgMs increased in both 3 and 6 mg/kg/day in a dose-dependent pattern, which was not concordant with the results in IgM-secreting PCs (**Figure 8B**). The antibody avidity index of the high-affinity Ag-specific IgMs over the total NP-specific IgMs showed increased ratios in both groups of 3 and 6 mg/kg/day treatments owing to the higher levels of high-affinity Ag-specific IgMs (**Figure 8C**). The result indicates that the effect of GW501516 on FcγRIIB might not be the only factor to influence the humoral immunity and affinity maturation. GW501516 might also affect the memory B cell response, Ab secretion, and class switch of centrocytes and T_{fh} activity.



Chapter 4

Discussion

Chapter 4 Discussion



4.1 FcγRIIB^{232T/T} mutant mice as a model for investigating the functional role of FcγRIIB in GC reaction

FcγRIIB act as the only inhibitory Fcγ receptor of immune response. Impairment of FcγRIIB leads to development of persistent GC reaction and autoimmune diseases.

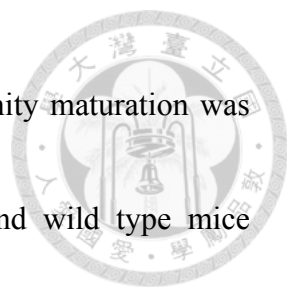
I232T is a single nucleotide polymorphism of Fcgr2B in human that is highly associated with SLE. As previously mentioned, the I232T SNP locates in the transmembrane domain, impairing signal transduction and stability during coengagement with BCR in the lipid raft. Despite that FcγRIIB^{232T/T} mutant mice are functionally impaired of the receptor on all the immune cells, FcγRIIB^{232T/T} mice did not present SLE symptoms even after immunization. Because FcγRIIB-deficient mice spontaneously develop lupus symptoms after 6 months of age, advanced age of FcγRIIB^{232T/T} is likely required to trigger lupus pathology. However, we can still observe impaired negative selection, larger GCs and more PCs in FcγRIIB^{232T/T} mice. On the other hand, FcγRIIB-deficient mice present with hyper-immunity and are used as a model for SLE. The properties of FcγRIIB^{232T/T} mice make them an ideal human disease-relevant model for research on

the role of Fcγ receptors in the GC reaction and also pharmacological manipulation of Fcγ receptors for vaccination, e.g. phenotype rescue, or the treatment of autoimmune disorders, as opposed to FcγRIIB-deficient mice.



4.2 Difference between FcγRIIB^{232T/T} mutant mice and wild type mice treated with nilotinib or GW501516

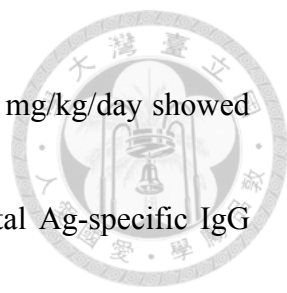
We tested nilotinib and GW501516 for the potential of manipulating the selection outcome of GC reaction. We hypothesized that nilotinib inhibits the downstream c-Abl signal pathway triggered by coengagement of FcγRIIB, negative selection and apoptosis of low-affinity centrocytes in the LZ were impaired, leading to accumulation of low-affinity GC B cells. For GW501516, it can reduce FcγRIIB expression levels, mimicking the condition of reduced FcγRIIB inhibitory activity. The timing of administering nilotinib and GW501516 was designed to meet the maximum negative selection and apoptosis of GC B cells, but to avoid affecting early phase GC reaction. As shown in **Figure 2**, FcγRIIB^{232T/T} mice remained impaired on affinity maturation till 35 days after primary immunization. For wild-type mice on day 28 after primary



immunization, the day for second booster, the circulating IgG affinity maturation was 0.8. Therefore, the baseline conditions for FcγRIIB^{232T/T} mice and wild type mice treated with nilotinib or GW501516 are different. We could reason that memory cells generated from the primary immunization are not exposed to nilotinib or GW501516, which might affect the secondary immune response. It is reasonable that by administering nilotinib or GW501516 cannot fully replicate the functional impairment in FcγRIIB-I232T polymorphism. After drug elimination, we expected that the affinity maturation would go on and FcγRIIB activity or expression would return to normal conditions. Thus, the risk for inducing autoimmune disease is expected to be low. The long-term effect requires further investigation.

4.3 Summary of the overall effect of GW501516 on GC reaction

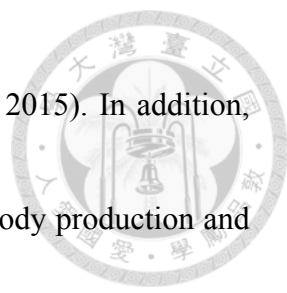
In this study, we showed that GW501516 at the dose of 3 and 6 mg/kg/day can influence the GC reaction, resulting in an increase of the numbers of total Ag-specific IgG PCs and serum levels of Ag-specific IgGs. The high-affinity Ag-specific PCs and Ag-specific IgG levels were not significantly different when compared with the control




group (**Figures 2 and 3**). However, GW501516 administration at 6 mg/kg/day showed paradoxical results in that some mice displayed lower levels of total Ag-specific IgG PCs, whereas some mice showed the opposite findings (**Figures 6 and 7**). Our results showed a concomitant increase of the low-affinity PCs and serum IgGs (**Figures 6 and 7**) in treated groups. These results support the involvement of GW501516 in GCs with negative influence on the affinity maturation reminiscent of the findings observed in FcγRIIB-232T mice. Interestingly, GW501516 appears to increase the numbers of high-affinity Ag-specific IgG ASCs and serum IgG. On the other hand, the levels of high-affinity Ag-specific IgM increased more markedly than the increased number of ASCs. As the extrafollicular ASCs mostly carry IgM on their surface and they do not undergo affinity maturation in the germinal center, we reasoned that GW501516 might have effects on the secretion of IgM but this needs to be further investigated.

4.4 Could GW501516 affect GC reaction other than FcγRIIB down-regulation induced by PPAR-δ activation?

A previous study demonstrates that PPAR-δ activation down-regulates the

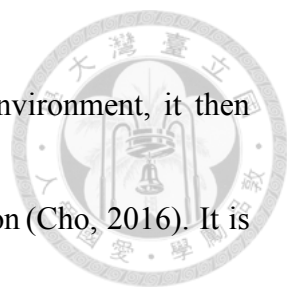


expression of FcγRIIB in a macrophage cell line (Adhikary, *et al.*, 2015). In addition, our previous study on FcγRIIB-I232T mice revealed enhanced antibody production and reduced affinity maturation (Jhou, *et al.*, 2018). The down-regulation of FcγRIIB in macrophages could be a result of direct regulation by PPAR-δ but whether the effect of PPAR-δ activation is the same in B cells remained unknown. On the other hand, PPAR-δ is a transcription factor with different functions on T cells, B cells and macrophages.ⁱⁱⁱ How activation of PPAR-δ might lead to alternation of the interaction between B cells and T_{fh} or between T_{fh} and B cells remains unclear. However, our preliminary data from the analysis of flow cytometric results did not show a significant change in surface FcγRIIB levels in CD11b⁺ myeloid cells in the spleen. A more detailed analysis of the phenotypes of GC myeloid cells, especially at the marginal zone of the GC is warranted. Unlike splenic macrophages, splenic B cells showed a trend of decreased expression of FcγRIIB at the dose of 6 mg/kg/day, suggesting greater drug sensitivity. However, the relative numbers of DZ and LZ GC B cells did not show significant differences in vehicle- and GW501516-treated mice, suggesting that GW501516 did not affect the differentiation of DZ GC B cells (centroblasts) into LZ



GC B cells (centrocytes) and not significantly influenced by Fc γ RIIB. A definitive answer can be obtained from inducible deletion of Fc γ RIIB gene at a defined time during GC reaction. Fc γ RIIB gene deleted at the same period of GW501516 administration after secondary immunization is expected to show more profound effects in the change of IgG PCs and their Abs secreted.


PPAR- δ activates signaling pathways that affect immune responses and inflammation. The phenomenon in humoral response observed in our study might be an integrated result from multiple factors. For instance, Bcl-6, an important transcription factor in selection of B cells entering the GC, is also a transcriptional repressor of PPAR- δ . GW501516 induces activation of PPAR- δ and leads to unbinding and activation of Bcl-6 (Coleman, *et al.*, 2013). In contrast, NF- κ B is a transcription factor involved in pro-inflammatory effects and it is suppressed during PPAR- δ activation by AMP kinase (AMPK) and SIRT1 (Barroso, *et al.*, 2011). PPAR- δ also modulates inflammatory responses that involve JAK-STAT pathway. On the other hand, GW501516 had been reported to increase fatty acid oxidation and glucose uptake in skeletal muscles via activation of AMPK, a kinase activated in hypoxic environment,



and PPAR- δ (Kramer, *et al.*, 2007). Since the GC is a hypoxic environment, it then suggests that energy metabolism might modulate antibody production (Cho, 2016). It is possible that PPAR- δ activation alters the metabolism in the GCs and then affects humoral immunity. It should be noted that our study focused on the response after a second booster of immunogen. The effect on memory B cells should also be considered for investigation. In addition, it is likely that the effect on the primary response will be different because of different natures in the production of IgM and IgG.

4.5 Pharmacological modulation of Fc γ RIIB activity is an applicable method for novel manipulation of immune response

Although the GW501516-mediated mechanisms of our findings are not clear at present, we showed immunomodulatory effects of GW501516, a PPAR- δ agonist, *in vivo*. The effects of widely used anti-diabetic drugs, such as metformin, TZDs, have been reported to be associated with PPARs activation. It is an interesting question to answer that if these anti-diabetic medications affect our immune response to pathogens and to vaccination. Importantly, our results reveal that PPAR- δ could be a potential



target for innovative adjuvants in vaccine development and the development of cross-protective effects of vaccines. On the flip side, PPAR- δ inactivation might be a prospective therapy toward autoimmune diseases. Our ongoing research aims to unravel the molecular mechanism of immunomodulatory effects of GW501516 and PPAR- δ activation both *in vitro* and *in vivo* by using conditional and inducible knockout mice of Fc γ RIIB gene and to modulate GC response using various candidate compounds.

4.6 Potential role of macrophages in the GC reaction to influence the generation of Ag-specific Abs

It has been reported that defective phagocytosis of macrophages can lead to autoimmunity (Fond and Ravichandran, 2016). Fc γ RIIB can block IC-mediated activation of Fc γ R and other activating receptors in macrophages. Moreover, overexpression of Fc γ RIIB in myeloid cells suppresses host immunity against bacterial infection. Conversely, Fc γ RIIB-deficient macrophages increase their phagocytic property (Brownlie, *et al.*, 2008). The gene transcription of Fc γ RIIB has been shown to be down-regulated in a macrophage cell line by PPAR- δ agonist (Adhikary *et al.*, 2015).

It is then crucial to determine whether the absence of FcγRIIB gene can promote macrophage function *in vivo*.



Splenic macrophage subpopulations are diverse and their functions remain elusive.

The unique tingible body macrophages (TBMs; Mer+DNaseI⁺) are predominantly scattered in the GC. TBMs express Mer receptor tyrosine kinase, which mediates phagocytic activity and regulates cytokine production (Rahman, 2011). They phagocytose apoptotic cells and thereby contain condensed chromatin fragments. TBMs are thought to play a role in down-regulation of GC reaction (Rahman, 2011). The marginal zone (MZ) surrounds lymphoid follicles, where MZ macrophages (MZMs; MARCO⁺CD169⁺) and metallophilic macrophages (MMMs; MOMA⁺) are abundantly present (McGaha and Karlsson, 2016). MZMs are specialized macrophages that phagocytose apoptotic materials entering the spleen from circulation to minimize the immunogenicity of autoantigens (McGaha *et al.*, 2011). MMMs distribute adjacent to the T- and B-cell-rich zones. Interestingly, MZMs and MMMs disappear when B cells were absent before birth or gradually depleted after birth, suggesting a critical role of B cells in the maintenance of splenic MZ structure (Nolte, *et al.*, 2004). Interaction with

MZ B cells is also crucial for efficient homing of MZMs and MMMs and for efficient removal of blood-borne pathogens coming into the MZ.



To the best of our knowledge, whether the fate of GC B cells during affinity maturation is influenced by macrophages, whether Fc γ RIIB regulates phagocytic activity of GC and MZ macrophages, and how macrophages might interact with B cells in the GC are all incompletely understood. We have recently generated conditional knockout mice of Fc γ RIIB gene in myeloid cells to investigate the potentially important role of macrophages in the selection of GC B cells. Moreover, this mouse strain will help explain and conclude our findings on the effects of GW501516 of macrophages during affinity maturation of GC reaction in secondary immunization.



Figures

Figure 1



(A)

Primary
Immunization

Sacrifice



(B)

Primary
Immunization

Second
Booster

Sacrifice



(C)

Primary
Immunization

Second
Booster

Sacrifice



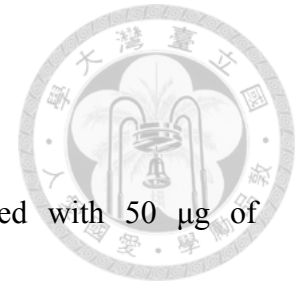


Figure 1. Mouse immunization schedules.

(A~C) 7-to-10-week-old female mice were primarily immunized with 50 μ g of NP20-CGG admixed with 50 μ l of alum intraperitoneally on day 1. The second booster was given on day 28 with the same antigen and route. The “x” denotes the day of collecting serum samples. Before the second booster, serum samples were collected on days 14 and 27. **(A)** Comparison of wild-type and Fc γ RIIB^{232T/T} mice. Mice were sacrificed on day 35 after primary immunization. Sera were collected on day 14, day 28 and day 35. No second booster was given. **(B)** C57BL/6 mice were daily given nilotinib at 2 mg/kg/day or vehicle intraperitoneally from the sixth day to the ninth day after the second booster. Mice were sacrificed on the tenth day after the second booster (day 38). Serum was collected on day 37. **(C)** C57BL/6 mice were daily given vehicle, GW501516 3 or 6 mg/kg/day intraperitoneally from the sixth day to the ninth day after the second booster. Mice were sacrificed on the tenth day after the second booster (day 38). Serum samples were collected on day 37.

Figure 2

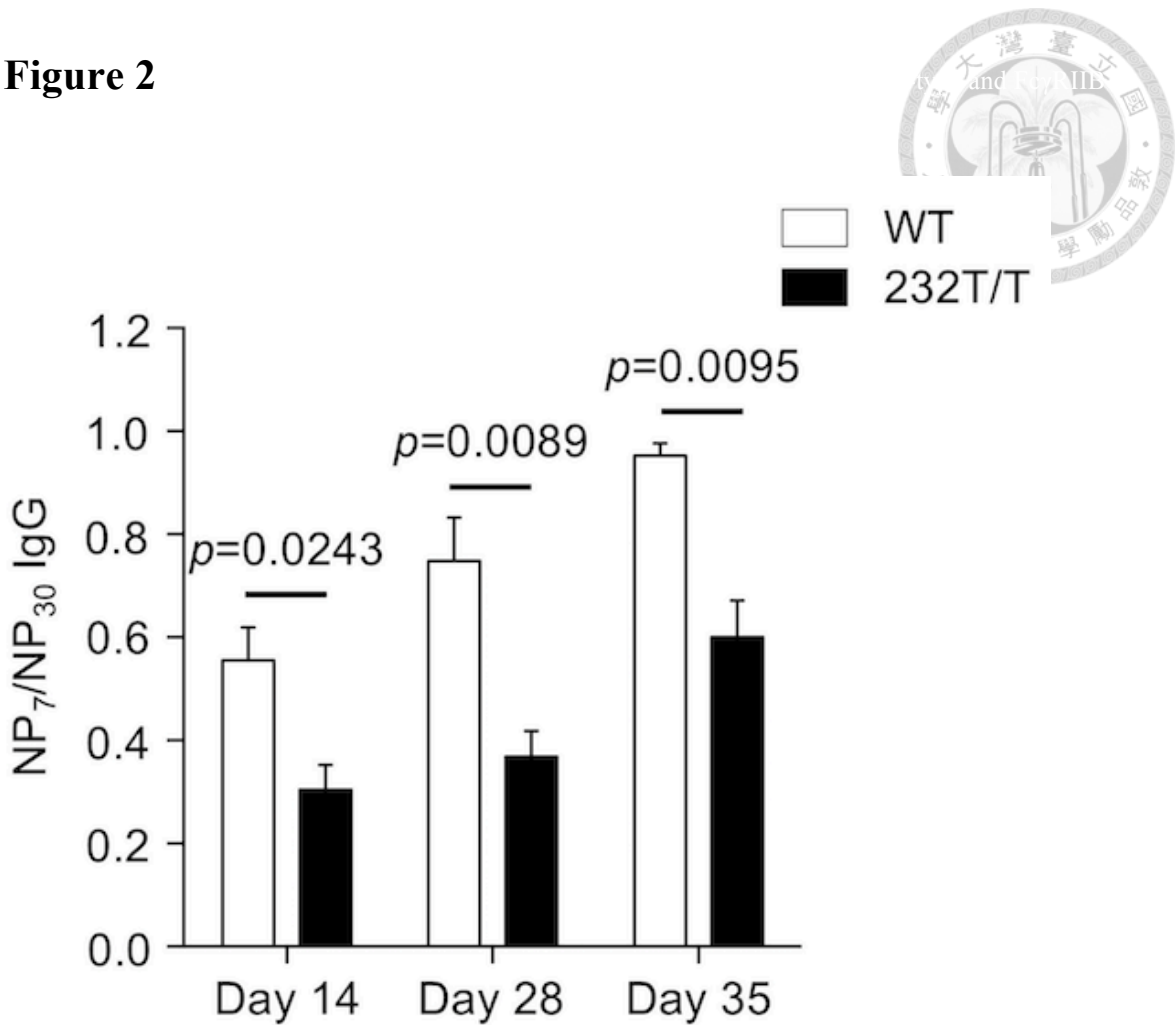


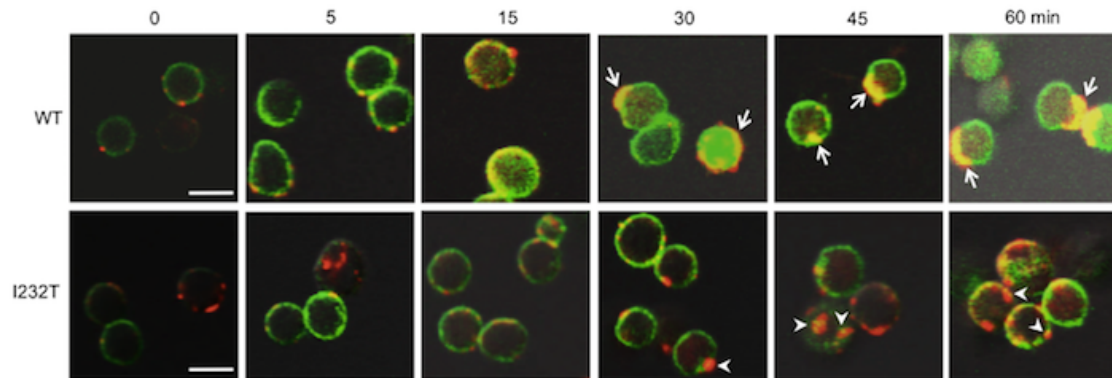
Figure 2. Analysis of the differences of affinity maturation status between wild-type and Fc γ RIIB^{232T/T} mice over time.

On days 14, 28 and 35 after the primary immunization with NP-CGG, sera were collected. The serum NP-specific IgG levels were analyzed by ELISA assay. The status of affinity maturation was measured by the OD₄₅₀ ratio of serum NP7-specific IgG/NP30-specific IgGs between wild-type (n=3) and Fc γ RIIB^{232T/T} (n=4) mice on day 14 ($P=0.0243$), day 28 ($P=0.0089$) and day 35 ($P=0.0095$).



Figure 3

(A)



F

(B)

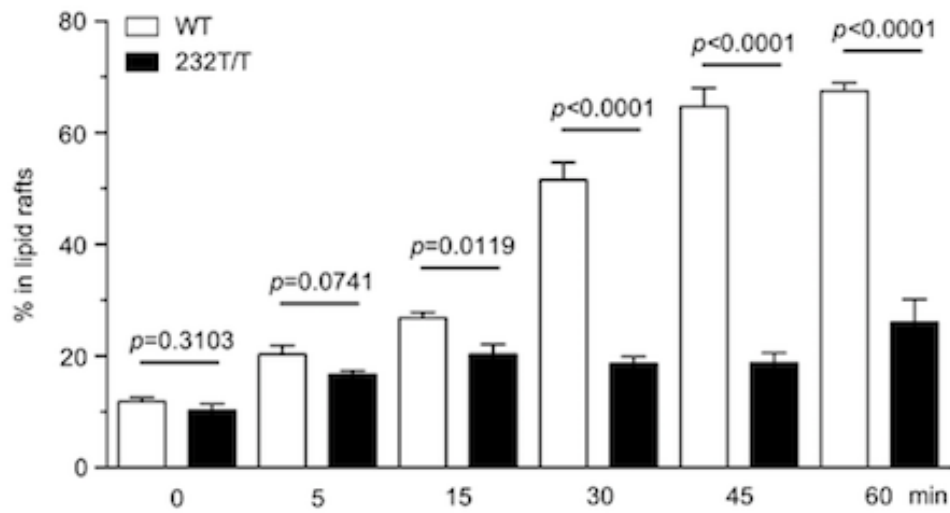




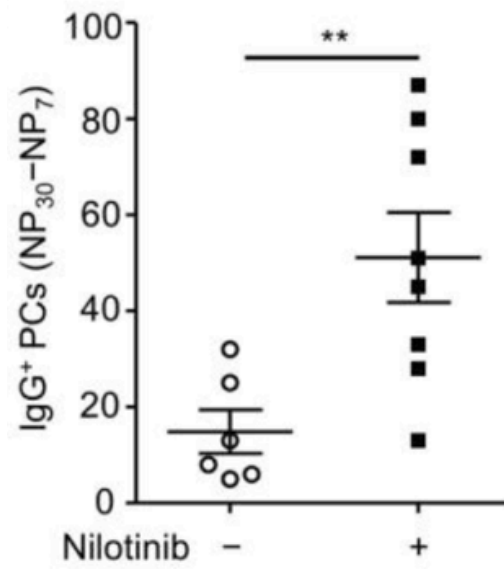
Figure 3. Compare FcγRIIB^{232T/T} mutant and wild type mice of FcγRIIB cluster in the lipid raft with confocal microscopy.

(A) Confocal image (400x magnification) of B-lymphocyte retrieved from the spleens of 8-week-old FcγRIIB^{232T/T} mutant and wild type mice. FITC-labeled cholera toxin B binds to the GM1 ganglioside of the lipid raft and display green fluorescence. Cy3-labeled anti-rabbit IgG binds to the anti-mouse IgM and display red fluorescence. FcγRIIB stabilized in the lipid raft would display yellow fluorescence. In wild type mice, cap structures were formed (arrows) at 30 to 60 min but FcγRIIB^{232T/T} mutant mice did not show much merged yellow fluorescence (arrow head). (B) Quantitative representation of FcγRIIB localized in the lipid raft with Metamorph analysis tool. FcγRIIB^{232T/T} mutant mice showed significant impaired lipid raft colocalization over 15 min ($P < 0.05$).

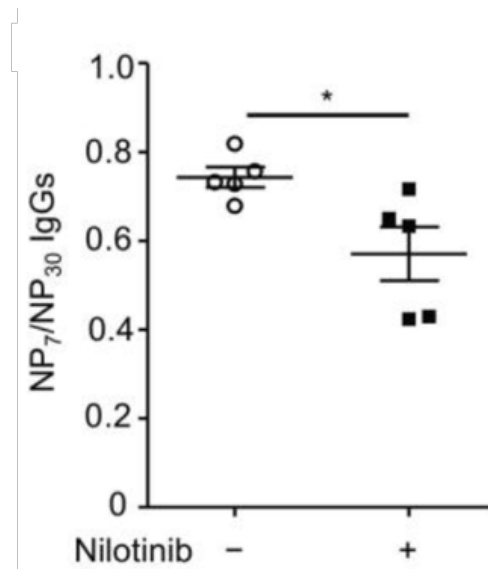
Figure 4



(A)



(B)



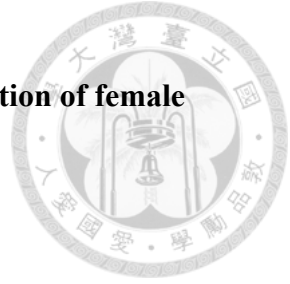


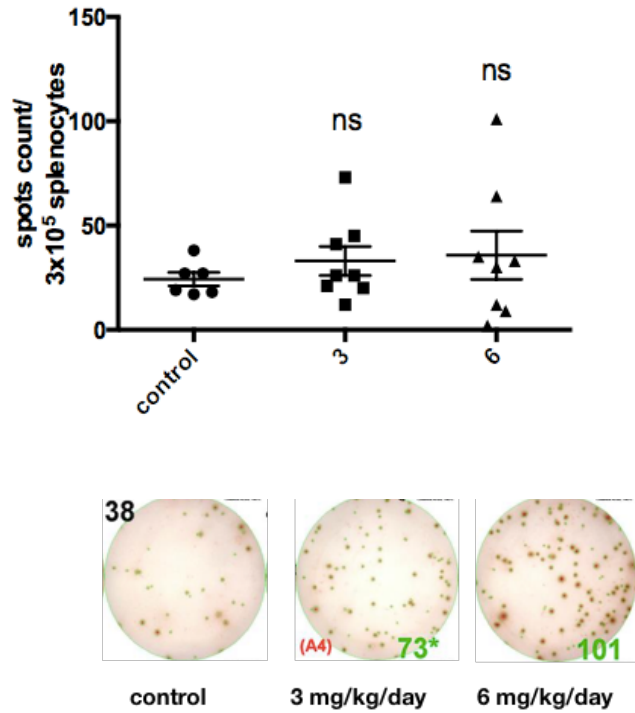
Figure 4. Analysis of the effect of nilotinib on the affinity maturation of female wild-type mice.

(A, B) Wild type female mice were given nilotinib 2 mg/kg/day or vehicle given from the seventh day to the ninth day after the second booster. **(A)** Analysis of IgG secreting PC numbers with ELISPOT assay. Number of low affinity NP-specific IgG secreting PCs per 2.4×10^4 splenocytes by subtracting the NP7 specific IgG-secreting PCs from NP30 specific IgG-secreting PCs. Comparisons between vehicle (n=6) and nilotinib-treated group (n=8) ($P=0.0087$). **(B)** Analysis of serum NP-specific IgG concentration by ELISA assay. The affinity maturation was measured by the OD450 ratio of serum NP7-specific IgG/NP30-specific IgG between vehicle (n=5) and nilotinib-treated group (n=5) ($P=0.0283$).

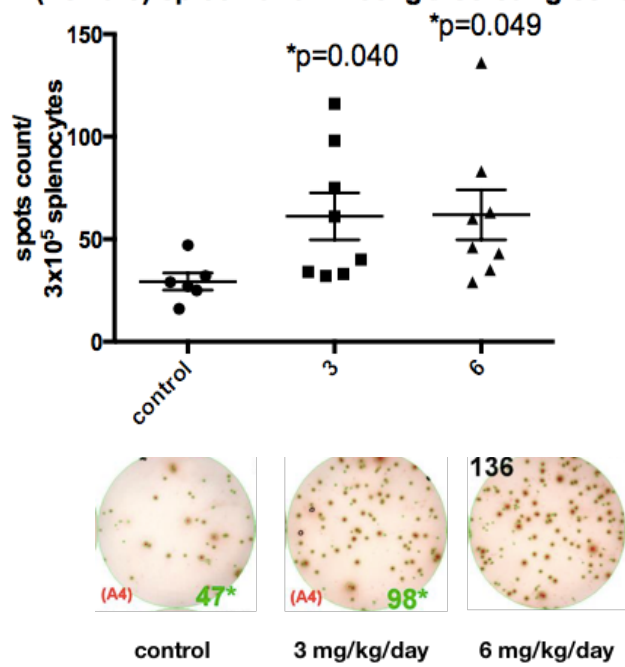
Figure 5



(A) (Female) spleen anti-NP7 IgG secreting cells



(B) (Female) spleen anti-NP30 IgG secreting cells





(C)

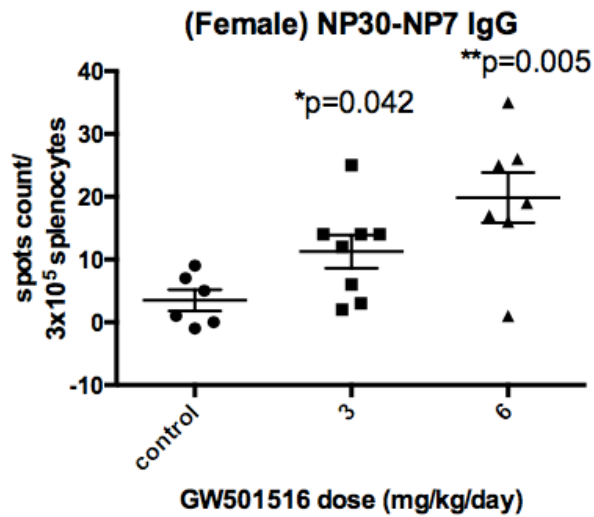


Figure 5. Analyzing IgG-secreting PCs in the spleen of female C57BL/6 mice immunized with two different GW501516 doses by ELISPOT assay.

(A, B) ELISPOT quantification (upper panel) and demonstrative graph (lower panel) of the high-affinity and total NP-specific IgG PCs per 3×10^5 splenocytes. Female C57BL/6 mice, 10 days after the second booster (day 39). Vehicle (n=6, as control group), GW501516 3 mg/kg/day (n=9), GW501516 6 mg/kg/day (n=7) were administered, respectively, during the sixth to the ninth day after the second booster. (A) High-affinity NP7-specific IgG-secreting PC count: GW501516 3 mg/kg/day (ns), 6

mg/kg/day (ns). **(B)** Total NP30-specific IgG-secreting PC count: GW501516 3

mg/kg/day ($P=0.040$), 6 mg/kg/day ($P=0.049$), compared with the control group.

(C) Low-affinity NP-specific IgG secreting PCs measure by subtracting the NP7

specific IgG-secreting PCs from NP30 specific IgG-secreting cells. Low-affinity

NP-specific IgG secreting PC count: GW501516 3 mg/kg/day ($P=0.042$), 6 mg/kg/day

($P=0.005$). Results were analyzed with unpaired, two-tailed student *t* test and shown as

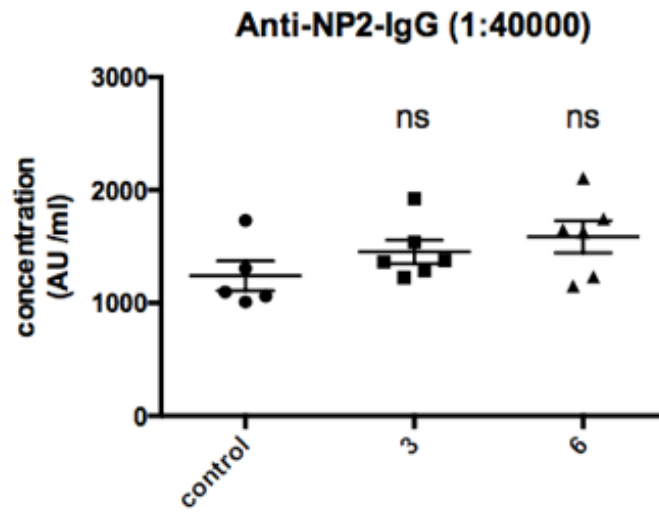
mean \pm SEM. * $P < 0.05$, ** $P < 0.01$, *** $P < 0.001$ and ns, no significance



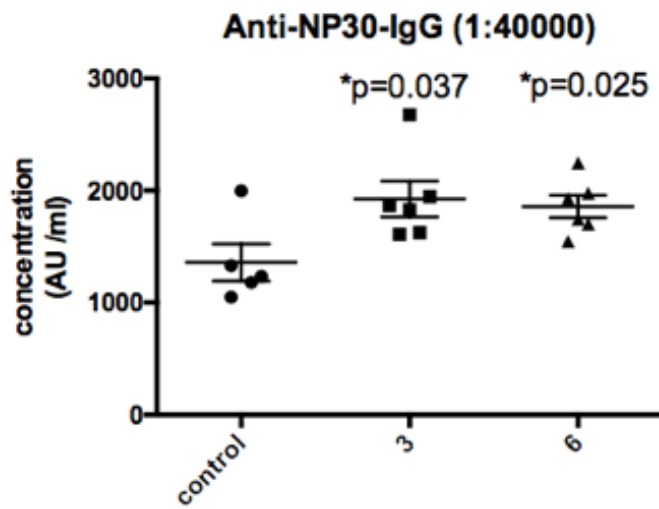
Figure 6



(A)



(B)



(C)

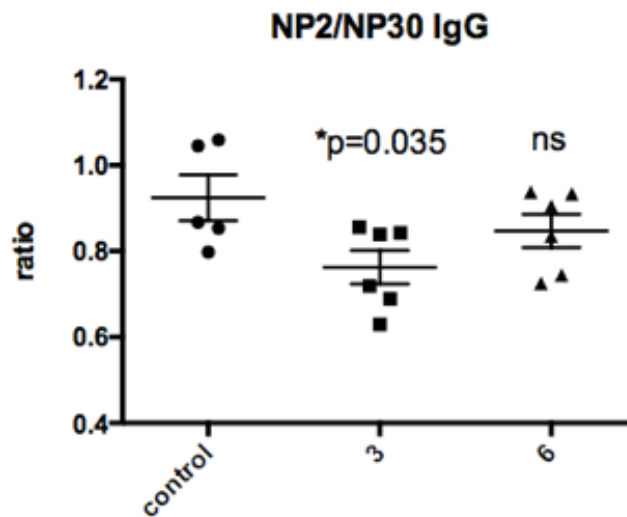




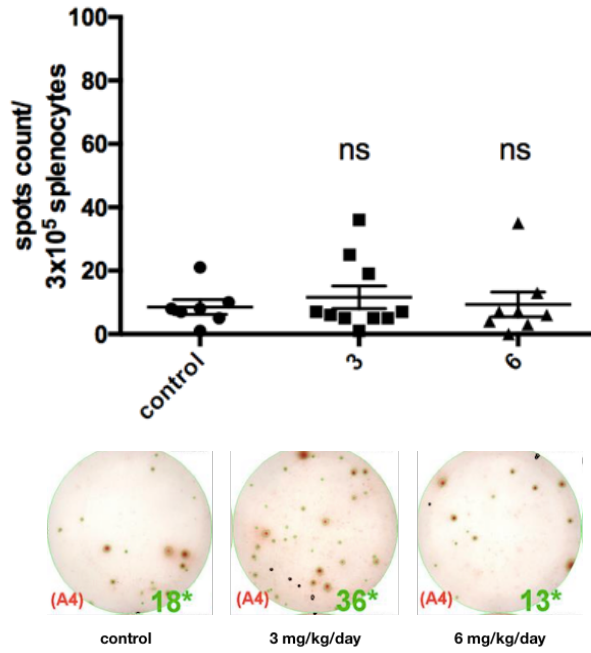
Figure 6. Measurement of serum IgG levels of female C57BL/6 mice immunized with two different GW501516 doses by ELISA assay.

(A, B) Serum high-affinity and total NP-specific IgGs in the serum of female C57BL/6 mice, 10 days after the second booster (day 39). Vehicle (n=5, as control group), GW501516 3 mg/kg/day (n=6), GW501516 6 mg/kg/day (n=6) were administered, respectively, during the sixth to the ninth day after the second booster. Serum was diluted in 4×10^4 folds. **(A)** Serum high-affinity NP2-specific IgG: GW501516 3mg/kg/day (ns), 6mg/kg/day (ns). **(B)** Serum total NP30-specific IgG of treatment with GW501516 3 mg/kg/day ($P=0.037$) or 6 mg/kg/day ($P=0.025$), compared with the control group. **(C)** The affinity maturation measurement by dividing the NP2 specific IgG serum level by the NP30 specific IgG serum levels. NP2/NP30: GW501516 3 mg/kg/day ($P=0.035$), 6 mg/kg/day (ns). Results were analyzed with unpaired, two-tailed student *t* test and shown as mean \pm SEM. * $P < 0.05$, ** $P < 0.01$, *** $P < 0.001$ and ns, no significance. AU denotes arbitrary units

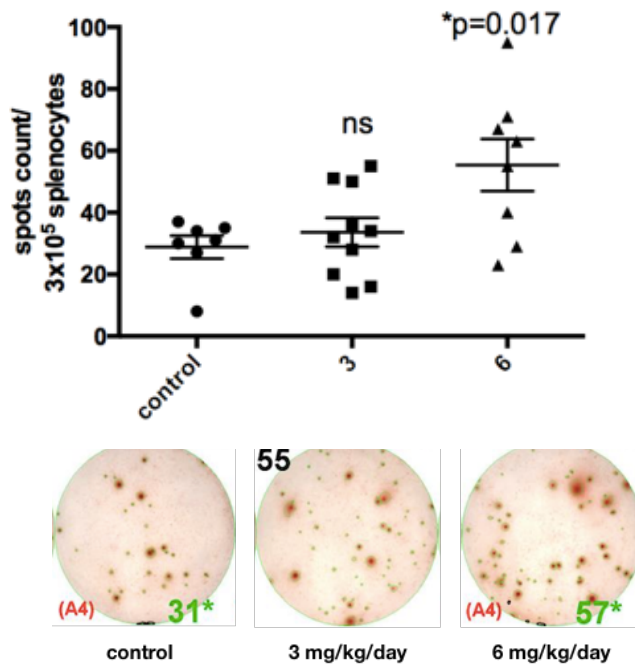
Figure 7



(A) (Female) spleen anti-NP7 IgM secreting cells



(B) (Female) spleen anti-NP30 IgM secreting cells



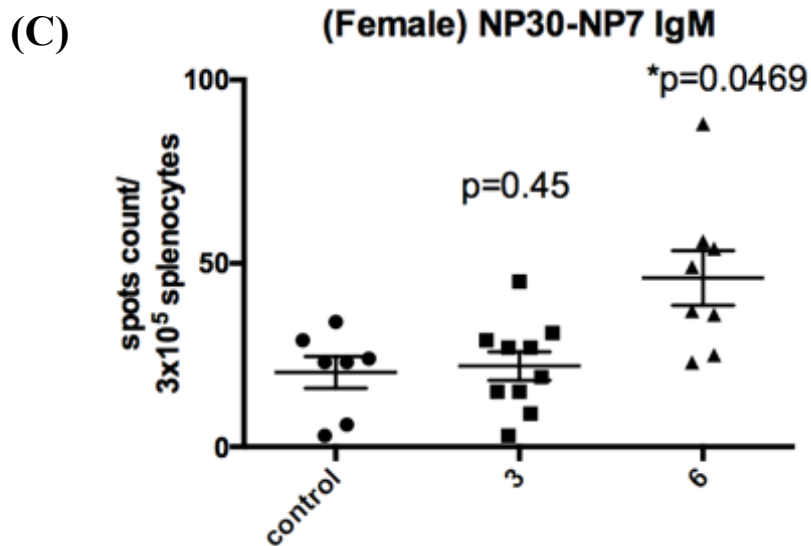


Figure 7. Analyzing IgM-secreting PCs in the spleen of female C57BL/6 mice immunized with two different GW501516 doses by ELISPOT assay

(A, B) ELISPOT quantification (upper panel) and demonstrative graph (lower panel) of high-affinity and total NP-specific IgM-secreting cells per 3×10^5 splenocytes of female C57BL/6 mice, 10 days after the second booster (day 39). Vehicle (n=7, as control group), GW501516 3 mg/kg/day (n=10), GW501516 6 mg/kg/day (n=8) were administered, respectively, during the sixth to the ninth day after the second booster. (A) High-affinity NP7-specific IgM-secreting PC count: GW501516 3 mg/kg/day (ns),

6mg/kg/day (ns). **(B)** Total NP30-specific IgM-secreting PC count: GW501516 3 mg/kg/day (ns), 6 mg/kg/day ($P=0.017$), compared with the control group.

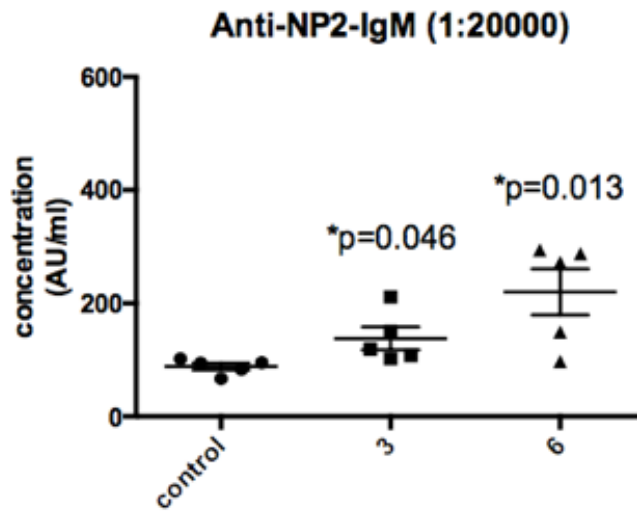


(C) Low-affinity NP-specific IgM secreting PCs measure by subtracting the NP7 specific IgM-secreting PCs from NP30 specific IgM-secreting PCs. Low-affinity NP-specific IgM secreting PC count: GW501516 3 mg/kg/day ($P=0.45$), 6 mg/kg/day ($P=0.0469$) Results were analyzed with unpaired, two-tailed student t test and shown as mean \pm SEM, * $P < 0.05$, ** $P < 0.01$, *** $P < 0.001$ and ns, no significance.

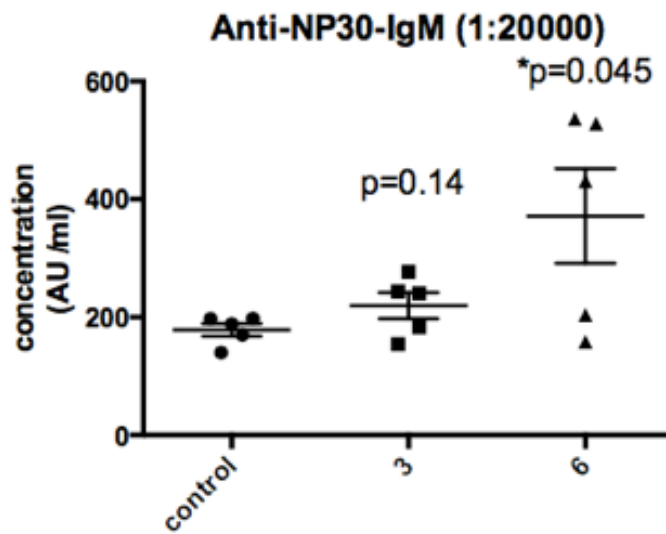
Figure 8



(A)



(B)



(C)

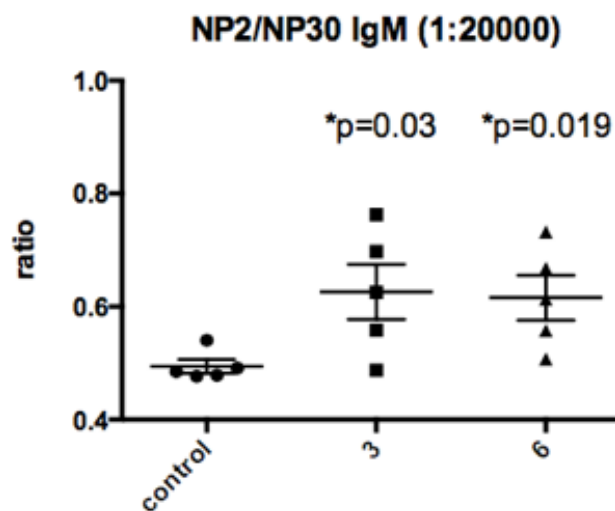




Figure 8. Measurement of the serum IgM levels of female C57BL/6 mice immunized with two different GW501516 doses by ELISA assay.

(A, B) Serum high-affinity and total NP-specific IgMs in the serum of female C57BL/6 mice, 10 days after the second booster (day 39). Vehicle (n=5, as control group), GW501516 3 mg/kg/day (n=5), GW501516 6 mg/kg/day (n=5) were administered, respectively, during the sixth to the ninth day after the second booster. Serum was diluted 2×10^4 times. (A) Serum high-affinity NP2-specific IgGs: GW501516 3 mg/kg/day ($P=0.046$), 6 mg/kg/day ($P=0.013$). (B) Serum total NP30-specific IgMs. GW501516 3 mg/kg/day ($P=0.14$), 6 mg/kg/day ($P=0.045$), compared with the control group. (C) Affinity maturation measured by dividing the NP2 specific IgM serum levels by the NP30 specific IgM serum levels. NP2/NP30: GW501516 3 mg/kg/day ($P=0.03$), 6 mg/kg/day ($P=0.019$). Results were analyzed with unpaired, two-tailed student *t* test and shown as mean \pm SEM. * $P < 0.05$, ** $P < 0.01$, *** $P < 0.001$ and ns, no significance. AU denotes arbitrary units.



References

Ademokun, Alexander A, and Dunn-Walters, Deborah (Sep 2010) , Immune responses: primary and secondary. *In: eLS*. John Wiley & Sons Ltd, Chichester. <http://www.els.net> [doi: 10.1002/9780470015902.a0000947.pub2]

Adhikary T, *et al.* (2015), The Transcriptional PPAR β/δ Network in human macrophages defines a unique agonist-induced activation state. *Nucleic Acids Research*, 43(10): 5033–5051

Allen C, Okada T, Cyster JG (2015), Germinal center organization and cellular dynamics. *Immunity*, 27(2): 190–202

Barroso E, Eyre E, Palomer X, Vázquez-Carrera M (2011), The peroxisome proliferator-activated receptor β/δ (PPAR β/δ) agonist GW501516 prevents TNF- α -induced NF- κ B activation in human HaCaT cells by reducing p65 acetylation through AMPK and SIRT1. *Biochemical Pharmacology*, 15, 81(4):534-543

Baxter D (2007), Active and passive immunity, vaccine types, excipients and licensing. *Occupational Medicine*, 57(8): 552–556

Cho SH, *et al.*(2016), Germinal centre hypoxia and regulation of antibody qualities by a hypoxia response system. *Nature*, 537: 234–238

Coleman JD, Thompson JT, Smith RW III, Prokopczyk B and Vanden Heuvel JP (2013), Role of peroxisome proliferator-activated receptor and B-Cell Lymphoma-6 in regulation of genes involved in metastasis and migration in pancreatic cancer cells. *PPAR Research* 2013:121956. [https:// doi: 10.1155/2013/121956](https://doi.org/10.1155/2013/121956)

Cox RL (2017), Rationally designed PPAR δ -specific agonists and their therapeutic potential for metabolic syndrome. *Proceedings of the National Academy of Sciences of*



the USA, 114(13): 3284–3285.

D'Ambrosio D, Fong DC, Cambier JC (1996), The SHIP phosphatase becomes associated with Fc γ RIIB1 and is tyrosine phosphorylated during 'negative' signaling. *Immunology Letter*, 54:77-82.

De Silva NS and Klein U (2015), Dynamics of B cells in germinal centres. *Nature Reviews Immunology*, 15: 137–148

Gefen T, *et al.* (2014), The effect of haptens on protein-carrier immunogenicity. *Immunology*, 144 (1), 116–126

Higashiyama H, Billin AN, Okamoto Y, Kinoshita M, Asano S (2007), Expression profiling of peroxisome proliferator-activated receptor-delta (PPAR-delta) in mouse tissues using tissue microarray. *Histochemistry and Cell Biology*, 127: 485–494

Jhou JP, *et al.* (17 May 2018), The lupus-associated Fc γ RIIB-I232T polymorphism results in impairment in the negative selection of low-affinity germinal center B cells via c-Abl. *Arthritis and Rheumatology*. [https://doi: 10.1002/art.40555](https://doi.org/10.1002/art.40555).

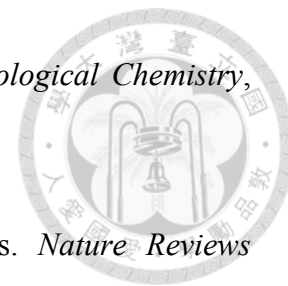
Kanyavuz A, Marey-Jarossay, Lacroix-Desmazes, Dimitrov JD (2019 February 4), Breaking the law: unconventional strategies for antibody diversification, *Nature Reviews of Immunology*. <https://doi.org/10.1038/s41577-019-0126-7>

Katrin F. Chua, Frederick W. Alt, and John P. Manis. (2002), The function of AID in somatic mutation and class switch recombination: upstream or downstream of DNA breaks. *The Journal of Experimental Medicine*, 195 (9): F37-41

Kono H, *et al.*(2005), Fc γ RIIB Ile232Thr transmembrane polymorphism associated with human systemic lupus erythematosus decreases affinity to lipid rafts and attenuates inhibitory effects on B cell receptor signaling. **Human Molecular Genetics**, 14(19): 2881-2892.

Kramer DT, *et al.* (2007), Role of AMP kinase and PPAR in the regulation of lipid and

glucose metabolism in human skeletal muscle. *The Journal of Biological Chemistry*, 282 (27): 19313–19320



Kurosaki T, Kometani K and Ise W (2015), Memory B cells. *Nature Reviews Immunology*, 15:149–159

Li X and Kimberly RP (2014), Targeting the Fc receptor in autoimmune disease.. *Expert Opinion on Therapeutic Targets*, 18:335-350

Li Z, Woo CJ, Maria D. Iglesias-Ussel MD, Ronai D, and Scharff MD. (2004) The generation of antibody diversity through somatic hypermutation and class switch recombination. *Genes and Development*, 18: 1-11

Luo Q, *et al.* (2012), The effect of PPAR δ agonists (HS00098) on serum lipid profiles in diet-induced obese rhesus monkeys. *Journal of Biomedical Science and Engineering*, 5: 439-447

Moldta B and Hessellb AJ (2014), Fc γ Rs across species linking adaptive and innate immunity. *Antibody Fc, Academic Press*: 145-157

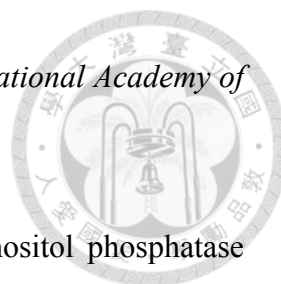
Mothe-Satney I, *et al.* (2016), A role for peroxisome proliferator-activated receptor beta in T cell development. *Scientific Reports*, 6:34317

Murphy K, Travers P, Walport M (2008), The humoral immune response. *Janeway's Immunobiology (7th Ed.)*, Garland Science, 9: 379-420

Newsholme SJ, *et al.* (2009), Mouse carcinogenicity study with GW501516, a PPAR delta agonist. *Toxicological science*, 108 (1)

Oda M, Sato-Nakamura N, Azuma T (2004), Molecular characterization of monovalent and multivalent hapten–protein conjugates for analysis of the antigen–antibody interaction. *Analytical Biochemistry*, 333: 365–371

Oliver WR Jr, *et al.* (2001), A selective peroxisome proliferator-activated receptor δ



agonist promotes reverse cholesterol transport. *Proceedings of the National Academy of Sciences of the USA*, 98(9): 5306–5311

Ono M, Bolland S, Tempst P, Ravetch JV (1996), Role of the inositol phosphatase SHIP in negative regulation of the immune system by the receptor Fc γ RIIB. *Nature*, 383(6597): 263-266.

Papavasiliou FN, Schatz DG (2002), Somatic hypermutation of review immunoglobulin genes: merging mechanisms for genetic diversity. *Cell*, Vol.109, S35–S44

Paul W. Manley, *et al.* (2010), Extended kinase profile and properties of the protein kinase inhibitor nilotinib, *Biochimica et Biophysica Acta*, 1804: 445–453

Pokrywka A, *et al.* (2014), Metabolic modulators of the exercise response: doping control analysis of an agonist of the peroxisome proliferator-activated receptor δ (GW501516) and 5-aminoimidazole-4-carboxamide ribonucleotide (AICAR). *Journal of physiology and pharmacology*, 65(4): 469-76

Poulsen LI, Siersbæk M and Mandrup S (2012), PPARs: Fatty acid sensors controlling metabolism. *Seminars in Cell & Developmental Biology*, 23(6): 631-639

Product information (2007), TASIGNA® (nilotinib) capsules, for oral use

Quinn CE, Hamilton PK, Lockhart CJ and McVeigh GE (2008), Thiazolidinediones: effects on insulin resistance and the cardiovascular system. *British Journal of Pharmacology*, 153(4): 636–645

Roghani A, Cragg MS, Frendeus B. (2016 February 26). Resistance is futile: targeting the inhibitory Fc γ RIIB (CD32B) to maximize immunotherapy. *Oncoimmunology*, 5 (2). [https://doi: 10.1080/2162402X.2015.1069939](https://doi.org/10.1080/2162402X.2015.1069939)

Schroeder HW and Cavacini L (2010), Structure and function of immunoglobulins. *Journal of Allergy and Clinical Immunology*, 125(202): S41–S52.



Shulman Z, *et al.* (2013), T follicular helper cell dynamics in germinal centers. *Science*, 341(6146): 673–677

Stavnezer J, Guikema JEJ, and Schrader CE. (2008) , Mechanism and regulation of class switch recombination. *Annual Review of Immunology*, 26: 261–292.

Stewart R, Hammond SA, Oberst M and Wilkinson RW. (2014) , The role of Fc gamma receptors in the activity of immunomodulatory antibodies for cancer. *Journal for Immunotherapy of Cancer* 2:29

Sun L, *et al.*, PPAR-delta modulates membrane cholesterol and cytokine-signaling in malignant B cells. *Leukemia*, Leukemia Research Fund, U.K 32(1)

Sznaidman ML, *et al.* (2003), Novel selective small molecule agonists for peroxisome proliferator-activated receptor delta (PPAR-delta)--synthesis and biological activity. *Bioorganic and Medicinal Chemistry Letters*, 13(9): 1517-1521.

Takemori T, Tarlinton D, Hiepe F, Andreas R (2015), Chapter 14 - B cell memory and plasma cell development. *Molecular Biology of B cells (2nd Ed.)*, Academic Press: 227-249

Tzeng SJ, Bolland S, Inabe K, Kurosaki T, Pierce SK (2005), The B cell inhibitory Fc receptor triggers apoptosis by a novel c-Abl family kinase-dependent pathway. *The Journal of Biological Chemistry*, 280: 35247-35254.

Victora GD and Nussenzweig MC (2012), Germinal centers. *Annual Review of Immunology*, 30:429–457

Wataru I and Tomohiro K (2018) Plasma cell differentiation during the germinal center reaction, *Immunological Reviews*, 288:64–74

World Health Organization (24-30 April 2017), *World Immunization Week*

Wu CC, *et al.* (2017), Structural basis for specific ligation of the peroxisome proliferator-activated receptor δ . *Proceedings of the National Academy of Sciences of the USA*, 114 (13):E2563-E2570

Yang H, Jiang H, Song Y, Chen DJ, Shen XJ, Chen JH (2018), Neutrophil CD16b crosslinking induces lipid raft-mediated activation of SHP-2 and affects cytokine expression and retarded neutrophil apoptosis. *Experimental Cell Research*, 362: 121–131

Zhang X and Young HA (2002), PPAR and immune system—what do we know? *International Immunopharmacology*, 2(8): 1029–1044

Zhang Y, Garcia-Ibanez L and Toellner KM (2016), Regulation of germinal center B - cell differentiation. *Immunological Reviews*, 270 (1): 8-19



Appendix

Publication List



1. Jhou JP, Yu IS, **Hwai H**, Chen CS, Chen PL, Tzeng SJ*. The lupus-associated Fcγ receptor IIb-I232T polymorphism results in impairment in the negative selection of low-affinity germinal center B cells via c-Abl in mice. *Arthritis and Rheumatology*. 2018 Nov;70(11):1866-1878. doi: 10.1002/art.40555.
2. **Hwai W**, Chen YY, Tzeng SJ*. B-cell ELISpot assay to quantify antigen-specific antibody-secreting cells in human peripheral mononuclear cells. In the 3rd edition of Handbook of ELISPOT in Springer/Humana Press book series “*Methods in Molecular Biology*” 2018;1808:133–141. doi: 10.1007/978-1-4939-8567-8_11.
3. Tseng TC, Huang DY, Lai LC, **Hwai H**, Hsiao YW, Jhou JP, Chuang EY, Tzeng SJ*. Dual immuno-renal targeting of 7-benzylidenenaltrexone alleviates lupus nephritis via FcγRIIB and HO-1. *Journal of Molecular Medicine (Berlin)* 2018 May;96(5):413-425. doi: 10.1007/s00109-018-1626-



Publications



The Lupus-Associated Fcγ Receptor IIb–I232T Polymorphism Results in Impairment in the Negative Selection of Low-Affinity Germinal Center B Cells Via c-Abl in Mice

Jyun-Pei Jhou, I-Shing Yu, Haw Hwai, Chih-Shan Chen,
Pei-Lung Chen, and Shiang-Jong Tzeng

Objective. Fcγ receptor IIb (FcγRIIb) is an essential negative regulator of B cells that blocks B cell receptor (BCR) signaling and triggers c-Abl–dependent apoptosis of B cells. FcγRIIb-deficient mice display splenomegaly with expansion of B cells, leading to lupus. FcγRIIb-I232T is a hypofunctional polymorphism associated with lupus susceptibility in humans, an autoimmune disease linked to diminished deletion of autoreactive B cells. In the context of the FcγRIIb-I232T polymorphism, we investigated the role of FcγRIIb in the deletion of low-affinity germinal center (GC) B cells, an important mechanism for preventing autoimmunity.

Methods. We generated FcγRIIb^{232T/T} mice to mimic human FcγRIIb-I232T carriers and immunized mice with chicken gamma globulin (CGG)–conjugated NP, a T cell–dependent antigen, to examine the response of GC B cells.

Results. Compared to wild-type (WT) mice, FcγRIIb^{232T/T} mice showed increased numbers of low-affinity NP-specific IgG and NP-specific B cells and plasma cells; additionally, the expression of a somatic mutation (W33L) in their V_H186.2 genes encoding high-affinity BCR was reduced. Notably, FcγRIIb^{232T/T} mice had a higher number of GC light zone B cells and showed less apoptosis than WT mice, despite having equivalent follicular helper T cell numbers and function. Moreover, phosphorylation of c-Abl was reduced in FcγRIIb^{232T/T} mice, and treatment of WT mice with the c-Abl inhibitor nilotinib during the peak of GC response resulted in reduced affinity maturation reminiscent of FcγRIIb^{232T/T} mice.

Conclusion. Our findings provide evidence of a critical role of FcγRIIb/c-Abl in the negative selection of GC B cells in FcγRIIb^{232T/T} mice. Importantly, our findings indicate potential benefits of up-regulating FcγRIIb expression in B cells for treatment of systemic lupus erythematosus.

Fcγ receptor IIb (FcγRIIb) is a low-affinity Fcγ receptor for IgG. The Fc portion of IgG binds to the second Ig domain located near the transmembrane region of FcγRIIb proteins (1,2). In B cells, FcγRIIb is an indispensable inhibitory regulator. FcγRIIb-deficient mice exhibit splenomegaly due to expansion of B cells and eventually develop lupus-like disease (3,4). Depending on the affinity of antigens to the B cell receptor (BCR), FcγRIIb can transduce 2 distinct inhibitory signals upon stimulation of IgG immune complexes (ICs) to block B cell function (5). When FcγRIIb is co-ligated to the BCR, FcγRIIb blocks BCR signaling for proliferation and differentiation, and when independently engaged, FcγRIIb triggers B cell apoptosis by a c-Abl–dependent mechanism (1,2,5). When the BCR and FcγRIIb are co-engaged, the cytoplasmic immunoreceptor tyrosine-based inhibition motif of FcγRIIb is phosphorylated by the Lyn kinase, followed by recruitment of the lipid phosphatase SH2 domain–containing inositol-5′-phosphatase (SHIP), which hydrolyzes PI(3–5)P₃ to antagonize phosphatidylinositol 3-kinase signals for activation and proliferation of B cells (6–8). On the other hand, when the antigen in IgG ICs has low or no affinity for BCRs, FcγRIIb can directly trigger apoptosis of B cells via c-Abl kinase (5). The FcγRIIb-dependent apoptosis of B cells has been proposed to play a role in the elimination of autoreactive B cells, which emerge as low-affinity B cells in the germinal center (GC) (9), but evidence from in vivo studies is largely lacking.

The human FcγRIIb-I232T polymorphic variant, in which the isoleucine at position 232 of FcγRIIb is

Supported by the Ministry of Science and Technology of the Executive Yuan of Taiwan (grant NSC99-2320-B-002-011).

Jyun-Pei Jhou, MS, I-Shing Yu, PhD, Haw Hwai, MD, Chih-Shan Chen, MS, Pei-Lung Chen, MD, PhD, Shiang-Jong Tzeng, MD, PhD: National Taiwan University, Taipei, Taiwan.

Address correspondence to Shiang-Jong Tzeng, MD, PhD, Graduate Institute of Pharmacology, National Taiwan University, Taipei 10051, Taiwan. E-mail: sjtzeng@ntu.edu.tw.

Submitted for publication August 14, 2017; accepted in revised form May 8, 2018.

replaced by threonine, is a risk allele for systemic lupus erythematosus (SLE). The prevalence of Fc γ RIIb-I232T carriers has been reported to be up to 40% of SLE patients in Africans and Southeast Asians (10–12). Biochemical and imaging analyses have revealed a decreased association of Fc γ RIIb-232T proteins with lipid microdomains on the plasma membranes, resulting in blocking the association with BCR that results in inhibitory signaling (13–15). Nevertheless, people carrying the Fc γ RIIb-232T allele are protected against malaria infection owing to enhanced antibody response (12,16,17). Conversely, these subjects are susceptible to autoimmune diseases, e.g., SLE (12). Consistent with these findings, the surface expression of wild-type (WT) Fc γ RIIb in memory B cells and plasma cells (PCs) is down-regulated in patients with SLE (18–20). Furthermore, a failure to up-regulate Fc γ RIIb expression on GC B cells has been found in lupus-prone mice regardless of their genetic background (21). These findings strongly suggest a role of Fc γ RIIb in the GC response and raise the question of whether the hypofunctional Fc γ RIIb-232T allele might result in abnormality in the clonal selection of B cells in GCs, particularly in the deletion of low-affinity autoreactive B cells.

The GC is a critical site for antigen-driven selection of GC B cells for differentiation into PCs to generate high-affinity antibodies for protective immunity. In response to antigen, GC B cells first undergo V(D)J gene hypermutation of their BCRs in the dark zone, followed by migration of GC B cells to the adjacent light zone for selection of cells with high affinity to antigen, a critical process known as affinity maturation (22–24). Importantly, while high-affinity GC B cells are positively selected for further development into memory B cells and PCs, GC B cells carrying mutated BCRs of low or no antigenic affinity are negatively selected for apoptosis (25,26). To investigate the pathogenesis of human lupus associated with the Fc γ RIIb-I232T polymorphism, we generated Fc γ RIIb^{232T/T} mice to mimic human Fc γ RIIb-I232T carriers. Given that IgG ICs are readily formed after secondary immunization (27,28), the surface expression level of Fc γ RIIb in GC B cells is up-regulated (21), and Fc γ RIIb activation can trigger apoptosis of B cells via c-Abl (5), we reasoned that the Fc γ RIIb-232T allele with reduced inhibitory function might result in abnormal negative selection of GC B cells. Whether the dysfunction of the Fc γ RIIb-I232T polymorphism is linked to a GC defect is virtually unexplored. In addition, the consequences of abnormal GC reaction in the pathogenesis of autoimmune diseases are incompletely understood. Importantly, new insights into the causal relationship between the Fc γ RIIb-I232T polymorphism and the pathogenesis of SLE may provide valuable implications

for therapeutic exploitation of Fc γ RIIb for patients with SLE and perhaps other autoimmune diseases.

MATERIALS AND METHODS

Reagents. Chicken gamma globulin-conjugated NP₂₀ (NP₂₀-CGG), bovine serum albumin (BSA)-conjugated NP₇, BSA-conjugated NP₃₀, and phycoerythrin (PE)-conjugated NP were purchased from LGC Biosearch Technologies. Imject Alum adjuvant was acquired from Thermo Scientific. F(ab')₂ goat anti-mouse IgG and IgM antibodies were purchased from Jackson ImmunoResearch. Mouse IgG isotypes and monoclonal antibodies (mAb) specific for CD16/32 (clone 2.4G2), PE-Cy7-conjugated CD19 (clone 1D3), BV421-conjugated CD138 (clone 281-2), PerCP-Cy5.5-conjugated CD11b (clone M1/70), Alexa Fluor 700-conjugated CD11c (clone HL3), and fluorescein isothiocyanate (FITC)-conjugated inducible costimulator (ICOS) (clone 7E.17G9) were purchased from BioLegend. Allophycocyanin (APC)-Cy7-conjugated B220 (clone RA3-6B2), BV605-conjugated CD86 (clone GL1), Alexa Fluor 647-conjugated GL-7 (clone GL-7), BV421-conjugated CXCR4 (clone 2B11), PE-Cy7-conjugated CD95 (clone Jo2), Alexa Fluor 647-conjugated CD4 (clone RM4-5), BV421-conjugated programmed death 1 (PD-1; clone J43), PE-conjugated CXCR5 (clone 2G8), and 7-aminoactinomycin D (7-AAD) were acquired from BD Biosciences. Ninety-six-well MultiScreen-HTS filter plates were acquired from Merck Millipore. Blood lancets were obtained from MEDipoint. Mouse reference serum was acquired from Bethyl Laboratories. Vectastain ABC kits containing biotinylated goat anti-rabbit IgG and rabbit anti-goat IgG mAb were purchased from Vector. Horseradish peroxidase (HRP)-conjugated isotype IgG and polyclonal antibodies specific to phospho-c-Abl (Y245) were obtained from Santa Cruz Biotechnology. The active caspase 3 mAb was purchased from Cell Signaling Technology. Nilotinib and DMSO were obtained from Selleckchem.

Fc γ RIIb^{232T/T} mice and immunization protocols. Fc γ RIIb^{232T/T} mice on a C57BL/6J background were generated at the gene knockout mouse core facility at the Center of Genomic Medicine of National Taiwan University (NTU). The ATT codon of isoleucine 231 in exon 5 of the *Fcgr2b* gene was mutated to ACT to encode threonine using a recombinering approach. A *neo* gene cassette flanked with *loxP* sequences was inserted into the intron 5 region. The targeting vector was then linearized for electroporation into JM8A3 embryonic stem cells (ESCs). Correctly targeted ESC clones were subsequently injected into C57BL/6 blastocysts to produce chimeras. Chimeric males were bred with C57BL/6 females to produce Fc γ RIIb^{232T/T} mice. To remove the *neo* cassette, Fc γ RIIb^{232T/T} mice were crossed with Sox2-Cre mice (Tg(Sox2-cre)1Amc/J), which were kindly provided by Dr. Ming-Ji Fann (National Yang-Ming University, Taipei, Taiwan). Male and female Fc γ RIIb^{232T/T} mice were bred to generate offspring carrying Fc γ RIIb^{232T/T} (WT), Fc γ RIIb^{232T/T} (heterozygote), or Fc γ RIIb^{232T/T} (homozygote) genotypes for experiments. All mice were maintained in specific pathogen-free conditions at the Center for Laboratory Animals in the College of Medicine of NTU. The protocols of animal use were reviewed, and the experiments were performed according to the guidelines approved by the Institutional Animal Care and Use Committee of the College of Medicine of NTU. Female mice (7–8 weeks old) were immunized with 50 μ g NP₂₀-CGG per mouse by

intraperitoneal injection. Nilotinib (2 mg/kg/day) was administered intraperitoneally once a day on days 7–9 after secondary immunization. Mice were killed the day after the last injection.

Flow cytometric analysis. Mouse splenocytes were stained with FITC-conjugated CD16/32 mAb for 10 minutes at 4°C, followed by addition of an antibody cocktail containing PE-Cy7-conjugated CD19, BV421-conjugated CD138, PerCP-Cy5.5-conjugated CD11b, Alexa Fluor 700-conjugated CD11c, Alexa Fluor 647-conjugated GL-7, and PE-conjugated NP for 20 minutes on ice. To distinguish GC light zone from dark zone B cells, mouse splenocytes were stained with FITC-conjugated CD16/32, APC-Cy7-conjugated B220, BV605-conjugated CD86, Alexa Fluor 647-conjugated GL-7, BV421-conjugated CXCR4, PE-Cy7-conjugated CD95, and PE-conjugated NP. Splenic follicular helper T (T_{fh}) cells were stained with the following mAb: APC-Cy7-conjugated B220, Alexa Fluor 647-conjugated CD4, BV421-conjugated PD-1, PE-conjugated CXCR5, FITC-conjugated ICOS, and BV605-conjugated CD69. Bone marrow cells were stained with FITC-conjugated CD16/CD32, BV421-conjugated CD138, PE-Cy7-conjugated CD19, PerCP-Cy5.5-conjugated CD11b, Alexa Fluor 700-conjugated CD11c, and PE-conjugated NP. Dead splenocytes and bone marrow cells were stained with 7-AAD for 5 minutes before being washed. Cells were processed for analysis using a multicolor LSRFortessa cytometer (BD Biosciences). Data were analyzed using FlowJo version 10.

Confocal microscopy. Splenic B cells from 8-week-old WT and FcγRIIb^{232T/T} mice were isolated (>98% purity) using a mouse B lymphocyte enrichment kit (catalog no. 557792; BD Biosciences) according to the manufacturer's instructions. Purified cells (2 × 10⁶/ml) were incubated with rabbit anti-mouse IgM (25 μg/ml) for 10 minutes on ice followed by Cy3-labeled goat anti-rabbit IgG (50 μg/ml) and FITC-labeled cholera toxin B (10 μg/ml), which binds the lipid raft resident protein ganglioside G_{M1}, for an additional 10 minutes. Cells were then placed on a shaker (200 revolutions per minute) and incubated at 25°C for the indicated times. After a brief wash, cells were immediately fixed with 4% paraformaldehyde for 10 minutes at room temperature before mounting on slides. Images were acquired, analyzed, and quantified using a Zeiss LSM 880 confocal microscope.

Enzyme-linked immunosorbent assay (ELISA). BSA-conjugated NP₇ or BSA-conjugated NP₃₀ (5 μg/ml) was added to 96-well high bind plates (100 μl/well; Corning) and incubated at 4°C overnight. Mouse serum samples were diluted to detect IgG (1:200,000) and IgM (1:15,000). After blocking and incubation at 4°C overnight, plates were washed, followed by addition of HRP-conjugated rabbit anti-mouse IgG (Fcγ-specific) (catalog no. 115-035-071; Jackson ImmunoResearch) or goat anti-mouse IgM (μ-specific) (catalog no. 115-035-075; Jackson ImmunoResearch) for a 1-hour incubation at room temperature. After washes, plates were developed with tetramethylbenzidine substrate and the reaction was quenched with 2N H₂SO₄. Plates were read at an optical density of 450 nm (OD_{450 nm}) and OD_{570 nm} using an ELISA plate reader (BioTek). The reading values of HRP activities were calculated using OD_{450 nm} minus OD_{570 nm}. Standard curves of IgM and IgG concentrations were generated using serially diluted samples of mouse reference serum.

Enzyme-linked immunospot (ELISpot) assay. ELISpot assay was performed as previously described (29,30), except that BSA-conjugated NP₇ and BSA-conjugated NP₃₀ were used as the immobilized antigens to capture NP-specific PCs. Briefly, HRP-conjugated goat anti-mouse IgG and IgM were

used for detection of PCs. Approximately 2 × 10⁴ cells/well and 1.6 × 10⁵ cells/well with 2-fold serial dilutions for the detection of IgG and IgM PCs, respectively, were incubated overnight at 37°C. Spots in wells were developed by addition of 50 μl per well of 3-amino-9-ethylcarbazole substrates and incubation for 30 minutes. After washes and complete air dry, plates were scanned to enumerate spots using a CTL S6 universal analyzer (Cellular Technology).

Immunohistochemical examination. Immunohistochemical analysis of mouse spleen sections was performed using standard procedures with Vectastain ABC kits. Deparaffinized sections (4 μm thick) were stained overnight at 4°C with antibodies specific to active caspase 3 or phospho-c-Abl according to the manufacturer's instructions. After washes with phosphate buffered saline (PBS)-Tween (PBS buffer with 0.1% [volume/volume] Tween 20), sections were incubated with a species-specific antibody conjugated with HRP for 1 hour at ambient temperature. Slides were washed thoroughly, followed by addition of 3,3'-diaminobenzidine substrates for development. Sections were counterstained with hematoxylin before mounting. Slides were photographed using an Axioplan 2 light microscope (Zeiss).

Sequence analysis of the V_H186.2 region of BCRs from NP+ GC B cells. Genomic DNA of sorted GC B cells (NP+B220+GL-7+IgG+; ~1,000 cells per mouse) was extracted using a QIAamp DNA micro kit (Qiagen). For the amplification of V_H186.2-J_H2 segments, 1 ng of genomic DNA was used as template, and polymerase chain reaction (PCR) products were generated from high-fidelity PrimeStar DNA polymerase (Takara Bio). The PCR primers have been described previously (31): forward primer, 5'-AGCTGTATCATGCTCTTCTTGGCA-3' and reverse primer, 5'-AGATGGAGGCCAGT-GAGGGAC-3' (31). Illumina libraries were generated from PCR products using a TruSeq library preparation kit and were sequenced using Illumina MiSeq to generate paired-end reads of 300 nucleotides. Raw sequencing data were aligned to mouse germline V_H186.2 sequences using Burrows-Wheeler aligner and SAMtools (32,33). The W33L mutation percentages in first complementarity-determining region sequences were compared with those in WT mice.

Statistical analysis. Bar graphs were plotted and analyzed using GraphPad Prism software version 6.0. Student's unpaired 2-tailed *t*-test was used for statistical analysis. The *t*-test was modified by Welch's correction in case of unequal variance. Tukey's test with one-way analysis of variance was used to compare multiple groups. Results are presented as the mean ± SEM. *P* values less than 0.05 were considered significant.

RESULTS

FcγRIIb^{232T/T} mice exhibit enhanced antibody production with reduced affinity maturation. Because the isoleucine 232 residue of human FcγRIIb is conserved in mice (NCBI accession nos. NP_001070657.1 and NP_003992.3), we generated a mouse line, termed the FcγRIIb^{232T/T} mouse line, which carries a point mutation of the isoleucine residue at position 231 (232 in humans) replaced by threonine (Figure 1A). Consistent with previous findings of live cell imaging (15), the surface FcγRIIb-232T proteins and lipid rafts were neither stably

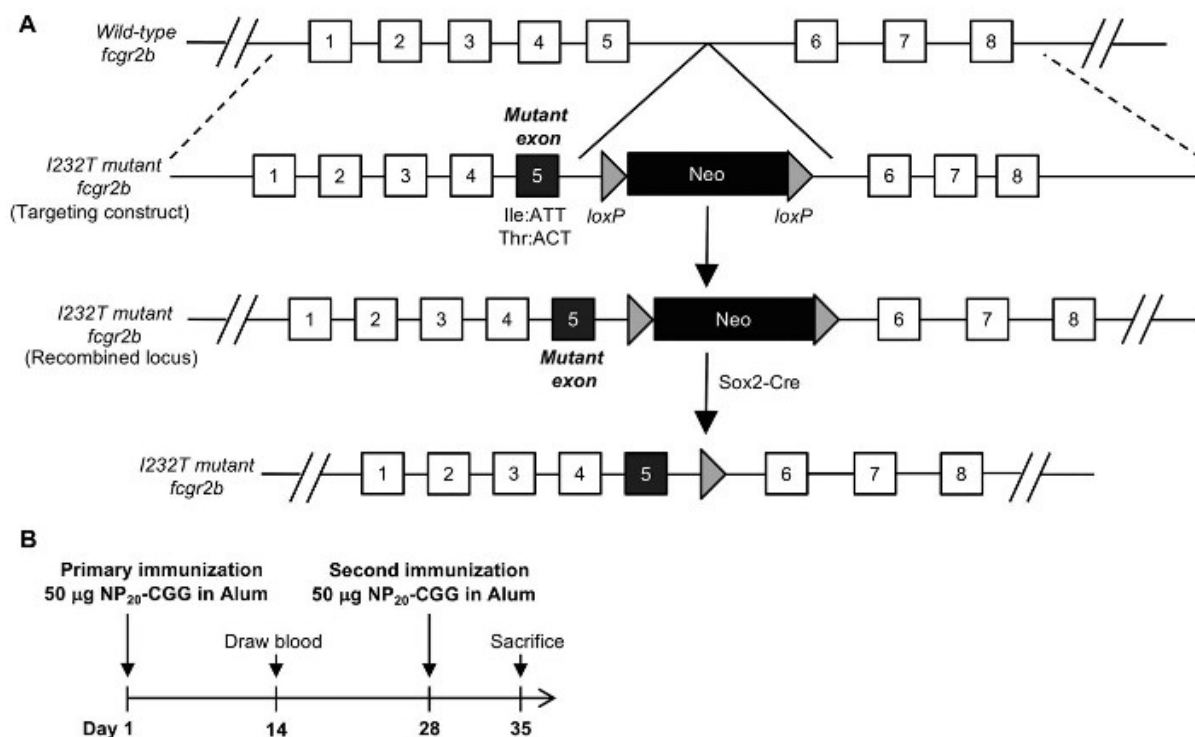


Figure 1. Generation of Fc γ receptor IIb (Fc γ RIIb)^{232T/T} mice and immunization schedule. **A**, Schematic diagram of the generation of Fc γ RIIb-1232T mutant mice. **B**, Schedule of immunization of mice with chicken gamma globulin-conjugated NP (NP₂₀-CGG). Wild-type and Fc γ RIIb^{232T/T} mice 7–8 weeks of age were each injected intraperitoneally with 50 μ g of NP₂₀-CGG proteins mixed with 50 μ l of alum. A second immunization was performed 4 weeks later.

associated nor co-clustered to form cap structures in splenic B cells (see Supplementary Figure 1, available on the *Arthritis & Rheumatology* web site at <http://onlinelibrary.wiley.com/doi/10.1002/art.40555/abstract>).

To investigate GC response, we immunized each WT and Fc γ RIIb^{232T/T} mouse by intraperitoneal injection with 50 μ g of NP₂₀-CGG mixed with an equal volume of alum. All mice received a booster injection with the same amount of NP₂₀-CGG on day 28 after primary immunization and were killed on day 35, when clonal selection was actively proceeding (24,25) (Figure 1B). Serum samples were collected on day 14 and day 35 and tested in ELISA plates coated with either IgG-specific antibodies to detect total serum IgG, NP₃₀ to detect NP-specific antibodies of all affinities, or NP₇ to detect high-affinity NP-specific antibodies (30,31). The serum levels of total IgG were significantly higher in Fc γ RIIb^{232T/T} mice than in WT mice following both primary immunization (day 14) ($P = 0.0035$) and secondary immunization (day 35) ($P = 0.032$) (Figure 2A).

Fourteen days after the primary immunization, Fc γ RIIb^{232T/T} mice produced similar levels of high-affinity NP-specific antibodies ($P = 0.5033$) but more than double the amount of low-affinity NP-specific antibodies compared to WT mice ($P < 0.05$) (Figure 2B). By day 35, seven days after secondary immunization, Fc γ RIIb^{232T/T} mice produced significantly more high-affinity and low-affinity NP-specific antibodies than WT mice ($P < 0.05$ for NP₇; $P < 0.01$ for NP₃₀) (Figure 2B). The ratio of high-affinity to total (low affinity plus high affinity) NP-specific IgG (NP₇-bound IgG: NP₃₀-bound IgG) was lower in the serum of Fc γ RIIb^{232T/T} mice than in that of WT mice, indicating reduced affinity maturation of antibodies ($P < 0.05$) (Figure 2B). Moreover, sequencing of the NP-specific V_H186.2 region of B cells expressing NP-specific BCRs showed a decreased percentage of W33L replacement, which gives rise to high-affinity BCR variants, in Fc γ RIIb^{232T/T} mice ($P < 0.001$) (Figure 2C). In addition, we found a trend toward a lower ratio of replacement to silent hypermutation in Fc γ RIIb^{232T/T} mice

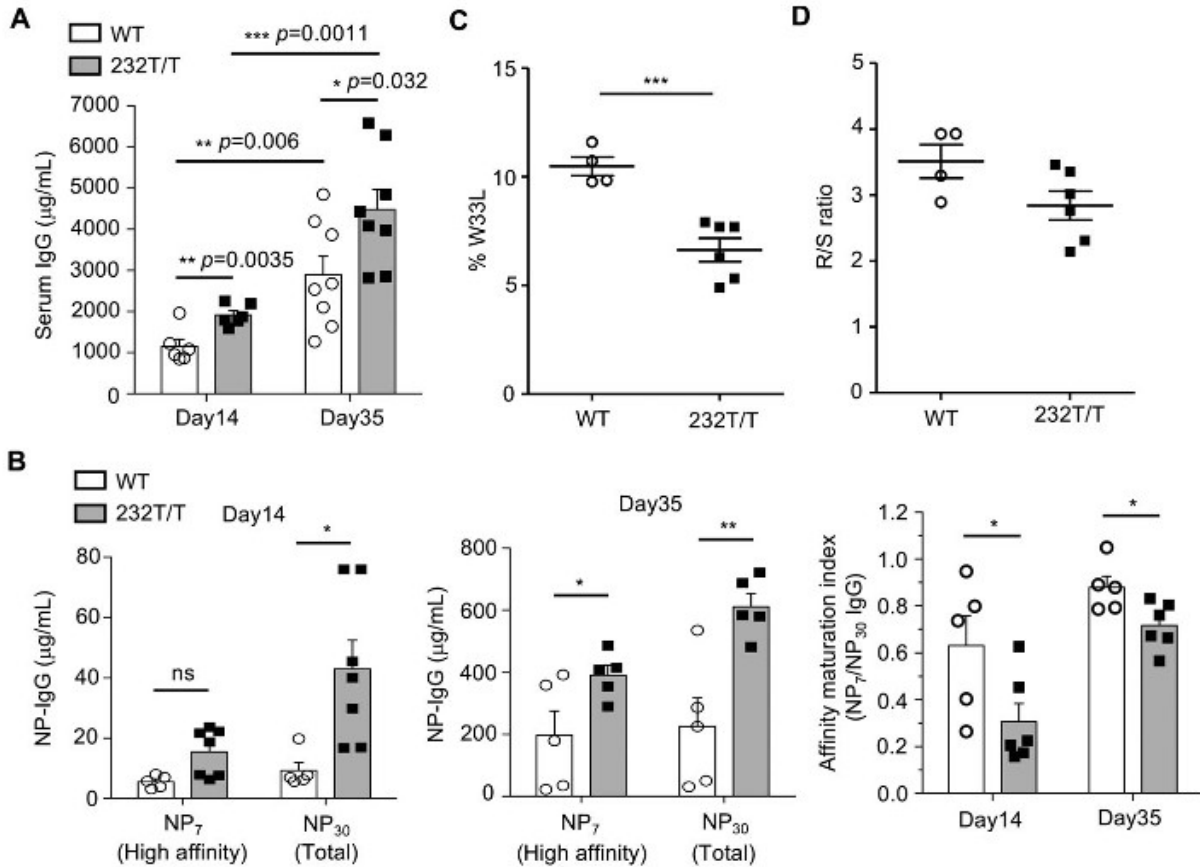


Figure 2. Enhanced NP-specific IgG production in immunized $\text{Fc}\gamma\text{RIIb}^{232\text{T}/\text{T}}$ mice. **A** and **B**, Serum levels of total IgG (**A**) and high-affinity NP₇ IgG and total NP₃₀ IgG (**B**) in wild-type (WT) mice and $\text{Fc}\gamma\text{RIIb}^{232\text{T}/\text{T}}$ mice 2 weeks after primary immunization (day 14) ($P = 0.0035$ for IgG, $P = 0.5033$ for NP₇, and $P = 0.0469$ for NP₃₀) and 1 week after secondary immunization (day 35) ($P = 0.032$ for IgG, $P = 0.0411$ for NP₇, and $P = 0.0068$ for NP₃₀). In **B**, the ratios of NP₇ to NP₃₀ IgG levels in serum on day 14 ($P = 0.0427$) and day 35 ($P = 0.0277$) after immunization are also shown. Symbols represent individual mice; bars show the mean \pm SEM ($n = 5\text{--}8$ mice per group). **C**, Frequency of W33L mutation in the V_H186.2 region of individual B cell receptor (BCR) genes of NP+ germinal center (GC) B cells in WT mice and $\text{Fc}\gamma\text{RIIb}^{232\text{T}/\text{T}}$ mice 7–8 days after primary immunization ($P = 0.0008$). **D**, Ratio of replacement mutations to silent mutations (R:S) in the V_H186.2 region in NP+ GC B cells in WT mice and $\text{Fc}\gamma\text{RIIb}^{232\text{T}/\text{T}}$ mice ($P = 0.0845$). In **C** and **D**, symbols represent individual mice; horizontal and vertical lines show the mean \pm SEM ($n = 4$ WT mice and 6 $\text{Fc}\gamma\text{RIIb}^{232\text{T}/\text{T}}$ mice). $*$ = $P < 0.05$; $**$ = $P < 0.01$; $***$ = $P < 0.001$. NS = not significant.

than in WT mice 8 days after primary immunization (Figure 2D). These results indicate a dysfunction in the affinity maturation of GC B cells in $\text{Fc}\gamma\text{RIIb}^{232\text{T}/\text{T}}$ mice.

Retention of low-affinity B cells in $\text{Fc}\gamma\text{RIIb}^{232\text{T}/\text{T}}$ mice after secondary immunization. Because affinity maturation was reduced in $\text{Fc}\gamma\text{RIIb}^{232\text{T}/\text{T}}$ mice compared to WT mice, we investigated whether the elimination of low-affinity antigen-specific B cells was abnormal in GCs. As shown in Figure 3A, the percentages of splenic CD19+ B cells in lymphocytes were comparable in WT and $\text{Fc}\gamma\text{RIIb}^{232\text{T}/\text{T}}$ mice. However, the percentage of NP+CD19+ B cells was substantially increased in

$\text{Fc}\gamma\text{RIIb}^{232\text{T}/\text{T}}$ mice compared to WT mice after secondary immunization. Similarly, the percentage of splenic CD19+CD138+ PCs in $\text{Fc}\gamma\text{RIIb}^{232\text{T}/\text{T}}$ mice was not different from that in WT mice, but the percentage of NP+CD19+CD138+ PCs was significantly increased in $\text{Fc}\gamma\text{RIIb}^{232\text{T}/\text{T}}$ mice ($P < 0.001$) (Figure 3B).

We next used ELISpot assays to quantify the numbers of splenic NP+ PCs. Consistent with an increased level of circulating NP₃₀+ IgG, a greater number of NP₃₀+IgG+ PCs was detected in $\text{Fc}\gamma\text{RIIb}^{232\text{T}/\text{T}}$ mice than in WT mice ($P < 0.05$) (Figure 3C). Further analysis of splenic NP+IgG+ PCs revealed no significant

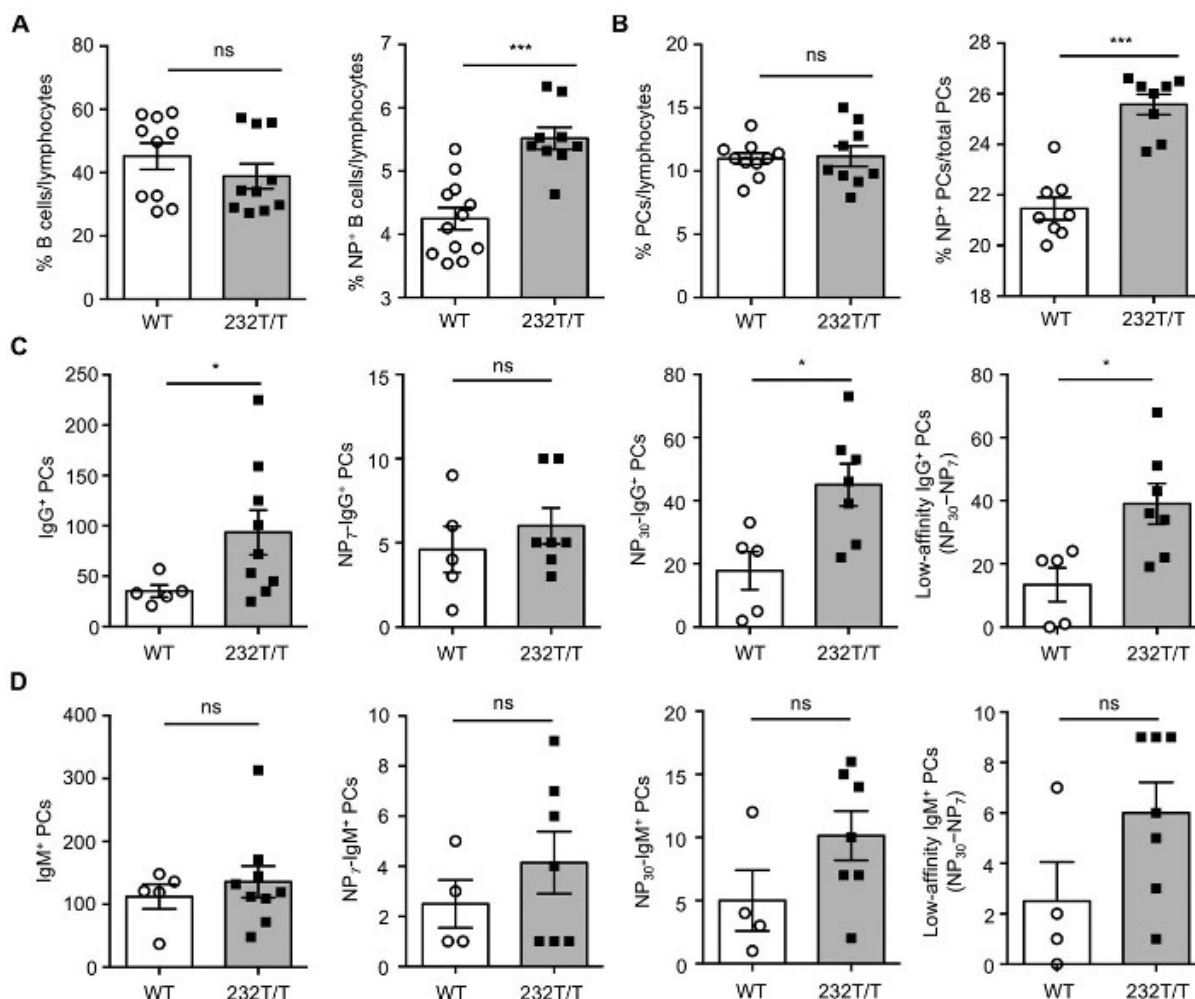


Figure 3. Increased frequency of low-affinity NP+IgG+ plasma cells (PCs) in the spleen in Fc γ receptor IIb (Fc γ RIIb)^{232T/T} mice after secondary immunization. **A and B.** Percentages of CD19+ B cells ($P = 0.2846$) and NP+CD19+ B cells ($P = 0.0007$) (**A**) and percentages of CD19+CD138+ PCs ($P = 0.8432$) and NP+CD19+CD138+ PCs ($P = 0.0009$) (**B**) in splenic lymphocytes from wild-type (WT) mice and Fc γ RIIb^{232T/T} mice on day 35, analyzed by flow cytometry. **C.** Splenic total IgG+ PCs ($P = 0.0315$), high-affinity NP₇-specific IgG+ PCs ($P = 0.4318$), total NP₃₀-specific IgG+ PCs ($P = 0.0168$), and low-affinity NP+IgG+ (NP₃₀ minus NP₇) PCs ($P = 0.0159$) in WT mice and Fc γ RIIb^{232T/T} mice on day 35, determined using enzyme-linked immunospot assays (using 6×10^3 cells to detect total PCs and 2.4×10^4 cells to detect NP+ PCs). **D.** Numbers of total IgM+ PCs ($P = 0.5412$), NP₇-specific IgM+ PCs ($P = 0.355$), NP₃₀-specific IgM+ PCs ($P = 0.116$), and low-affinity NP+IgM+ (NP₃₀ minus NP₇) PCs ($P = 0.0864$) in WT mice and Fc γ RIIb^{232T/T} mice. Symbols represent individual mice; bars show the mean \pm SEM ($n = 8$ – 12 WT mice and 8 – 10 Fc γ RIIb^{232T/T} mice in **A** and **B**; $n = 5$ WT mice and 7 – 9 Fc γ RIIb^{232T/T} mice in **C**; $n = 4$ – 5 WT mice and 7 – 9 Fc γ RIIb^{232T/T} mice in **D**). * = $P < 0.05$; *** = $P < 0.001$. NS = not significant.

differences in the numbers of high-affinity NP₇+ PCs between WT and Fc γ RIIb^{232T/T} mice. In contrast, compared to WT mice, the numbers of low-affinity IgG+ PCs (NP₃₀+ PCs minus NP₇+ PCs) increased ~ 3 -fold in Fc γ RIIb^{232T/T} mice ($P < 0.05$) (Figure 3C). These differences were not observed when the numbers of NP+IgM+ PCs were compared between WT and Fc γ RIIb^{232T/T} mice (Figure 3D), suggesting a specific IgG-associated effect

through Fc γ RIIb. Of interest, we found that the numbers of low-affinity NP+IgG+ PCs were also significantly increased in heterozygous Fc γ RIIb-232T mice compared to WT mice (see Supplementary Figure 2, available on the *Arthritis & Rheumatology* web site at <http://onlinelibrary.wiley.com/doi/10.1002/art.40555/abstract>). These findings suggest that Fc γ RIIb-232T might impede recruitment of sufficient amounts of WT receptors to reach the threshold

required for efficient induction for apoptosis. Consistent with this notion, we previously demonstrated that Fc γ RIIb-mediated apoptosis is dependent on the signal strength transduced from the receptor oligomers (5).

Tfh cell number and function in switching IgG isotypes are not altered in Fc γ RIIb^{232T/T} mice. Because the generation of PCs is influenced by Tfh (CD4+B220+PD-

1+ICOS+) cells, which provide help, e.g., interleukin-21, to GC B cells to further their differentiation into PCs and to class-switch Ig isotypes (32,33), we examined the numbers of splenic Tfh cells to determine their contributions to the increase in NP+IgG+ PCs in Fc γ RIIb^{232T/T} mice. As shown in Figure 4A, the numbers of Tfh cells were comparable between immunized WT and Fc γ RIIb^{232T/T}

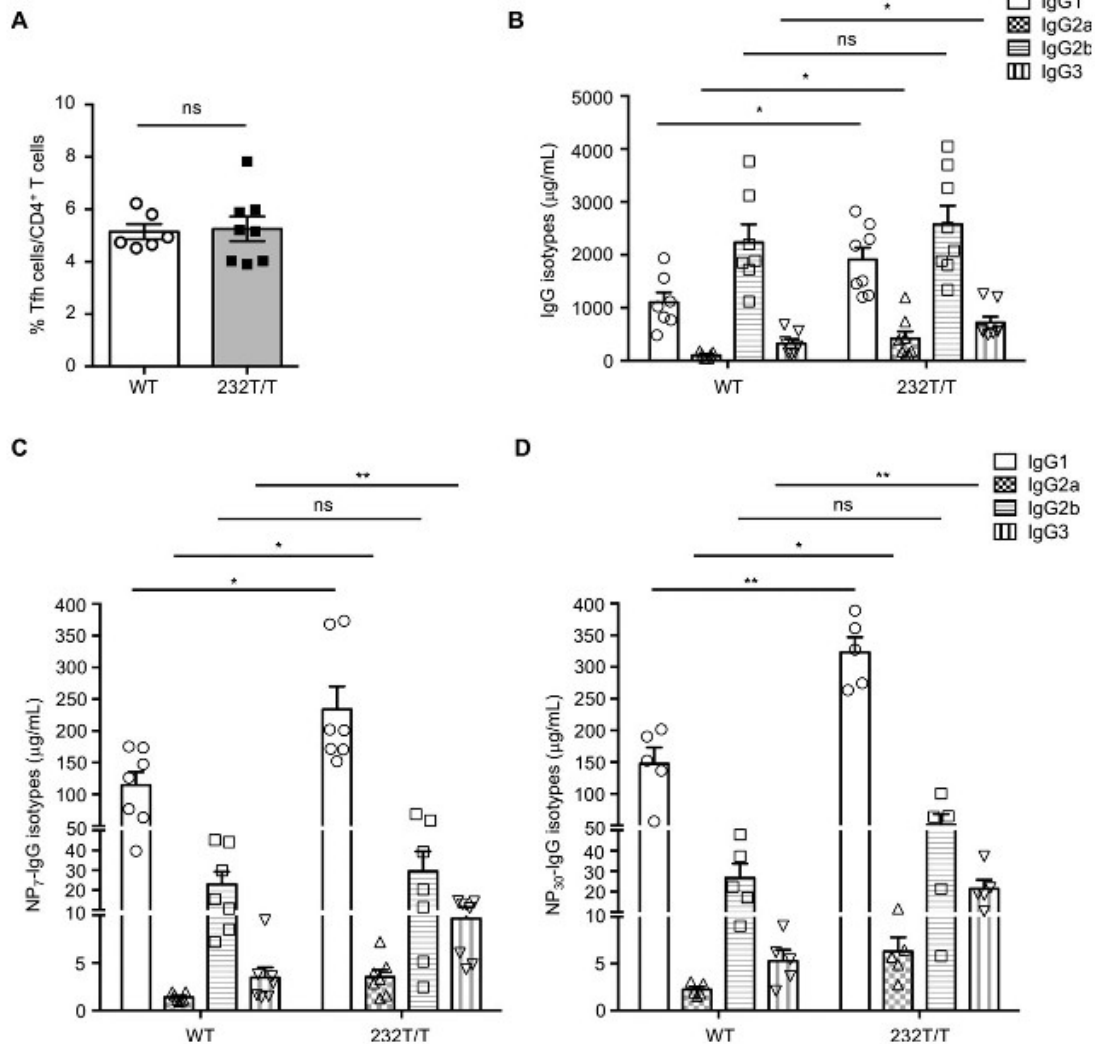


Figure 4. Splenic follicular helper T (Tfh) cell numbers and serum titers of class-switched NP+ IgG isotypes in wild-type (WT) and Fc γ receptor IIb (Fc γ RIIb)^{232T/T} mice. **A**, Percentages of Tfh cells (CD4+B220– programmed death 1–positive inducible costimulator–positive) in splenic T cells in WT mice and Fc γ RIIb^{232T/T} mice on day 35 ($P = 0.8622$). **B**, Serum concentrations of IgG1 ($P = 0.0098$), IgG2a ($P = 0.0076$), IgG2b ($P = 0.9813$), and IgG3 ($P = 0.045$) in immunized WT mice and Fc γ RIIb^{232T/T} mice. **C** and **D**, Serum levels of high-affinity NP₇-specific IgG isotypes (IgG1 [$P = 0.0137$], IgG2a [$P = 0.0178$], IgG2b [$P = 0.5956$], and IgG3 [$P = 0.0091$]) (**C**) and total NP₃₀-specific IgG isotypes (IgG1 [$P = 0.0011$], IgG2a [$P = 0.0283$], IgG2b [$P = 0.217$], and IgG3 [$P = 0.0079$]) (**D**) in WT and Fc γ RIIb^{232T/T} mice. Symbols represent individual mice; bars show the mean \pm SEM ($n = 6$ WT mice and 8 Fc γ RIIb^{232T/T} mice in **A**; $n = 7$ WT mice and 8 Fc γ RIIb^{232T/T} mice in **B**; $n = 5$ –7 mice per group in **C** and **D**). * = $P < 0.05$; ** = $P < 0.01$. NS = not significant.

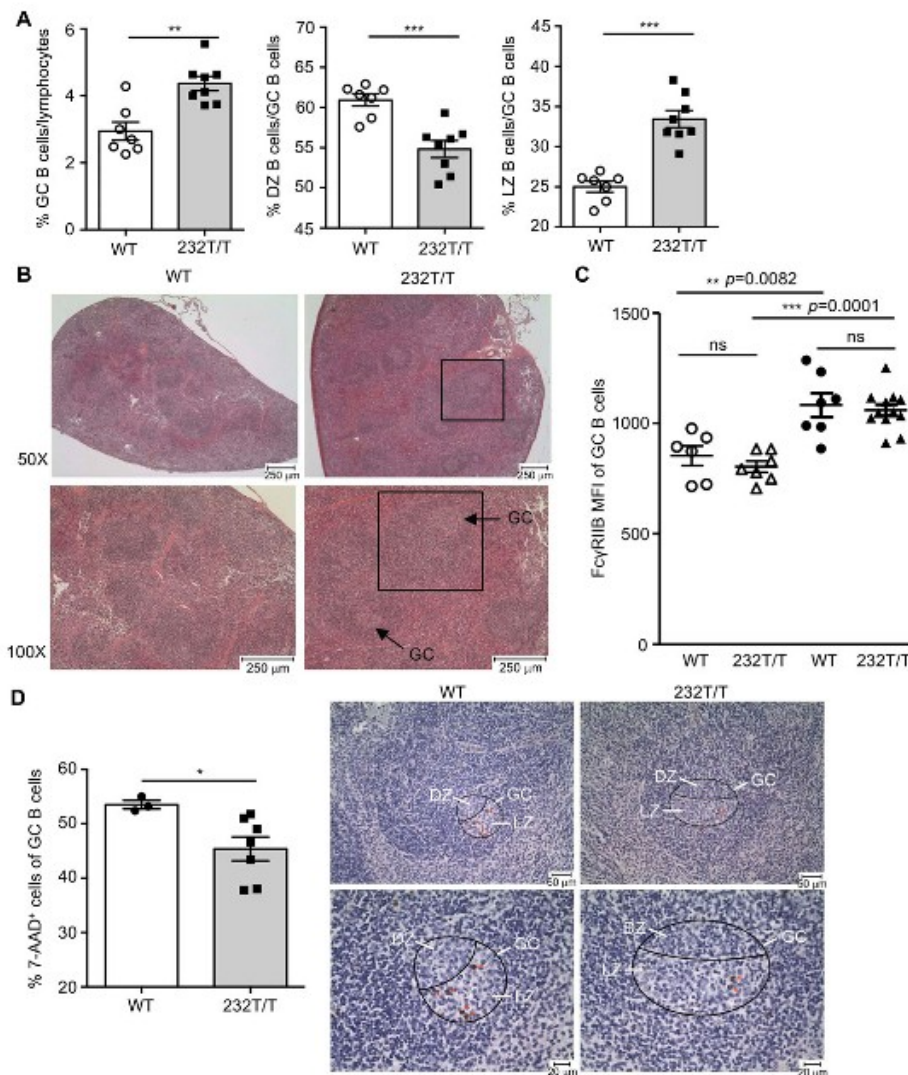


Figure 5. Increased numbers of light zone (LZ) germinal center (GC) B cells and reduced numbers of apoptotic GC B cells in Fc γ receptor IIb (Fc γ RIIb)^{232T/T} mice after secondary immunization. **A**, Percentages of splenic CD19+GL-7+ GC B cells ($P = 0.0011$), dark zone (DZ) NP+ GC B cells ($P = 0.0005$), and light zone NP+ GC B cells ($P = 0.0002$) in WT mice and Fc γ RIIb^{232T/T} mice. Symbols represent individual mice; bars show the mean \pm SEM ($n = 7$ WT mice and 8 Fc γ RIIb^{232T/T} mice). **B**, Representative splenic sections from WT and Fc γ RIIb^{232T/T} mice showing the size of GCs. Bottom panels are higher-magnification views of the top panels. The boxed areas show follicles. **C**, Surface expression levels of Fc γ RIIb on GC B cells in age-matched nonimmunized WT and Fc γ RIIb^{232T/T} mice (open symbols) ($P = 0.3613$) and immunized WT and Fc γ RIIb^{232T/T} mice on day 35 (solid symbols) ($P = 0.7026$). There was a significant difference in expression of Fc γ RIIb in nonimmunized WT mice versus immunized WT mice ($P = 0.0082$) and in nonimmunized Fc γ RIIb^{232T/T} mice versus immunized Fc γ RIIb^{232T/T} mice ($P = 0.0001$). Symbols represent individual mice; horizontal and vertical lines show the mean \pm SEM ($n = 6$ nonimmunized WT mice, 7 nonimmunized Fc γ RIIb^{232T/T} mice, 7 immunized WT mice, and 11 immunized Fc γ RIIb^{232T/T} mice). MFI = mean fluorescence intensity. **D**, Left, Percentages of 7-aminoactinomycin D (7-AAD)+GL-7+ GC B cells in WT mice and Fc γ RIIb^{232T/T} mice ($P = 0.0484$). Symbols represent individual mice; bars show the mean \pm SEM ($n = 3$ WT mice and 7 Fc γ RIIb^{232T/T} mice). Right, Staining for active caspase 3 to detect apoptotic GC B cells in the light zone of GCs (encircled areas) in splenic sections from WT and Fc γ RIIb^{232T/T} mice. * = $P < 0.05$; ** = $P < 0.01$; *** = $P < 0.001$. NS = not significant.

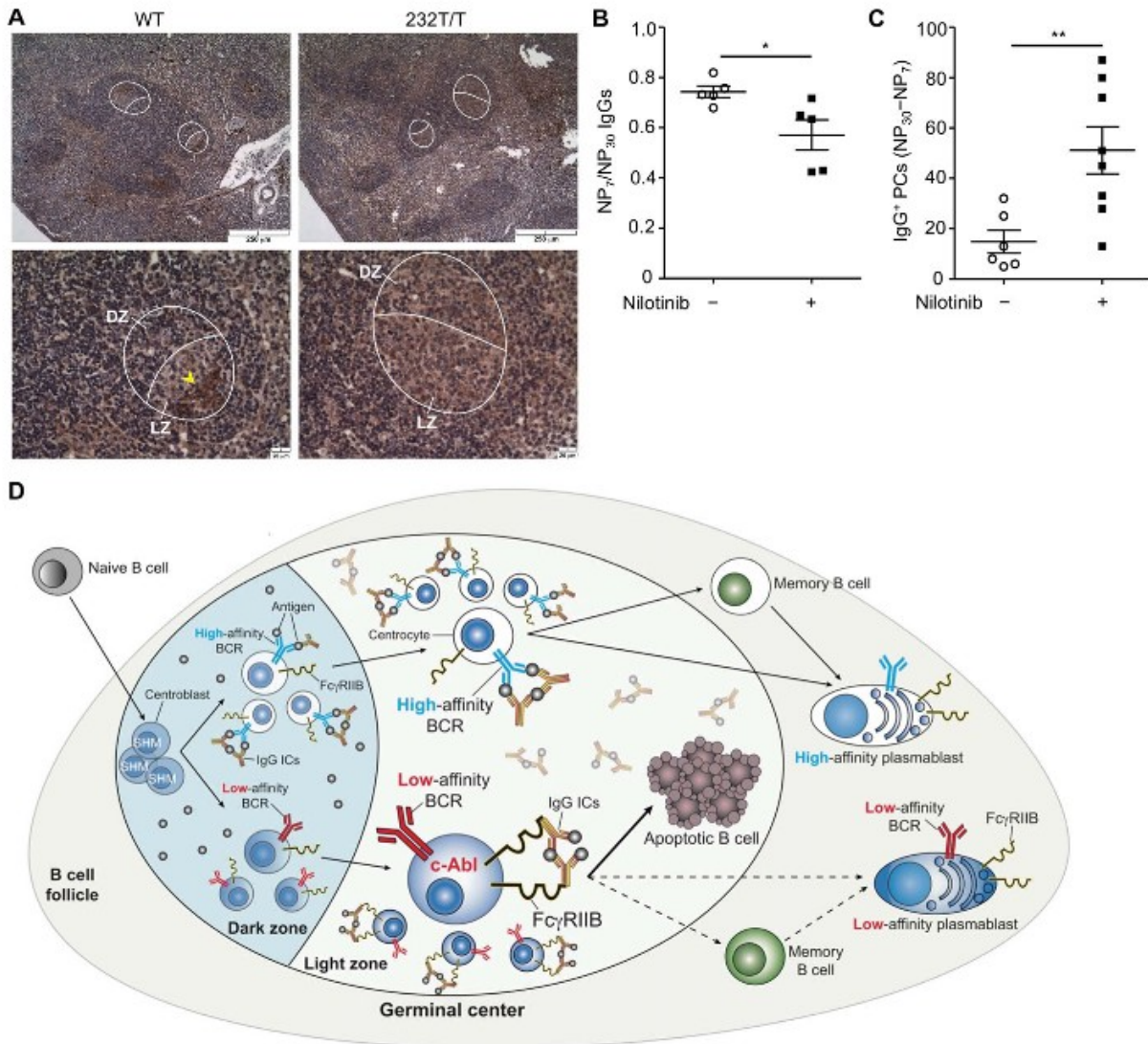


Figure 6. Association of reduced c-Abl activation with retention of low-affinity germinal center (GC) B cells in mice after secondary immunization. **A**, Reduced staining of phospho-c-Abl (Y245)+ GC B cells (arrowhead) in Fcγ receptor IIIb (FcγRIIb)^{232T/T} mice compared to wild-type (WT) mice. Female WT mice (7–8 weeks old) were immunized as described in Figure 1B. Mice were treated with either vehicle or nilotinib (2 mg/kg/day) on days 7–9 after the second immunization. Encircled areas show GCs. Bottom panels show higher-magnification views of the top panels. **B** and **C**, Ratio of NP₇ to NP₃₀ serum IgG ($P = 0.0283$) (**B**) and number of low-affinity NP+IgG+ (NP₃₀ minus NP₇) plasma cells in splenocytes (2.4×10^4) ($P = 0.0087$) in vehicle-treated WT mice and nilotinib-treated WT mice. Symbols represent individual mice; horizontal and vertical lines show the mean \pm SEM ($n = 5$ –6 vehicle-treated mice and 5–8 nilotinib-treated mice). * = $P < 0.05$; ** = $P < 0.01$. **D**, Illustration of the crucial role of FcγRIIb in the negative selection of low-affinity GC B cells via c-Abl in the light zone of GCs in response to IgG immune complexes (ICs) in secondary immunization in WT mice (solid lines). Broken lines represent FcγRIIb^{232T/T} mice. BCR = B cell receptor; SHM = somatic hypermutation.

mice ($P = 0.8622$) despite an increased number of NP+ PCs in FcγRIIb^{232T/T} mice (Figure 3). Consistent with increased serum levels of total IgG in FcγRIIb^{232T/T} mice

(Figure 2A), the serum concentrations of IgG1, IgG2a, and IgG3 isotypes were all significantly higher in immunized FcγRIIb^{232T/T} mice than WT mice ($P < 0.05$)

(Figure 4B). Similarly, the serum levels of high-affinity (NP₇)-specific and total NP+ (NP₃₀)-specific IgG isotypes remained higher in Fc γ RIIb^{232T/T} mice than in WT mice (Figures 4C and D).

Reduced apoptosis of B cells in GC light zones of immunized Fc γ RIIb^{232T/T} mice. To further delineate the abnormality of GC response in Fc γ RIIb^{232T/T} mice, we quantified NP+CD19+GL-7+ GC B cells and found that Fc γ RIIb^{232T/T} mice exhibited more splenic NP+ GC B cells than WT mice (Figure 5A). When GC dark zone (CD86^{low}CXCR4^{high}) and light zone (CD86^{high}CXCR4^{low}) B cells were analyzed and compared, we found a decreased percentage of GC dark zone B cells ($P < 0.001$) (Figure 5A) but an increased percentage of GC light zone B cells ($P < 0.001$) (Figure 5A) in Fc γ RIIb^{232T/T} mice. Moreover, we detected an increase in the size of GCs in splenic sections from immunized Fc γ RIIb^{232T/T} mice (Figure 5B). It has been shown that the surface expression of Fc γ RIIb in GC B cells is up-regulated in normal mice (16). We examined the Fc γ RIIb expression levels in GC B cells and found no significant differences in Fc γ RIIb expression between WT and Fc γ RIIb^{232T/T} mice either before or after immunization (Figure 5C). Because clonal selection of GC B cells occurs primarily in the light zone of GCs (17–22), we next investigated the apoptosis of GC B cells to determine the extent of negative selection of low-affinity B cells after secondary immunization. Consistent with an increase in GC B cell numbers in Fc γ RIIb^{232T/T} mice, the percentage of dead GC B cells was significantly decreased in these mice ($P < 0.05$) (Figure 5D). Significantly fewer apoptotic GC B cells, which were stained by active caspase 3 mAb, were detected in Fc γ RIIb^{232T/T} mice after secondary immunization (Figure 5D).

Blocking c-Abl activity in WT mice during clonal selection recapitulates the GC phenotype of Fc γ RIIb^{232T/T} mice. Because Fc γ RIIb is known to mediate apoptosis via c-Abl kinase in response to IgG ICs in B cells (5), we investigated the expression of active c-Abl (p-Y245) proteins in GC B cells. In WT mice, phospho-c-Abl proteins were readily detectable and mainly localized in the light zone of GCs, where affinity maturation and clonal selection occur. In contrast, the levels of phospho-c-Abl proteins were substantially decreased in the GCs of Fc γ RIIb^{232T/T} mice (Figure 6A). It has been reported that the apoptosis of GC B cells peaks during days 7–9 after secondary immunization (34). Thus, to determine whether c-Abl activity is crucial for Fc γ RIIb to negatively regulate GC B cells, we treated WT mice with nilotinib (2 mg/kg/day) to block c-Abl kinase activity during the peak period when GC B cells undergo apoptosis for selection after secondary immunization. Indeed, the serum titers of NP+ IgG displayed reduced affinity maturation

in nilotinib-treated mice ($P < 0.05$) (Figure 6B). Moreover, the number of low-affinity NP+IgG+ PCs (NP₃₀ PCs minus NP₇ PCs) was significantly increased after c-Abl kinase activity was blocked in WT mice ($P < 0.01$) (Figure 6C). Thus, the findings in antibodies produced from nilotinib-treated WT mice are reminiscent of the GC defect observed in Fc γ RIIb^{232T/T} mice after secondary immunization (Figures 2 and 3).

DISCUSSION

In this study, we showed for the first time that compromised inhibitory activity of Fc γ RIIb-232T proteins results in insufficient deletion of low-affinity antigen-specific GC B cells and reduces affinity maturation in clonal selection. Consequently, the resultant increase in low-affinity antigen-specific GC B cells leads to a corresponding increase in low-affinity antigen-specific IgG in circulation in Fc γ RIIb^{232T/T} mice (Figures 2 and 3). Compared to WT mice, the number of GC light zone B cells was increased in Fc γ RIIb^{232T/T} mice due to a decrease in the apoptosis of GC B cells and in the phosphorylation of c-Abl proteins (Figures 5 and 6). Furthermore, administration of nilotinib to WT mice to block c-Abl kinase activity at the peak of apoptosis of GC B cells in clonal selection resulted in reduced affinity maturation reminiscent of the phenotype of immunized Fc γ RIIb^{232T/T} mice. The involvement of c-Abl in the clonal selection of GC B cells is a novel and important finding. The newly identified, crucial role of Fc γ RIIb in regulating the stringency of affinity maturation by triggering apoptosis to delete low-affinity GC B cells via c-Abl is illustrated in Figure 6D.

Because Fc γ RIIb^{232T/T} mice display a higher serum level of high-affinity NP-specific IgG, the reduced inhibition of Fc γ RIIb-232T on BCRs might have the potential to promote the proliferation of GC B cells. Indeed, numbers of GC B cells increased in Fc γ RIIb^{232T/T} mice after secondary immunization (Figure 5A). Nevertheless, the increased number of B cells was largely due to an increase in low-affinity B cells, since no increase in high-affinity IgG+ PCs was observed in Fc γ RIIb^{232T/T} mice (Figure 3). This leads us to conclude that the retention of low-affinity B cells is more a consequence of insufficient apoptosis rather than insufficient inhibition of proliferation of GC B cells in Fc γ RIIb^{232T/T} mice. In addition, because low-affinity B cells are intrinsically less competitive than high-affinity cells for antigen stimulation, the increased survival of low-affinity Fc γ RIIb^{232T/T} GC B cells is positively associated with reduced apoptosis. One important caveat is that low-affinity antigen-specific GC B cells may have a chance to undergo further affinity maturation when the competition with high-affinity B cells becomes reduced in late

GCs (35). However, in the persistence of Fc γ RIIb-232T dysfunction, repeated immunization generates a new pool of low-affinity B cells, which normally should have been deleted. Consistent with this finding, the serum level of low-affinity antigen-specific IgG and the number of IgG+ PCs remained significantly increased after secondary immunization in Fc γ RIIb^{232T/T} mice (Figures 2 and 3).

These findings raise the possibility of undesired consequences of enhanced immune response due to the presence of the Fc γ RIIb-232T allele. For example, low-affinity memory B cells might persist in peripheral lymphoid organs, and low-affinity PCs emigrated from GCs into circulation might be able to become long-term residents in the bone marrow to secrete low-affinity antibodies (36). An additional caveat is that because serum NP+ IgG display increasing affinity maturation in WT mice over time but remain reduced in Fc γ RIIb^{232T/T} mice after primary immunization, the contribution of extrafollicular response to influence the outcome of low-affinity B cells is likely limited (Supplementary Figure 3, available on the *Arthritis & Rheumatology* web site at <http://onlinelibrary.wiley.com/doi/10.1002/art.40555/abstract>).

Consistent with previous findings in living cells (14,15), Fc γ RIIb-I232T proteins appear to form small raft-associated clusters rather than coalesced caps for signal amplification as compared to receptors in WT mice at 30–60 minutes (see Supplementary Figure 1, available on the *Arthritis & Rheumatology* web site at <http://onlinelibrary.wiley.com/doi/10.1002/art.40555/abstract>). The resultant diminished recruitment of SHIP to Fc γ RIIb-232T therefore can account for reduced inhibition on B cells in response to IgG ICs. However, mice deficient in the *Ship* gene show no differences from WT mice in antibody production after immunization with a T cell-dependent antigen (37). Nevertheless, when the *Ship* gene is specifically deleted in B cells, they are indeed more sensitive to antigen activation than WT cells in vitro (38).

Surprisingly, the number of NP+ GC B cells and the serum level of NP+ IgG decreased markedly after NP-CGG immunization. It appears that hyperactive BCR signaling in SHIP-deficient GC B cells directly induces apoptosis of both low- and high-affinity B cells (38). Thus, a tightly regulated balance between Fc γ RIIb/SHIP and Fc γ RIIb/c-Abl pathways in response to IgG ICs is crucial for normal outcome of GC reaction. Consistent with this notion, an increased sensitivity to Fc γ RIIb-dependent apoptosis might contribute in part to the GC phenotype in mice with SHIP deficiency in B cells. Indeed, loss of SHIP in DT40 B cells enhances Fc γ RIIb-induced apoptosis (9). We previously showed that apoptosis of B cells induced by Fc γ RIIb is dependent on c-Abl, but independent of SHIP, suggesting a decisive role of c-Abl when activated (5).

In the GC, low-affinity B cells are outcompeted by high-affinity B cells for antigen stimulation and Tfh cell help, thereby lacking survival advantages (39,40). In the present study, we provided evidence of a new role of the Fc γ RIIb/c-Abl signaling pathway to participate in the negative selection of low-affinity B cells. Consistent with our findings, enhancing survival of GC B cells by overexpression of the *Bcl-x_L* gene in mice results in reduced affinity maturation (41). Similarly, mice overexpressing *Bcl-2* show decreased negative selection of GC B cells (42,43). These findings indicate that enhanced BCR signaling can increase the survival of low-affinity B cells to avoid negative selection. Whether these low-affinity B cells might have overcome the apoptotic induction from Fc γ RIIb to escape deletion is of interest for future studies. Meanwhile, it has been demonstrated that low-affinity autoreactive B cells are more sensitive to CpG double-stranded DNA-induced differentiation into PCs than high-affinity B cells (44,45). Thus, low-affinity autoreactive B cells are able to efficiently expand independent of antigen stimulation if they can escape from elimination in GCs. Because autoreactive B cells are routinely generated in response to a foreign antigen in normal mice, e.g., resulting from host immune response against pathogens (46), low-affinity autoreactive B cells, which are likely generated from time to time, need to be deleted when they emerge in GCs to prevent autoimmunity.

Our findings indicate that in Fc γ RIIb-232T allele carriers, the persistent presence of low-affinity B cells and especially PCs may gradually become a key contributor that puts them at risk of developing autoimmune diseases over time. Reduced surface expression levels of WT Fc γ RIIb in the B cells of SLE patients may result in susceptibility to the presence of low-affinity B cells (18–20). Accordingly, because transgenic mice overexpressing *Fcgr2b* in B cells exhibit reduced SLE disease severity (47), it will be of interest to investigate whether regimens that up-regulate the surface expression level of Fc γ RIIb-232T proteins to enhance their inhibition can restore competency to negatively regulate low-affinity GC B cells for therapeutic exploitation.

ACKNOWLEDGMENTS

We thank Miss Yu-Syuan You and Mr. Tsung-Chih Tseng for excellent technical assistance. We acknowledge Dr. Shu-Wha Lin for the technical assistance and service provided by the Gene Knockout Mouse Core of the NTU Center for Genomic Medicine, College of Medicine, National Taiwan University. We also appreciate the services provided by the staff of the First Core Laboratory at the College of Medicine, National Taiwan University and the RCF7 Laboratory of the Department of Medical Research at National Taiwan University Hospital.

AUTHOR CONTRIBUTIONS

All authors were involved in drafting the article or revising it critically for important intellectual content, and all authors approved the final version to be published. Dr. Tzeng had full access to all of the data in the study and takes responsibility for the integrity of the data and the accuracy of the data analysis.

Study conception and design. Zhou, Tzeng.

Acquisition of data. Zhou, Yu, Hwai, C.-S. Chen, Tzeng.

Analysis and interpretation of data. Zhou, Hwai, P.-L. Chen, Tzeng.

REFERENCES

- Daeron M. Fc receptors as adaptive immunoreceptors. *Curr Top Microbiol Immunol* 2014;382:131–64.
- Espeli M, Smith KG, Clatworthy MR. Fc γ RIIB and autoimmunity. *Immunol Rev* 2016;269:194–211.
- Bolland S, Ravetch JV. Spontaneous autoimmune disease in Fc γ RIIB-deficient mice results from strain-specific epistasis. *Immunity* 2000;13:277–85.
- Tiller T, Kofer J, Kreschel C, Busse CE, Riebel S, Wickert S, et al. Development of self-reactive germinal center B cells and plasma cells in autoimmune Fc γ RIIB-deficient mice. *J Exp Med* 2010;207:2767–78.
- Tzeng SJ, Bolland S, Inabe K, Kurosaki T, Pierce SK. The B cell inhibitory Fc receptor triggers apoptosis by a novel c-Abl family kinase-dependent pathway. *J Biol Chem* 2005;280:35247–54.
- Chacko GW, Tridandapani S, Damen JE, Liu L, Krystal G, Coggeshall KM. Negative signaling in B lymphocytes induces tyrosine phosphorylation of the 145-kDa inositol polyphosphate 5-phosphatase, SHIP. *J Immunol* 1996;157:2234–8.
- D'Ambrosio D, Fong DC, Cambier JC. The SHIP phosphatase becomes associated with Fc γ RIIB1 and is tyrosine phosphorylated during 'negative' signaling. *Immunol Lett* 1996;54:77–82.
- Ono M, Bolland S, Tempst P, Ravetch JV. Role of the inositol phosphatase SHIP in negative regulation of the immune system by the receptor Fc γ RIIB. *Nature* 1996;383:263–6.
- Pearse RN, Kawabe T, Bolland S, Guinamard R, Kurosaki T, Ravetch JV. SHIP recruitment attenuates Fc γ RIIB-induced B cell apoptosis. *Immunity* 1999;10:753–60.
- Siriboonrit U, Tsuchiya N, Sirikong M, Kyogoku C, Bejrachandra S, Suthipinittharm P, et al. Association of Fc γ receptor IIB and IIB polymorphisms with susceptibility to systemic lupus erythematosus in Thais. *Tissue Antigens* 2003;61:374–83.
- Chen JY, Wang CM, Ma CC, Luo SF, Edberg JC, Kimberly RP, et al. Association of a transmembrane polymorphism of Fc γ receptor IIB (FCGR2B) with systemic lupus erythematosus in Taiwanese patients. *Arthritis Rheum* 2006;54:3908–17.
- Willcocks LC, Carr EJ, Niederer HA, Rayner TF, Williams TN, Yang W, et al. A defuncting polymorphism in FCGR2B is associated with protection against malaria but susceptibility to systemic lupus erythematosus. *Proc Natl Acad Sci U S A* 2010;107:7881–5.
- Kono H, Kyogoku C, Suzuki T, Tsuchiya N, Honda H, Yamamoto K, et al. Fc γ RIIB Ile232Thr transmembrane polymorphism associated with human systemic lupus erythematosus decreases affinity to lipid rafts and attenuates inhibitory effects on B cell receptor signaling. *Hum Mol Genet* 2005;14:2881–92.
- Sohn HW, Pierce SK, Tzeng SJ. Live cell imaging reveals that the inhibitory Fc γ RIIB destabilizes B cell receptor membrane-lipid interactions and blocks immune synapse formation. *J Immunol* 2008;180:793–9.
- Xu L, Xia M, Guo J, Sun X, Li H, Xu C, et al. Impairment on the lateral mobility induced by structural changes underlies the functional deficiency of the lupus-associated polymorphism Fc γ RIIB-T232. *J Exp Med* 2016;213:2707–27.
- Clatworthy MR, Willcocks L, Urban B, Langhorne J, Williams TN, Peshu N, et al. Systemic lupus erythematosus-associated defects in the inhibitory receptor Fc γ RIIB reduce susceptibility to malaria. *Proc Natl Acad Sci U S A* 2007;104:7169–74.
- Waisberg M, Tarasenko T, Vickers BK, Scott BL, Willcocks LC, Molina-Cruz A, et al. Genetic susceptibility to systemic lupus erythematosus protects against cerebral malaria in mice. *Proc Natl Acad Sci U S A* 2011;108:1122–7.
- Mackay M, Stanevsky A, Wang T, Aranow C, Li M, Koenig S, et al. Selective dysregulation of the Fc γ IIB receptor on memory B cells in SLE. *J Exp Med* 2006;203:2157–64.
- Su K, Yang H, Li X, Li X, Gibson AW, Cafardi JM, et al. Expression profile of Fc γ RIIB on leukocytes and its dysregulation in systemic lupus erythematosus. *J Immunol* 2007;178:3272–80.
- Isaak A, Gergely P Jr, Szekeres Z, Prechl J, Poór G, Erdei A, et al. Physiological up-regulation of inhibitory receptors Fc γ RII and CR1 on memory B cells is lacking in SLE patients. *Int Immunol* 2008;20:185–92.
- Rahman ZS, Manser T. Failed up-regulation of the inhibitory IgG Fc receptor Fc γ RIIB on germinal center B cells in autoimmune-prone mice is not associated with deletion polymorphisms in the promoter region of the Fc γ RIIB gene. *J Immunol* 2005;175:1440–9.
- MacLennan IC, Gray D. Antigen-driven selection of virgin and memory B cells. *Immunol Rev* 1986;91:61–85.
- French DL, Laskov R, Scharff MD. The role of somatic hypermutation in the generation of antibody diversity. *Science* 1989;244:1152–7.
- Gitlin AD, Shulman Z, Nussenzweig MC. Clonal selection in the germinal centre by regulated proliferation and hypermutation. *Nature* 2014;509:637–40.
- MacLennan IC. Germinal centers. *Annu Rev Immunol* 1994;12:117–39.
- De Silva NS, Klein U. Dynamics of B cells in germinal centres. *Nat Rev Immunol* 2015;15:137–48.
- Goins CL, Chappell CP, Shashidharamurthy R, Selvaraj P, Jacob J. Immune complex-mediated enhancement of secondary antibody responses. *J Immunol* 2010;184:6293–8.
- Qin D, Wu J, Vora KA, Ravetch JV, Szakal AK, Manser T, et al. Fc γ receptor IIB on follicular dendritic cells regulates the B cell recall response. *J Immunol* 2000;164:6268–75.
- Tzeng SJ. The isolation, differentiation, and quantification of human antibody-secreting B cells from blood: ELISpot as a functional readout of humoral immunity. *J Vis Exp* 2016;118:e54582.
- Tzeng SJ, Li WY, Wang HY. Fc γ RIIB mediates antigen-independent inhibition on human B lymphocytes through Btk and p38 MAPK. *J Biomed Sci* 2015;22:87–98.
- Dominguez-Sola D, Victora GD, Ying CY, Phan RT, Saito M, Nussenzweig MC, et al. The proto-oncogene MYC is required for selection in the germinal center and cyclic reentry. *Nat Immunol* 2012;13:1083–91.
- Li H, Durbin R. Fast and accurate short read alignment with Burrows-Wheeler transform. *Bioinformatics* 2009;25:1754–60.
- Li H, Handsaker B, Wysoker A, Fennell T, Ruan J, Homer N, et al. The sequence alignment/map format and SAMtools. *Bioinformatics* 2009;25:2078–9.
- Saitoh HA, Maeda K, Yamakawa M. In situ observation of germinal center cell apoptosis during a secondary immune response. *J Clin Exp Hematop* 2006;46:73–82.
- Dal Porto JM, Haberman AM, Kelsoe G, Shlomchik MJ. Very low affinity B cells form germinal centers, become memory B cells, and participate in secondary immune responses when higher affinity competition is reduced. *J Exp Med* 2002;195:1215–21.
- Jacob J, Kelsoe G. In situ studies of the primary immune response to (4-hydroxy-3-nitrophenyl)acetyl. Part II. A common clonal origin for periarteriolar lymphoid sheath-associated foci and germinal centers. *J Exp Med* 1992;176:679–87.
- Helgason CD, Kalberer CP, Damen JE, Chappel SM, Pineault N, Krystal G, et al. A dual role for Src homology 2 domain-containing inositol-5-phosphatase (SHIP) in immunity: aberrant development



- and enhanced function of B lymphocytes in *ship*^{-/-} mice. *J Exp Med* 2000;191:781–94.
38. Leung WH, Tarasenko T, Biesova Z, Kole H, Walsh ER, Bolland S. Aberrant antibody affinity selection in SHIP-deficient B cells. *Eur J Immunol* 2013;43:371–81.
 39. Shulman Z, Gitlin AD, Targ S, Jankovic M, Pasqual G, Nussenzweig MC, et al. T follicular helper cell dynamics in germinal centers. *Science* 2013;341:673–7.
 40. Shulman Z, Gitlin AD, Weinstein JS, Lainez B, Esplugues E, Flavell RA, et al. Dynamic signaling by T follicular helper cells during germinal center B cell selection. *Science* 2014;345:1058–62.
 41. Takahashi Y, Cerasoli DM, Dal Porto JM, Shimoda M, Freund R, Fang W, et al. Relaxed negative selection in germinal centers and impaired affinity maturation in *bcl-xL* transgenic mice. *J Exp Med* 1999;190:399–410.
 42. Hande S, Notidis E, Manser T. Bcl-2 obstructs negative selection of autoreactive, hypermutated antibody V regions during memory B cell development. *Immunity* 1998;8:189–98.
 43. Smith KG, Light A, O'Reilly LA, Ang SM, Strasser A, Tarlinton D. Bcl-2 transgene expression inhibits apoptosis in the germinal center and reveals differences in the selection of memory B cells and bone marrow antibody-forming cells. *J Exp Med* 2000;191:475–84.
 44. Rui L, Vinuesa CG, Blasioli J, Goodnow CC. Resistance to CpG DNA-induced autoimmunity through tolerogenic B cell antigen receptor ERK signaling. *Nat Immunol* 2003;4:594–600.
 45. Viglianti GA, Lau CM, Hanley TM, Miko BA, Shlomchik MJ, Marshak-Rothstein A. Activation of autoreactive B cells by CpG dsDNA. *Immunity* 2003;19:837.
 46. Ray SK, Putterman C, Diamond B. Pathogenic autoantibodies are routinely generated during the response to foreign antigen: a paradigm for autoimmune disease. *Proc Natl Acad Sci U S A* 1996;93:2019–24.
 47. Brownlie RJ, Lawlor KE, Niederer HA, Cutler AJ, Xiang Z, Clatworthy MR, et al. Distinct cell-specific control of autoimmunity and infection by FcγRIIb. *J Exp Med* 2008;205:883–95.



Chapter 11

B-Cell ELISpot Assay to Quantify Antigen-Specific Antibody-Secreting Cells in Human Peripheral Blood Mononuclear Cells

Haw Hwai, Yi-Ying Chen, and Shiang-Jong Tzeng

Abstract

Peripheral blood is commonly used to assess the cellular and humoral immune responses in clinical studies. It is a convenient sample to collect for immunological research as compared to the surgically excised and biopsied lymphoid specimens. To determine the functional status of immune system from peripheral blood, the enzyme-linked immunospot (ELISpot) assay is a popular method of choice owing to its high sensitivity, great accuracy, and easy performance. The ELISpot allows detection and quantification of cellular functionality at the single-cell level. Therefore, ELISpot assay is commonly applied to detect cytokines and cytotoxic granules released from T cells as well as to measure antibodies secreted from B cells. Because the ELISpot assay has been increasingly used for evaluation of the vaccine efficacy in clinical trials, standardization and reproducibility are crucial to minimize assay variability amongst samples from different sources. Here we introduce methods to isolate human peripheral blood mononuclear cells (PBMCs) for quantification of the antigen-specific antibody-secreting cells using the ELISpot assay.

Key words Enzyme-linked immunospot (ELISpot), B cells, Antibody-secreting cells (ASCs), Peripheral blood mononuclear cells (PBMCs), Vaccine

1 Introduction

The ELISpot assay was originally developed by Dr. Cecil Czerkinsky in 1983 for the purpose to detect antigen (Ag)-specific antibody (Ab)-secreting cells (ASCs) [1]. Over the years, the ELISpot has become an important method for the detection and quantification of ASCs in vaccine research. The technology of ELISpot assay is a combination of enzyme-linked immunoabsorbance assay (ELISA) and western blotting to enable quantification of a specific cell population based on their secretory molecules with superior sensitivity to detect a single positive cell [2]. Therefore, ELISpot assay has been increasingly adopted for the identification and enumeration of cytokine-producing T cells as well as Ag-specific ASCs [2–4]. Although the conventional ELISA and flow cytometry-based

cytokine bead arrays and intracellular staining can provide extremely useful information of the cells, they have less sensitivity and accuracy than ELISpot in the quantification of rare Ag-specific cells [5, 6]. These advantages make the ELISpot assay frequently applied to directly monitor Ag-specific B-cell response in PBMCs.

In an ELISpot assay for detecting Ag-specific ASCs, the polyvinylidene difluoride (PVDF) membranes in a 96-well microtiter plate require pre-coating with the Ag to be assayed. After blocking and washing steps, purified PBMCs are serially diluted to seed into wells of the ELISpot plate for incubation. The Ag-specific ASCs secrete Abs, which are captured directly on the membrane surface by the immobilized Ag to prevent diffusion into culture medium. Subsequent detection steps utilize a detection Ab, typically conjugated with horseradish peroxidase (HRP) or alkaline phosphatase (AP) enzyme, in order to visualize the secretory fingerprint of individual ASCs [7]. Because ELISpot is capable of detecting a single Ag-specific cell, direct *ex vivo* measurement of Ag-specific ASCs from PBMCs is frequently adopted in vaccine trials [8, 9]. *In vitro* differentiation of memory B cells from PBMCs into ASCs is an option for long-term assessments of vaccine-induced humoral response [10–12]. Because the processing of blood samples is amenable to scale up, ELISpot assay is suitable for investigating Ag-specific Ab response in a large-scale and multicenter vaccine trial.

The protocols described include isolation of PBMCs (~1 h) and detection of total and Ag-specific IgG ASCs (~4 h) in small amounts of blood (~10 mL). Other than culturing cells overnight, the hands-on steps normally take less than 6 h. The whole procedures can be performed in a resource-poor setting.

2 Materials

2.1 Isolation of Human PBMCs

1. Autoclaved double distilled water (ddH₂O).
2. Sterile 0.5 M ethylenediaminetetraacetic acid (EDTA) solution (9.3 g of EDTA disodium and 1.12 g of NaOH dissolved in 50 mL ddH₂O).
3. Blood sample drawing equipment: tourniquet, rubber gloves, disinfection swabs, 3M micropore tape, adhesive dressing, and needle disposal box.
4. 10 mL syringe with 20G or 22G needle.
5. Sterile 15 and 50 mL conical tubes.
6. Red blood cells (RBC) lysis buffer: 155 mM NH₄Cl, 10 mM NaHCO₃, 0.1 mM EDTA.
7. Autoclaved phosphate-buffered saline (PBS, NaCl 137 mM, KCl 2.7 mM, Na₂HPO₄ 10 mM, KH₂PO₄ 2 mM, pH 7.4) and PBS-T (PBS with 0.1% Tween 20).

8. RPMI 1640 culture medium supplemented with 10% fetal calf serum (FCS), 10 mM penicillin/streptomycin, and 10 mM L-glutamine (*see* **Notes 1** and **2**).
9. Centrifuge machine that allows spinning 10 and 50 mL conical tubes at $500 \times g$.
10. Trypan blue solution (0.5%).
11. Hemocytometer (Hausser Scientific, Horsham, PA, USA) to count PBMCs under the microscope.
12. Upright microscope equipped with bright-field illumination and phase contrast condenser.
13. A protocol approved by the Internal Review Board (IRB) of investigators' institutions for the use of human blood to perform ELISpot assays. Note: the protocol (no. 201307019RINB) to use human peripheral blood was approved by the IRB of National Taiwan University Hospital for this study.

2.2 ELISpot Assays

1. PVDF membrane-bottomed 96-well filter plates, 0.45 μm pore size (Merck Millipore, Billerica, MA, USA).
2. Tetanus toxin.
3. Goat anti-human IgG conjugated with alkaline phosphatase (AP) (Fc γ fragment specific).
4. Bromochloroindolyl phosphate-nitro blue tetrazolium (BCIP/NBT) substrate solution (Sigma-Aldrich, St. Louis, MO, USA).
5. C.T.L. ImmunoSpot analyzer (Cellular Technology Limited, Cleveland, OH, USA).

3 Methods

3.1 Isolation of Human PBMCs

1. Collect 10 mL of venous blood from a donor with a tube containing 20 μL of 0.5 M EDTA (final concentration: 5 mM) (*see* **Notes 3** and **4**).
2. Transfer blood into a 50 mL conical tube.
3. Fill tube to 50 mL with RBC lysis buffer and incubate at room temperature (RT) for 5 min (*see* **Notes 5** and **6**).
4. Spin down cells at $500 \times g$ (or 1500 rpm) at RT for 5 min.
5. Decant supernatant carefully.
6. Resuspend PBMCs with 10 mL of sterile PBS.
7. Centrifuge at $500 \times g$ for 5 min.
8. Decant supernatant carefully.

9. Resuspend PBMCs gently with 1 mL of culture medium.
10. Take 10 μL , transfer into an Eppendorf tube, and add 90 μL culture medium (10 \times dilution).
11. Mix cells 1:1 with trypan blue dye and incubate 1–2 min at RT.
12. Pipette 20 μL from the mixture into a V-shaped well of one side of hemocytometer under a coverslip.
13. Count cells under the phase contrast microscope using 20 \times lens (*see Note 7*).
14. Aliquot desired numbers of cells into separate Eppendorf tubes.
15. Cells are ready for seeding into the ELISpot plate (Fig. 1).

3.2 ELISpot Assays

1. Pre-wet the membranes with 30 μL of 35% ethanol per well in ELISpot plates for 30 s. Avoid touching the membrane in wells at all times during pipetting (*see Note 8*).
2. Decant ethanol.
3. Add 150 μL of sterile ddH₂O into each well and incubate at RT for 5 min.
4. Decant ddH₂O.
5. Add 200 μL of sterile PBS into each well and incubate at RT for 3 min.
6. Decant PBS.
7. Pre-coat the plate with 50 μL per well of 10 $\mu\text{g}/\text{mL}$ of Ag (e.g., tetanus toxin) (*see Note 9*).
8. Incubate overnight at 4 $^{\circ}\text{C}$ (preferred) or alternatively at 37 $^{\circ}\text{C}$ for 2 h.
9. Empty the wells and wash with 200 μL of PBS per well for three times.
10. Decant PBS thoroughly.
11. Add 200 μL of culture medium per well for blocking at RT for 2 h.
12. Decant culture medium and briefly wash wells with 200 μL of PBS.
13. Seed 5×10^5 , 2.5×10^5 , 1.25×10^5 PBMCs per donor's sample into wells, respectively. Bring up volume to 100 μL in wells with culture medium (*see Note 10*).
14. Incubate the plate in a 37 $^{\circ}\text{C}$ incubator with 5% CO₂ overnight. Do not shake or move the plate (*see Note 11*).
15. Decant cells and culture medium.
16. Wash the plate with 200 μL per well of PBS-T at RT for 3 min for five times (*see Note 12*).

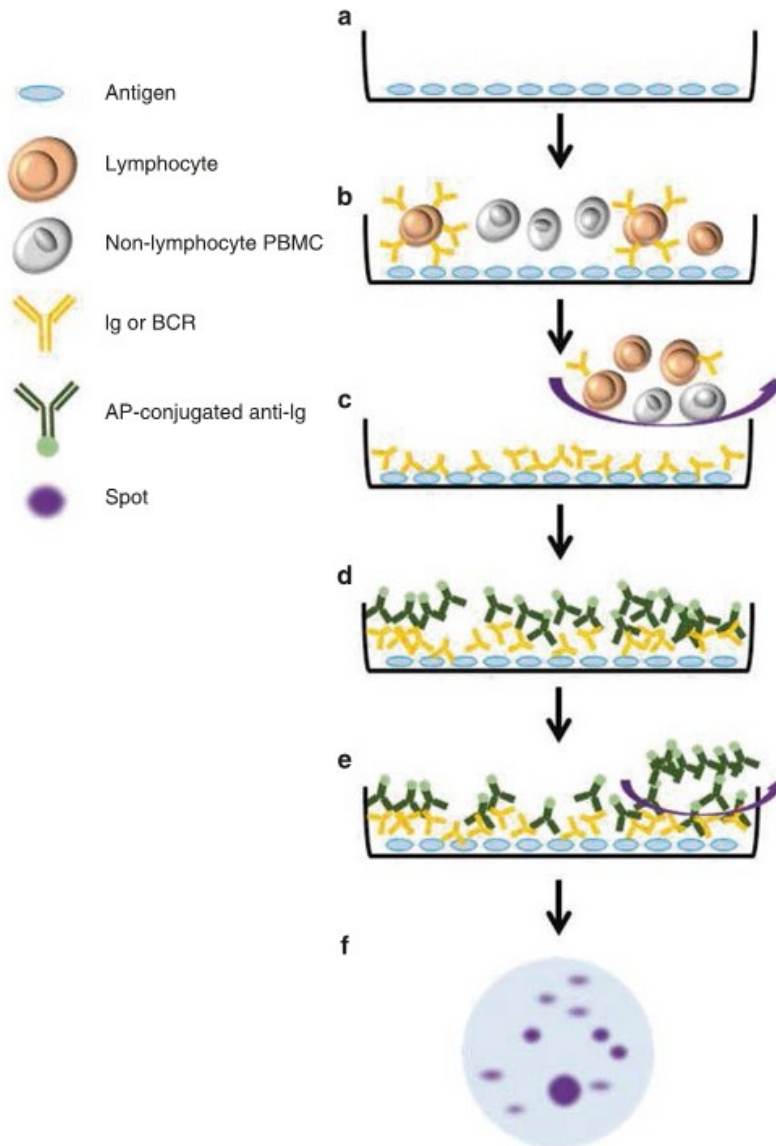


Fig. 1 A schematic flowchart of ELISpot assay to detect Ag-specific ASCs. (A) Pre-coat the wells of the ELISpot plate with an Ag, e.g., tetanus toxin. (B) Seed serial diluted PBMCs into wells of the plate, respectively. Culture overnight (minimum: 8 h). (C) Wash off cells with PBS-T. (D) Add AP-conjugated detection Abs specific to IgM, IgG, or IgA. (E) Wash off unbound Abs. (F) Develop the spots with BCIP/NBT substrate solution

17. Add goat anti-human IgG-AP (Fc γ -specific, 1:5000 in PBS with 1% BSA) into wells and incubate at RT for 2 h in the dark.
18. Wash the plate three times with 200 μ L of PBS-T.
19. Add 50 μ L of BCIP/NBT substrate solution and incubate at RT. Purple-colored spots normally appear in 10–30 min (*see Note 13*).

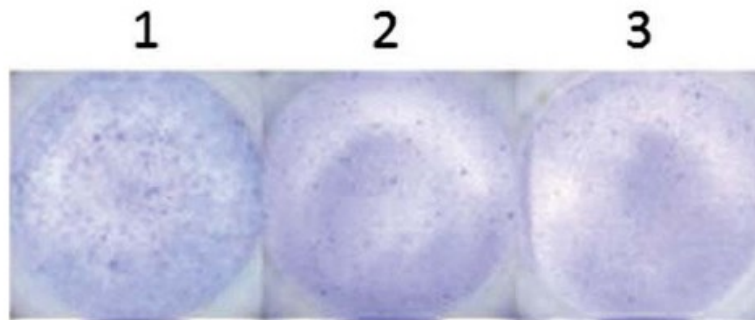


Fig. 2 Representative ELISpot images of tetanus toxin-specific IgG ASCs detected from PBMCs. PBMCs were isolated from a healthy donor 2 weeks after receiving a booster of tetanus toxin. ELISpot plate was pre-coated with 50 μL /well of tetanus toxin (10 $\mu\text{g}/\text{mL}$ in PBS). Aliquots of 5×10^5 , 2.5×10^5 , and 1.25×10^5 PBMCs (#1, #2 and #3) were seeded into wells of the ELISpot plate, respectively. Tetanus toxin-specific IgG ASCs were detected and illustrated

20. Stop enzymatic reaction by adding 100 μL ddH₂O into each well to prevent over-development of spots.
21. Take the underdrain off the plates and wash both sides of the membrane with tap water (*see Note 14*).
22. Allow plates completely air dried and store plates in the dark before scanning (*see Note 15*).
23. Count the spots on membrane surface (Fig. 2) using a C.T.L analyzer or an automated plate reader equipped with an image acquisition and analysis unit (*see Note 16*).

4 Notes

1. Complements in FCS may inhibit or destroy cells, e.g., via complement-dependent cytotoxicity, or affect the results of immunoassays, e.g., via binding to the Fc portion of Abs. If this is a concern, inactivate the serum at 56 °C for 30 min. Filtrate serum with a 0.2 μm sterile filter if precipitates occur after cooling.
2. If human serum is necessary to replace FCS in culture medium, pre-test the serum in different batches to avoid nonspecific activation to cultured cells, which may cause background spot formation. Heat inactivation of human serum before use is recommended.
3. Vacutainer blood collection tubes, which contain 1–2% of spray-dried K₂EDTA, are often adopted in vaccine trials. K₂EDTA is recommended by the CLSI (Clinical & Laboratory Standards Institute) and the ICSH (International Council for Standardization in Hematology). It is important to mix the sample immediately after collection to ensure no blood clot formation.

4. If sodium citrate is used as the anticoagulant, add 1 part sodium citrate (3.2% or 0.109 M) to 9 parts blood. Incubate at RT for 5 min [13].
5. Ficoll gradient is also commonly used to prepare PBMCs from fresh blood [7, 14]. Make sure no mixing of blood with Ficoll to gain good separation of buffy coat and high yield of PBMCs. In our experience, the purity and the yield of PBMCs isolated from either direct RBC lysis or Ficoll gradient methods are comparable.
6. Purified PMBCs can be cryopreserved until use. Typically, PBMCs can be frozen and stored at $1-2 \times 10^6$ cells/mL in cold cryoprotective medium containing 90% FCS and 10% dimethyl sulfoxide (v/v).
7. The hemocytometer is generally divided into nine major squares of 1 mm² area in the middle square part. Add ~20 μ L of cell suspension between hemocytometer and cover glass. The goal is to distribute roughly 50–100 cells/square. Count five squares—typically four corner and the center squares. Take the average of cellular counts per square, multiply it by the dilution factor (multiply by 1 if not diluted) and then multiply by 10^4 = the number of cells/mL. Alternatively, an automated cell counter is quick and convenient and highly suitable for processing multiple samples at a time.
8. Pre-wetting of the PVDF membrane with 35–70% ethanol or methanol improves hydrophobicity and greatly increases protein binding. By contrast, the nitrocellulose membrane-bottomed filter plates require no pre-treatment and they are not compatible with ethanol or methanol.
9. To detect all ASCs in PBMCs, the plate can be pre-coated with a single Ab, the F(ab')₂ fragment of anti-human (IgM + IgG + IgA). Use F(ab')₂ fragment of Ig rather than the whole Ig to reduce background signals resulting from potential cross-reactivity of Fc fragment with the detection Abs [7].
10. Seeding of serial diluted PBMCs is necessary to obtain a quantifiable number of spots for counting. The practical limit of spot detection generally depends on the number of cells seeded to form a tight monolayer on the membrane surface. Typically, $2-3 \times 10^5$ PBMCs in a well is recommended. The goal is to get ~50–200 spots. Although up to a maximum of 10^6 cells is acceptable for detection of rare events, it should be noted that over-seeding of cells may lead to piling up of cells and compromise the linearity between cell input and spot frequency.
11. Disturbing cultured cells in the plate may cause the development of weakly stained and fuzzy spots and the formation of “snail trail” or “comet tail” spots. Do not stack plates to prevent the edge effect—few or no spots at the outer wells of the plate.

12. Squirt bottle is preferred over multichannel pipettes for manual wash to prevent damaging of the membrane. When a microplate washer is used, make sure the protruding prongs are properly adjusted to avoid puncturing the membrane. An automatic plate washer is highly convenient and effective. After completing the wash, tap the plates on a dry paper towel to remove residual liquid contents to prevent increasing background signals. Repeat tapping motion when necessary.
13. BCIP/NBT reaction produces an insoluble NBT diformazan end product that is blue to purple in color. Alternatively, use AEC (9-ethylcarbazol-3-amine) substrate solution for HRP-conjugated Abs. If using biotinylated detection Abs, incubate with streptavidin-AP or -HRP proteins before adding respective substrate solutions.
14. For enzymatic reaction steps, removing the base of the plate before addition of substrates can further reduce background signals as reagents can leak through the membrane into the bottom underdrain of the plate.
15. It is necessary to allow the ELISpot plate completely air dried in the dark before analysis in that wet membranes appear dark and obscure the detection of weak and small spots.
16. Spot counting can be performed manually via a dissecting microscope.

Acknowledgments

This study was supported by a research grant from the Ministry of Science and Technology of the Executive Yuan of Taiwan (NSC99-2320-B-002-011).

References

1. Czerkinsky CC, Nilsson LA, Nygren H et al (1983) A solid-phase enzyme-linked immunospot (ELISPOT) assay for enumeration of specific antibody-secreting cells. *J Immunol Methods* 65:109–121
2. Saletti G, Çuburu N, Yang JS et al (2013) Enzyme-linked immunospot assays for direct ex vivo measurement of vaccine-induced human humoral immune responses in blood. *Nat Protoc* 8:1073–1087. <https://doi.org/10.1038/nprot.2013.058>
3. Wulf M, Hoehn P, Trinder P (2009) Identification and validation of T-cell epitopes using the IFN- γ ELISPOT assay. *Methods Mol Biol* 524:439–446. https://doi.org/10.1007/978-1-59745-450-6_32
4. Sedegah M (2015) The ex vivo IFN- γ enzyme-linked immunospot (ELISpot) assay. *Methods Mol Biol* 1325:197–205. https://doi.org/10.1007/978-1-4939-2815-6_16
5. Hagen J, Zimmerman R, Goetz C et al (2015) Comparative multi-donor study of IFN γ secretion and expression by human PBMCs using ELISPOT side-by-side with ELISA and flow cytometry assays. *Cell* 4:84–95. <https://doi.org/10.3390/cells4010084>
6. Pike KA, Hui C, Krawczyk CM (2016) Detecting secreted analytes from immune cells: an overview of technologies. *Methods Mol Biol* 1458:111–124. https://doi.org/10.1007/978-1-4939-3801-8_9

7. Tzeng SJ (2016) The isolation, differentiation, and quantification of human antibody-secreting B cells from blood: ELISpot as a functional readout of humoral immunity. *J Vis Exp*. <https://doi.org/10.3791/54582>
8. Ahlén G, Frelin L (2016) Methods to evaluate novel hepatitis C virus vaccines. *Methods Mol Biol* 1403:221–244. https://doi.org/10.1007/978-1-4939-3387-7_11
9. Fiore-Gartland A, Manso BA, Friedrich DP et al (2016) Pooled-peptide epitope mapping strategies are efficient and highly sensitive: an evaluation of methods for identifying human T cell epitope specificities in large-scale HIV vaccine efficacy trials. *PLoS One* 11:e0147812. <https://doi.org/10.1371/journal.pone.0147812>
10. Crotty S, Aubert RD, Glidewell J et al (2004) Tracking human antigen-specific memory B cells: a sensitive and generalized ELISPOT system. *J Immunol Methods* 286:111–122
11. Weiss GE, Ndungu FM, McKittrick N et al (2012) High efficiency human memory B cell assay and its application to studying *Plasmodium falciparum*-specific memory B cells in natural infections. *J Immunol Methods* 375(1–2):68–74. <https://doi.org/10.1016/j.jim.2011.09.006>
12. Tzeng SJ, Li WY, Wang HY (2015) FcγRIIB mediates antigen-independent inhibition on human B lymphocytes through Btk and p38 MAPK. *J Biomed Sci* 22:87–98. <https://doi.org/10.1186/s12929-015-0200-9>
13. Wiese J, Didwania A, Kerzner R et al (1997) Use of different anticoagulants in test tubes for analysis of blood lactate concentrations: Part 2. Implications for the proper handling of blood specimens obtained from critically ill patients. *Crit Care Med* 25:1847–1850
14. Heine G, Sims GP, Worm M et al. (2011) Isolation of human B cell populations. *Curr Protoc Immunol* Chapter 7, Unit 7.5. doi:<https://doi.org/10.1002/0471142735.im0705s94>



Dual immuno-renal targeting of 7-benzylidenenaltrexone alleviates lupus nephritis via FcγRIIB and HO-1

Tsung-Chih Tseng¹ · Duen-Yi Huang¹ · Liang-Chuan Lai^{2,3} · Haw Hwai¹ · Yi-Wen Hsiao³ · Jyun-Pei Jhou¹ · Eric Y. Chuang^{3,4} · Shiang-Jong Tzeng¹

Received: 21 September 2017 / Revised: 18 December 2017 / Accepted: 5 February 2018 / Published online: 5 March 2018
© Springer-Verlag GmbH Germany, part of Springer Nature 2018

Abstract

Known as a selective $\delta 1$ opioid receptor (DOR1) antagonist, the 7-benzylidenenaltrexone (BNTX) is also a DOR1-independent immunosuppressant with unknown mechanisms. Here we investigated if BNTX could be beneficial for diseased MRL/lpr lupus mice. We treated mice with 0.5, 2, 5 or 10 mg/kg/day of BNTX for 2 weeks. At as low as 2 mg/kg/day, BNTX significantly improved splenomegaly and lymphadenopathy. Notably, B cell numbers, particularly autoreactive plasma cells, were preferentially reduced; moreover, BNTX enhanced surface expression of FcγRIIB, an immune complex (IC)-dependent apoptotic trigger of B cells. Consequently, serum autoantibody concentrations were significantly decreased, leading to diminished glomerular IC deposition and renal fibrosis, thereby improving proteinuria. Microarray and pathway analyses revealed heme oxygenase-1 (HO-1) and p38 MAPK as key mediators of BNTX-induced upregulation of FcγRIIB. Moreover, HO-1 expression was also induced by BNTX via p38 MAPK at renal proximal tubules to further cytoprotection. Taken together, we demonstrate that BNTX can alleviate lupus nephritis by reducing autoreactive B cells via FcγRIIB and by augmenting renal protection via HO-1. Accordingly, we propose a new strategy to treat lupus nephritis via such a dual immuno-renal targeting using either a single agent or combined agents to simultaneously deplete B cells and enhance renal protection.

Key messages

- 7-Benzylidenenaltrexone (BNTX) alleviates lupus nephritis in diseased MRL/lpr mice.
- BNTX reduces autoreactive plasma cell numbers and serum autoantibody titers.
- BNTX upregulates FcγRIIB levels via p38 MAPK and HO-1 to reduce B cell numbers.
- Reduction of immune complex deposition and fibrosis by BNTX improves proteinuria.
- BNTX induces HO-1 via p38 MAPK to enhance protection of renal proximal tubules.

Keywords 7-Benzylidenenaltrexone (BNTX) · Lupus nephritis · FcγRIIB · B cells · Heme oxygenase-1 (HO-1) · p38 MAPK

Electronic supplementary material The online version of this article (<https://doi.org/10.1007/s00109-018-1626-9>) contains supplementary material, which is available to authorized users.

✉ Shiang-Jong Tzeng
sjtzeng@ntu.edu.tw

¹ Graduate Institute of Pharmacology, National Taiwan University, Taipei, Taiwan

² Graduate Institute of Physiology, National Taiwan University, Taipei, Taiwan

³ Bioinformatics and Biostatistics Core, Center of Genomic Medicine, College of Medicine, National Taiwan University, Taipei, Taiwan

⁴ Graduate Institute of Biomedical Electronics and Bioinformatics, National Taiwan University, Taipei, Taiwan

Introduction

The opioid system consists of three classical naloxone-sensitive receptors— μ -opioid receptors (MORs), κ -opioid receptors (KORs) and δ -opioid receptors (DORs), and a naloxone-insensitive receptor—the non-classical nociceptin/orphanin FQ receptors. Opioids have well-known effects on analgesia and addiction and other complex pharmacological properties [1]. For example, opioids, e.g. morphine, are immunosuppressants, of which inhibitory effects are attributed to the MORs and KORs rather than DORs [2]. Distinct from the modulators of MORs and KORs, DOR agonists actually stimulate immune function [2–4], whereas DOR antagonists, e.g. BNTX and naltrindol, suppress immune cells [5]. Based on the differences of pharmacological attributes, DORs can be classified into DOR1 and DOR2 subtypes. However, only a receptor gene, termed *Oprd1*, has been identified in mammals and no evidence of splicing variants of DOR transcripts exists [6]. Additionally, in some cases DOR1 and DOR2 antagonists actually have entirely different physiological effects. For instance, unlike BNTX, the DOR2 antagonist naltriben is not immunosuppressive [5]. Nevertheless, the clear functional dichotomy between agonists and antagonists of DORs on the immune system indicates their therapeutic potentials for immunological disorders.

BNTX was originally synthesized as a selective DOR1 antagonist in 1992 [7]. Shortly, data from human peripheral blood mononuclear cells (PBMCs) revealed the inhibitory effects of BNTX on cell proliferation and cytokine production [5]. Intriguingly, however, BNTX remains suppressive to splenocytes isolated from the DOR-deficient mice, thereby indicating a DOR-independent inhibition [8]. Since the turn of the century, the cellular targets and molecular mechanisms of BNTX-induced immunosuppression have not been addressed.

To explore the therapeutic potential of BNTX for autoimmune diseases, we adopted MRL/lpr lupus mice to investigate whether BNTX can confer beneficial effects to lupus nephritis. The MRL/lpr mice were born with a spontaneous loss-of-function mutation in *Fas* gene, leading to a breach of peripheral tolerance in T cells and development of a lupus disease driven by Th1 helper T cells [9]. Because the MRL/lpr mouse strain displays the cardinal pathology of lupus nephritis, it is commonly used as a pre-clinical model of systemic lupus erythematosus (SLE) to evaluate drug efficacy on the disease activity. Of importance, the present available therapies are unsatisfactory in reversing or delaying the progression of lupus nephritis, in which glomeruli become inflamed owing to deposition of excess immune complexes (ICs) from circulation or direct autoantibody deposition. Without effective treatment, chronically inflamed glomeruli gradually become fibrotic followed by aggravation of proteinuria and progression to renal failure [10]. Such an unmet medical need prompts

researchers to develop new, effective and safe therapeutics for SLE patients.

Materials and methods

Reagents

BNTX and Abs specific to p38 MAPK and ERK were obtained from Santa Cruz Biotechnology (Dallas, TX, USA). Naloxone, naltrindole, tin protoporphyrin IX and dimethyl sulfoxide (DMSO) were purchased from Selleckchem (Houston, TX, USA). SB203580 and U0126 were acquired from Calbiochem (San Diego, CA, USA). F(ab')₂ fragment of goat anti-mouse IgG and μ chain-specific goat anti-mouse IgM were purchased from Jackson ImmunoResearch Laboratories (West Grove, PA, USA). Mouse monoclonal Abs: CD19-PE-Cy7 (clone 1D3), CD16/32 (clone 2.4G2), CD138-BV421 (clone 281-2), CD11b-PerCP-Cy5.5 (clone M1/70), CD11c-AlexaFluor 700 (clone HL3) and GL7-AlexaFluor 647 (clone GL7), and 7-aminoactinomycin D (7-AAD) were acquired from BioLegend (San Diego, CA, USA). Mouse IgG isotypes and IgM were obtained from SouthernBiotech (Birmingham, AL, USA). Abs specific to phospho-p38 MAPK (Thr180/Tyr182), phospho-ERK (Thr202/Tyr204) and β actin were purchased from Cell Signaling Technology (Danvers, MA, USA). Ninety six-well MultiScreen HTS filter plates were acquired from Merck Millipore (Billerica, MA, USA). Blood lancet was obtained from MEDipoint, Inc. (Mineola, NY, USA). Vectastain ABC kits were purchased from Vector Laboratories (Burlingame, CA, USA). Urine analysis strips were acquired from Macherey-Nagel (Duren, Germany).

Mice

The MRL/lpr mice were obtained from Jackson Laboratory and maintained in specific pathogen-free conditions at the Center for Laboratory Animals of College of Medicine of National Taiwan University. The protocols for animal experiments conformed to the guidelines approved by the Institutional Animal Care and Use Committee (IACUC) of College of Medicine of National Taiwan University. Full-blown female mice of 17 weeks old with the severity of proteinuria (++/+++ on urinalysis strip tests) were randomly divided into groups for treatment with vehicle (PBS) or a defined dose of BNTX for 14 days via intra-peritoneal route. Mice were sacrificed on the following day after the last treatment.

Enzyme-linked immunosorbent assay (ELISA)

To detect anti-dsDNA autoantibodies, 50 µg/ml methylated BSA (Sigma-Aldrich) was added into 96-well plates to incubate at 37 °C for 1 h, followed by overlaying 10 µg/ml of calf thymus DNAs (Invitrogen, Carlsbad, CA, USA) for additional incubation at 4 °C overnight. Mouse serum samples were diluted (1:100) to measure concentrations of anti-dsDNA IgM and IgG. Mouse IgM

and IgG were included to generate standard curves for quantification. Horseradish peroxidase (HRP)-conjugated Fcγ-specific rabbit anti-mouse IgG and µ-specific goat anti-mouse IgM Abs were used for detection. Plates were scanned and read at OD₄₅₀ and OD₅₇₀ nm wavelengths using an ELISA reader (BioTek, Winooski, VT, USA). The difference of OD readings (OD₄₅₀ minus OD₅₇₀) of each sample was plotted against standard curves for calculation of concentration.

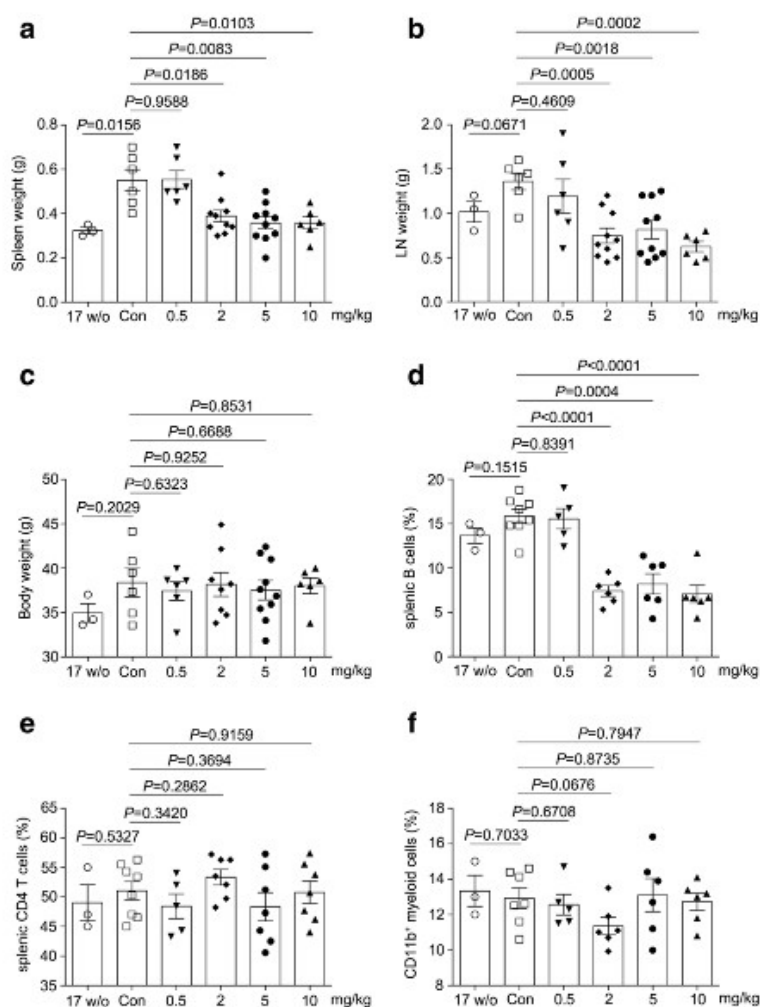


Fig. 1 BNTX treatment improved splenomegaly and lymphadenopathy in MRL/lpr mice with full-blown disease. MRL/lpr mice of 17 weeks old (w/o) were treated with vehicle- ($n = 6$, open circle) or a defined dose (0.5, 2, 5 or 10 mg/kg/day, $n = 6$ –10, closed symbols) of BNTX. Before and after treatments, the weights of **a** spleen ($P = 0.9588, 0.0186, 0.0083, 0.0103$), and **b** mesenteric lymph nodes ($P = 0.4609, 0.0005, 0.0018, 0.0002$) and **c** the body weight ($P = 0.6323, 0.9252, 0.6688, 0.8531$) of control (vehicle) versus BNTX-treated (0.5, 2, 5 or 10 mg/kg/day) mice were measured and compared. The percentages of **d** CD19⁺ B cells ($P = 0.8391, < 0.0001, 0.0004, < 0.0001$), **e** CD3⁺CD4⁺ T cells ($P = 0.342, 0.2862, 0.3694, 0.9159$) and **f** CD11b⁺ myeloid cells ($P = 0.6708,$

0.676, 0.8735, 0.7947) in splenocytes were quantified and compared between vehicle- ($n = 6$ open circle) and BNTX-treated (0.5, 2, 5 or 10 mg/kg/day, $n = 5$ –6) groups. Mice of 17 weeks of age ($n = 3$) were included as a pre-treatment control in comparisons. The results of group comparisons were illustrated with bar graphs and statistical analyses were shown as mean \pm SEM. Representative symbols of each group: 17 w/o control (open circles), 19 w/o vehicle-treated control (open squares), BNTX 0.5 mg/kg (closed down triangles), 2 mg/kg (closed diamonds), 5 mg/kg (closed circles) and 10 mg/kg (closed up triangle). Asterisks indicate significant differences of * $P < 0.05$, ** $P < 0.01$, *** $P < 0.001$ between groups

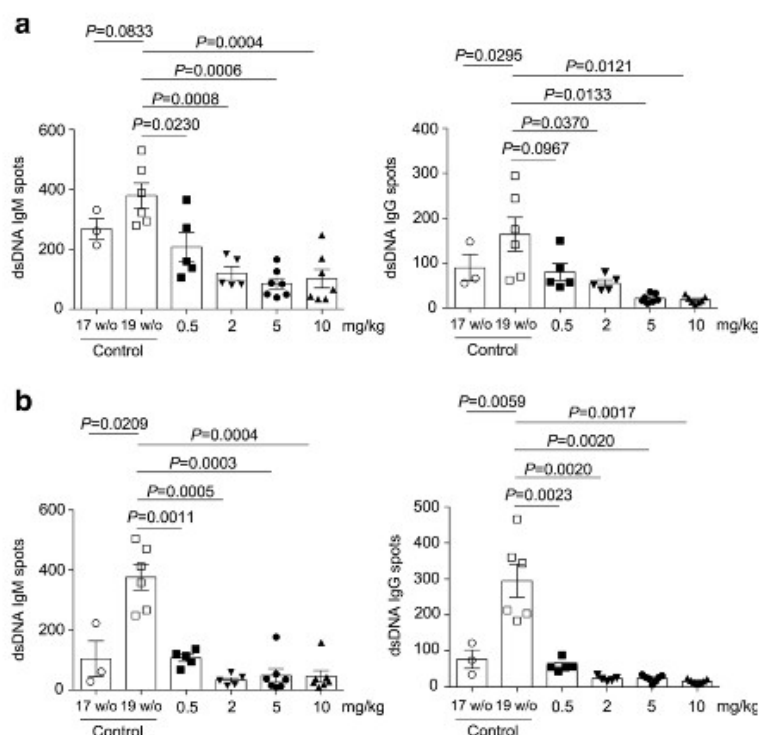


Fig. 2 BNTX treatment decreased PC numbers in the spleen and bone marrow of MRL/*lpr* mice. ELISpot assays were performed to quantify the numbers of **a** dsDNA-IgM (left panel, $P=0.023$, 0.0008 , 0.0006 and 0.0004) and dsDNA-IgG PCs (right panel, $P=0.0967$, 0.037 , 0.0133 and 0.0121) in splenocytes (3.2×10^5 cells) as well as **b** dsDNA-IgM (left panel, 3.2×10^5 cells; $P=0.0011$, 0.0005 , 0.0003 and 0.0004) and dsDNA-IgG PCs (right panel, 6.4×10^5 cells; $P=0.0023$, 0.002 , 0.002 and 0.0017) in the bone marrow of vehicle- versus BNTX-treated MRL/

lpr (0.5, 2, 5, 10 mg/kg/day) mice, respectively. Mice of 17 weeks of age ($n=3$) were included as a pre-treatment control in comparisons. Representative symbols of each group: 17 w/o before treatment, open circles ($n=3$); 19 w/o vehicle-treated control group, open squares ($n=6$); BNTX-treated groups: 0.5 mg/kg (closed squares, $n=5$), 2 mg/kg (closed down triangles, $n=5$), 5 mg/kg (closed circles, $n=7$) and 10 mg/kg (closed up triangles, $n=7$)

Flow cytometry

Single-cell suspension of total unfractionated splenocytes ($1-2 \times 10^6$ cells/mouse) were stained with CD32-FITC, CD138-

BV421, CD19-PE-Cy7, CD11b-PerCP-Cy5.5, CD11c-AlexaFluor 700, and GL7-AlexaFluor 647 mAbs to quantify cell subsets by LSRFortessa flow cytometer (BD Biosciences). Dead cells were excluded by 7-AAD staining. BJAB B cells

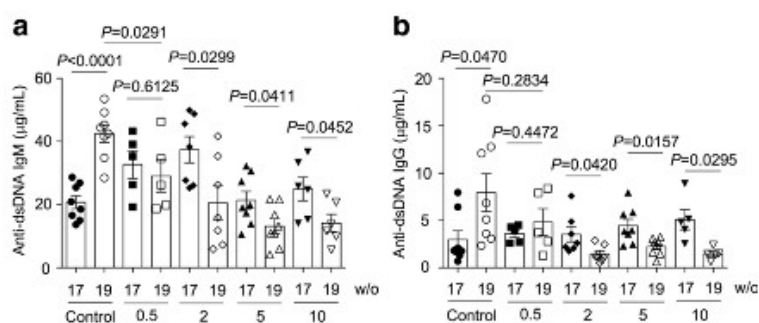
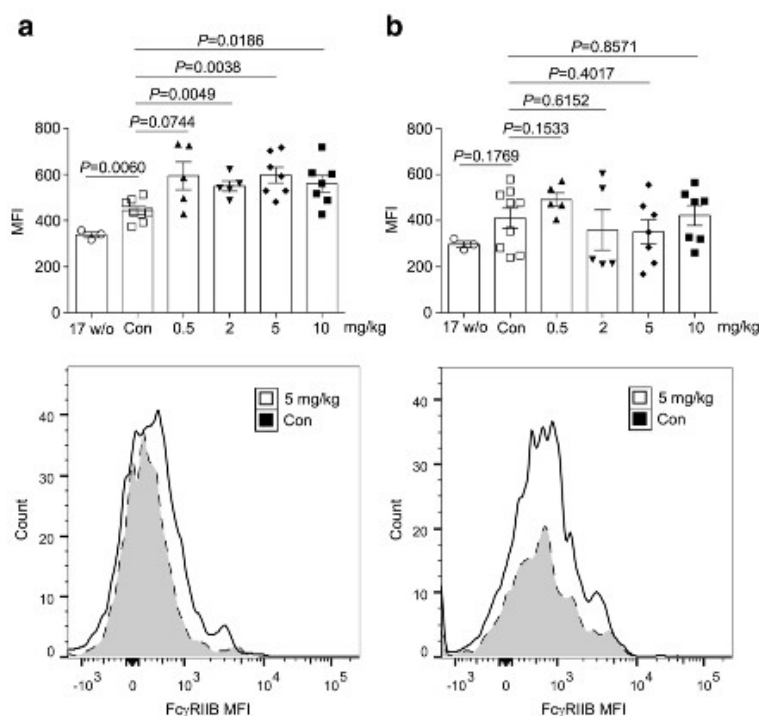


Fig. 3 BNTX treatment reduced serum titers of autoantibodies in MRL/*lpr* mice. Before (17 weeks old) and after (19 weeks old) vehicle or BNTX (0.5, 2, 5, 10 mg/kg/day) treatments, serum levels of **a** anti-dsDNA IgM ($P<0.0001$, 0.6125 , 0.0299 , 0.0411 and 0.0452) and **b** anti-dsDNA IgG ($P=0.047$, 0.4472 , 0.042 , 0.0157 and 0.0295) of

vehicle- ($n=8$) and BNTX-treated (0.5, 2, 5, 10 mg/kg/day, $n=5-8$) MRL/*lpr* mice were determined by ELISAs. Mouse serum samples were 100-fold diluted with PBS for anti-dsDNA IgM and IgG, respectively. Control mice of 17 weeks of age ($n=3$) before treatment were included for comparisons

Fig. 4 BNTX treatment up-regulated the surface expression level of FcγRIIB of B cells in MRL/lpr mice. Bar graphs of the expression levels (MFIs) of FcγRIIB were illustrated to compare **a** CD19⁺ B cells ($P = 0.0744, 0.0049, 0.0038$ and 0.0186) and **b** CD11b⁺ myeloid cells ($P = 0.1533, 0.6152, 0.4017$ and 0.8571) of control ($n = 8-9$) versus BNTX-treated (0.5, 2, 5, 10 mg/kg/day, $n = 5-7$) groups, respectively. Representative plots were illustrated at lower panels



were treated with vehicle (DMSO) or indicated concentrations of BNTX for 24 h and stained with CD32-FITC (clone FLI8.26, BD Biosciences) and 7-ADD for cytometric analysis. The percentages of immune cell subsets and mean fluorescence intensity (MFI) of the surface FcγRIIB levels were analyzed and quantified by FlowJo, version 10 (FLOWJO, LLC, Ashland, OR, USA). Single-cell suspension of total bone marrow cells was prepared by mechanical dispersion of marrow extracted from both femur bones of mice.

Enzyme-linked immunospot (ELISpot) assay

ELISpot assays were performed as previously described [11]. Briefly, splenocytes and bone marrow cells ($3.2-6.4 \times 10^5$ /well) were serially diluted (2-fold) for detection of IgG and IgM dsDNA plasma cells (PCs), were incubated at 37 °C overnight. After washes with PBS-T, HRP-conjugated goat Abs specific to μ or γ chain (1:5000) were added for 1-h incubation at room temperature. Spots were developed by addition of 50 μ l/well of 3-amino-9-ethylcarbazole substrate (BD Biosciences) to incubate for 20–30 min. Plates were scanned to enumerate spots using the C.T.L. S6 Universal Analyzer.

Immunohistochemistry examination

Four μ m thick of paraffin-embedded kidney sections were incubated with rabbit polyclonal Abs specific to

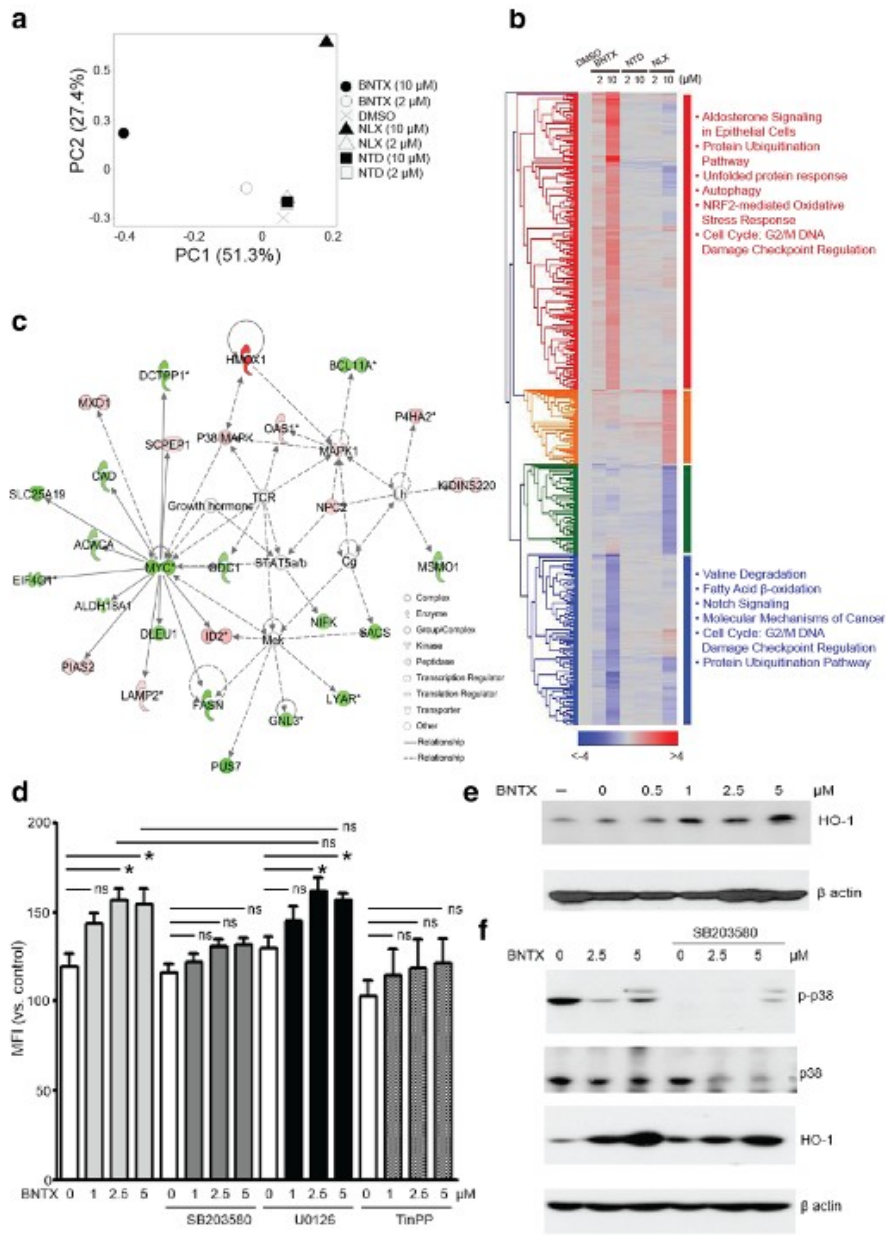
mouse HO-1 (CUSABIO Biotech Co., Baltimore, MD, USA) at 4 °C overnight. After washes, HRP-conjugated anti-rabbit Abs were added for 1-h incubation at room temperature. Slides were washed thoroughly before adding the 3,3'-diaminobenzidine substrates for development. Sections were counterstained with hematoxylin before mounting. An Axioplan 2 light microscope (Zeiss, Oberkochen, Germany) was used to photograph sections. The degrees of IC deposition in the renal glomeruli were determined by staining with HRP-conjugated goat anti-mouse IgM at room temperature for 1 h. Collagen fibers were stained by a Masson's trichrome staining kit (Sigma-Aldrich) to assess fibrosis in kidneys. MetaMorph software (Molecular Devices, Sunnyvale, CA, USA) was used to quantify areas of interest in tissue sections.

Urine biochemistry analysis

Urine creatinine was measured by Roche Cobas C111 chemistry analyzer (Roche Diagnostics). Bradford protein assay was used to measure the protein concentrations of 24-h urine samples from MRL/lpr mice before and after treatments.

Immunoblotting

BJAB B cells and NRK-52E cells (ATCC CRL-1571, provided by Dr. Shuei-Liong Lin) were cultured in



RPMI 1640 and DMEM, respectively, both of which were supplemented with 10% fetal calf serum. BJAB B cells (2×10^6 /ml) and NRK-52E cells (90% confluence) were treated with indicated concentrations of BNTX for 24 h. Cells were lysed with RIPA buffer for SDS-PAGE and subject to western blotting using Abs specific to HO-1 (CUSABIO), p38 MAPK, phospho-p38 MAPK, ERK, phospho-ERK and β actin, respectively. ImageJ software was used to quantify the relative abundance of respective proteins by normalization to β actin proteins.

RNA extraction and microarray analysis

BJAB cells (2×10^6 /ml) with treated with 2 or 10 μM of BNTX, naltrindol and naloxone for 9 h. Total RNAs of each sample were extracted with Trizol (Life Technologies, Carlsbad, CA, USA). The RNA concentration and quality were determined using a NanoDrop ND-1000 spectrophotometer (NanoDrop Technologies, Wilmington, DE, USA) and an Agilent 2100 Bioanalyzer (Agilent Technologies, Palo Alto, CA, USA) to calculate the RNA integrity number (RIN). Total

Fig. 5 BNTX treatment activated p38 MAPK and HO-1 proteins to upregulate expression levels of FcγRIIB in B cells. **a** BJAB B cells (2×10^6 /ml) were treated with vehicle (DMSO), 2 or 10 μM of BNTX, naltrindole (NTD) and naloxone (NLX), respectively. To analyze the intensity distribution of microarray results, PCA was conducted to compare global gene expression profiles among samples. **b** DEGs were identified for further clustering by calculating their euclidean distances and then visualized by heatmap. Significant ingenuity canonical pathways in clusters were depicted. Blue color represents downregulation while red color indicates upregulation. Different color depths reveal the genes' expression values. **c** IPA was performed for network identification of DEGs of BNTX-responsive genes. Red color represents upregulated genes while blue color indicates down-regulated genes of datasets of BNTX. Molecules highlighted in white from IPA database are highly connected with DEGs. **d** Surface expression levels of FcγRIIB of BJAB B cells in the absence (vehicle control) versus presence of 1, 2.5 and 5 μM of BNTX for 24 h, respectively. Bar graphs of cytometric analyses on the expression levels of FcγRIIB (MFI vs. control) of control versus BNTX-treated cells ($P=0.053$, 0.013 and 0.0267). Expression levels of surface FcγRIIB of BJAB B cells with the addition of 10 μM of SB203580 ($P=0.6859$, 0.4153 and 0.8571), U0126 ($P=0.2114$, 0.0265 and 0.0178) or tin protoporphyrin IX (TinPP) ($P=0.5475$, 0.4638 and 0.3379) with or without 1, 2.5 and 5 μM of BNTX, respectively, for 24 h were compared. **e** BJAB B cells treated with either vehicle (DMSO) or BNTX (0.5, 1, 2.5 and 5 μM) for 24 h were subject to immunoblot analysis using Abs specific to HO-1 and β actin, respectively. A representative blot from three independent experiments was shown. **f** Western blotting results of BNTX-treated (0, 2.5 and 5 μM) BJAB B cells in the absence or presence of SB203580 (10 μM) for 24 h using indicated Abs. Representative results from three independent experiments were shown

RNA samples with $A_{260}/A_{280} = 1.8$ – 2.0 were assessed for RNA integrity. Samples with $RIN > 9$ were processed for gene expression profiling. The RNA concentration of samples was adjusted to the 50 ng/μl with DEPC-treated H_2O . A total of 500 ng RNAs per sample were converted to double-stranded cDNA, followed by an amplification step with in vitro transcription to generate biotin-labeled cRNA (Ambion, Austin, TX, USA). A total of 1.5 g cRNA was subsequently hybridized to Illumina Human HT-12 v4.0 beadchip (Illumina, San Diego, CA, USA) at 58 °C at the Illumina Bead Station. After hybridization for 14–20 h, the BeadChip was stained by Cy3 and washed. The intensities of the bead's fluorescence were detected by the Illumina Bead Array Reader, and the results were analyzed using GenomeStudio v2010.1 software. The R software with Bioconductor packages was used for data analysis and data visualization. Raw intensity data were preprocessed by log₂ transformation and then normalized by quantile normalization using 'limma' package of R. Normalized values of each sample were further divided with the values of control sample (DMSO treated cells). The differentially expressed genes (DEGs) were defined with absolute log₂ fold-change value ≥ 1 . The similarity of the composition of each sample was analyzed by principal component analysis (PCA) using 'ggfortify' package of R. A hierarchical clustering analysis was applied to identify the expression pattern of DEGs and the results were visualized as a heatmap

using 'pheatmap' package of R. The canonical pathway was conducted by ingenuity pathway analysis (IPA) program and analyzed based on ingenuity knowledge base (content version: 39480507; release date: 2017-09-14). Fisher's exact test was used to determine the enrichment of differentially expressed proteins in a given canonical pathway.

Statistics

Statistical analysis was performed using two-tailed unpaired Student's *t* test to compare groups with Welch's correction in the presence of unpaired variance. Graphs and histograms were plotted using GraphPad Prism 6.0 (GraphPad Software, Inc., San Diego, CA, USA). All results were shown as mean \pm standard error (SEM). * $P < 0.05$, ** $P < 0.01$, and *** $P < 0.001$ denote degrees of statistical significance between compared groups. NS indicates no significance.

Results

BNTX treatment improves splenomegaly and lymphadenopathy in MRL/lpr lupus mice with full-blown disease

Because of entirely unknown efficacy of BNTX in animals, various doses were applied to female MRL/lpr mice of 17 weeks old when serum anti-dsDNA titers and proteinuria were evident [9]. Mice were treated with either vehicle (PBS) or BNTX at 0.5, 2, 5, or 10 mg/kg/day for 2 weeks by intraperitoneal route. As shown in Fig. 1a, BNTX treatment significantly improved splenomegaly at as low as 2 mg/kg/day ($P=0.0186$), but not 0.5 mg/kg/day ($P=0.9586$), compared with mice treated with vehicle. Likewise, 2 mg/kg/day ($P=0.005$), but not 0.5 mg/kg/day ($P=0.4609$), of BNTX treatment significantly reduced lymphadenopathy compared with control mice (Fig. 1b). No significant changes of the body weight of mice were observed up to 10 mg/kg/day of BNTX treatment, suggesting a considerable dose range for therapy (Fig. 1c). We next examined whether BNTX treatment altered the numbers of immune cells in the spleen. While B cells continued to expand in vehicle-treated mice, the percentages of CD19⁺ B cells were decreased ~30–50% after treatment with 2 to 10 mg/kg/day of BNTX (Fig. 1d; $P=0.8391$, < 0.0001 , 0.0004 and < 0.0001 for 0.5, 2, 5 and 10 mg/kg/day, respectively). By contrast, the percentages of CD3⁺CD4⁺ T cells ($P=0.342$, 0.2862, 0.3694 and 0.9159) and CD11b⁺ myeloid cells ($P=0.6708$, 0.0676, 0.8735 and 0.7947) were not significantly altered by various doses (0.5, 2, 5 and 10 mg/kg/day) of BNTX treatment compared with control mice (Fig. 1e, f).

BNTX treatment reduces splenic and bone marrow autoreactive PC numbers and decreases serum autoantibody concentrations in MRL/lpr mice

Because B cells were selectively reduced after BNTX treatment (Fig. 1d), we examined possible alteration of the numbers of autoreactive PCs, which in lupus are responsible for secreting autoantibodies to form excess immune complexes (ICs) to deposit in tissues. We used the ELISpot assay for its great sensitivity and accuracy to quantify the numbers of PCs [11]. In control mice, the numbers of splenic anti-dsDNA IgM ($P = 0.0833$) and IgG ($P = 0.0295$) PCs continued to increase substantially (Fig. 2a). In contrast, after 0.5, 2, 5 or 10 mg/kg/day of BNTX treatment, we found a remarkable more than 50% decrease of the numbers of splenic anti-dsDNA IgM dose-dependently compared with vehicle-treated mice ($P = 0.023$, 0.0008, 0.0006 and 0.0004) (Fig. 2a). To a similar extent, the numbers of anti-dsDNA IgG ($P = 0.0967$, 0.0037, 0.0133 and 0.0121) decreased after BNTX treatment (0.5, 2, 5 and 10 mg/kg/day) as compared to vehicle-treated mice (Fig. 2a). Importantly, BNTX treatment reduced the numbers of anti-dsDNA PCs not only in the spleen but also in the bone marrow, where long-lived PCs reside [12]. In the bone marrow, the numbers of anti-dsDNA IgM ($P = 0.0011$, 0.0005, 0.0003 and 0.0004) and IgG ($P = 0.0023$, 0.002, 0.002 and 0.0017) PCs significantly declined in BNTX-treated (0.5, 2, 5 and 10 mg/kg/day) mice as compared to control mice, respectively (Fig. 2b).

We next examined the consequence of reduced numbers of anti-dsDNA PCs on the autoantibody production following various doses (0.5 to 10 mg/kg/day) of BNTX treatment. Indeed, the serum concentrations of anti-dsDNA IgM ($P = 0.6125$, 0.0299, 0.0411, 0.0452) and IgG ($P = 0.4472$, 0.042, 0.0157, 0.0295) autoantibodies were decreased by ~50% after 2, 5 and 10 mg/kg/day of BNTX treatment in comparison to control mice, respectively (Fig. 3a, b). In vehicle-treated mice, the serum levels of anti-dsDNA IgM ($P < 0.0001$) and IgG ($P = 0.047$) continued to increase as the disease progressed (Fig. 3a, b).

BNTX treatment upregulates the surface expression level of FcγRIIB in B cells in MRL/lpr mice

FcγRIIB is an essential negative regulator of B cells. We and others have shown that FcγRIIB can mediate apoptosis of B cells induced by ICs particularly in the PCs [13–16]. We then investigated the potential contribution of FcγRIIB in the reduction of PC numbers in response to BNTX treatment. Except for 0.5 mg/kg/day ($P = 0.0744$), treatment with 2, 5 or 10 mg/kg/day ($P = 0.0049$, 0.0038 and 0.0186) of BNTX enhanced the surface expression of FcγRIIB in splenic CD19⁺ B cells by ~20–30% as compared to control MRL/lpr mice (Fig. 4a).

Although CD11b⁺ myeloid cells also express FcγRIIB, their expression levels were not significantly altered after various doses of BNTX treatment (Fig. 4b).

BNTX treatment induces HO-1 gene expression and regulatory networks distinct from naltrindole and naloxone

In addition to BNTX, naltrindole, a non-selective DOR antagonist, and naloxone, a pan-opioid receptor antagonist, can not only antagonize DORs but also confer immunosuppressive effects [5, 8]. Moreover, BNTX, naltrindole and naloxone remain immunosuppressive to splenocytes isolated from DOR-deficient mice [8]. We then decided to unravel the mechanisms of BNTX and to determine if BNTX induced specific genes distinct from naltrindole and naloxone to inhibit B cells. Because continuous treatment with BNTX for 2 weeks reduced B cells by FcγRIIB-mediated apoptosis in the spleen and bone marrow might affect retrieval of RNAs of interest (Figs. 1, 2 and 3), we decided to perform microarray analysis using BJAB B cells, which is a commonly used human B cell line, to compare the gene expression profiles of BNTX, naltrindole and naloxone. Specific genes responsible for BNTX action could then be identified for further investigation. Total RNA samples of BJAB B cells in response to 2 or 10 μM of BNTX, naltrindole and naloxone were separately collected and purified to perform microarray profiling of global gene expression. Responsive genes with concentration-dependent changes in expression were further analyzed to identify drug-specific gene signatures. To our surprise, the PCA showed virtually no similarities in DEG profiles of B cells treated with BNTX, naltrindole and naloxone, respectively (Fig. 5a). Moreover, clustering analysis of their gene expression profiles showed distinct groups of upregulated and downregulated genes (Fig. 5b and Supplemental Tables 1, 2). Notably, HO-1 transcripts were abundantly induced up to 4 folds among the genes specifically in response to BNTX (Supplemental Table 3). When we used ingenuity pathway analysis (IPA) to classify relevant pathways and regulatory networks of differentially expressed genes, HO-1 was predicted to independently interact with p38 MAPK and MAPK1 (a. k. a. ERK2, extracellular signal-regulated kinase-2) (Fig. 5c). HO-1 upregulation by BNTX was also linked to downregulation of several genes in the c-myc regulatory network (Fig. 5c).

HO-1 and p38 MAPK promote upregulation of FcγRIIB in response to BNTX in B cells

To validate the findings from microarray experiments, we performed flow cytometry to investigate the influence of p38 MAPK, ERK and HO-1 on the expression level of FcγRIIB in B cells. As shown in Fig. 5d, BNTX-mediated

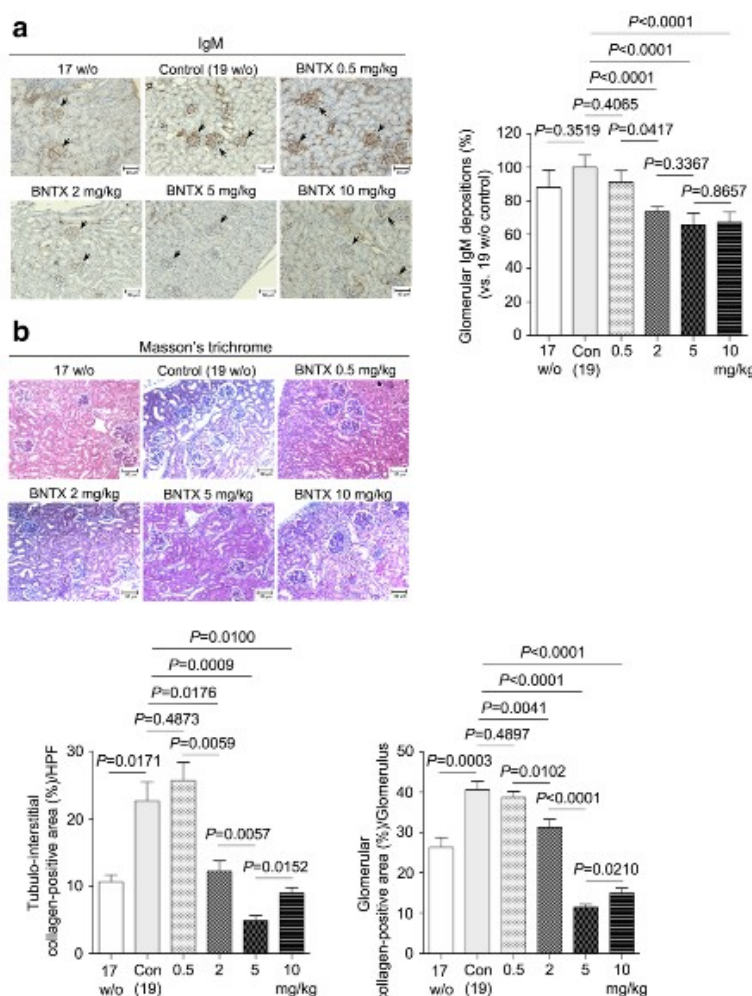


Fig. 6 BNTX treatment decreased IC deposition, reduced fibrosis and improved proteinuria in diseased MRL/lpr mice. **a** Glomerular deposition of IgM ICs in renal sections of control versus BNTX-treated (0.5, 2, 5, 10 mg/kg/day) mice was examined. Control mice of 17 weeks of age ($n = 3$) before treatment were included for comparisons. Three or four mouse kidneys of each group were analyzed. (Right panel) Bar graphs showed comparisons of control (vehicle-treated, 19 w/o) versus 0.5 mg/kg/day ($P = 0.4065$), 2 mg/kg/day ($P < 0.0001$), 5 mg/kg/day ($P < 0.0001$) and 10 mg/kg/day ($P < 0.0001$) of BNTX-treated mice before and after treatment. **b** Kidneys from control ($n = 4$) and BNTX-treated ($n = 3-4$) MRL/lpr mice were sectioned and stained with Masson's trichrome solutions. Representative images (magnification $\times 100$) of renal sections from control (17 w/o and vehicle-treated) and BNTX-treated mice were illustrated. Scale bars, 50 μm . Intensities of collagen deposition (stained blue) in the glomerular and tubulo-interstitial areas were quantified and averaged in each high-power field

(HPF) (> 5 glomeruli/HPF and > 5 HPFs/section/mouse). Quantifications of tubulo-interstitial and glomerular stained regions of control (19 w/o) versus 0.5 mg/kg/day ($P = 0.4873$ and 0.4897), 2 mg/kg/day ($P = 0.0176$ and 0.0041), 5 mg/kg/day ($P = 0.0009$ and < 0.0001) and 10 mg/kg/day ($P = 0.01$ and < 0.0001) of BNTX-treated mice were compared and illustrated as bar graphs. **c** Urinary protein/creatinine ($\mu\text{g}/\text{mg}$) ratios of control ($n = 6$) versus BNTX-treated (0.5, 2, 5, 10 mg/kg/day, $n = 5-8$) mice, respectively. Bar graphs illustrated alterations of severity of proteinuria between control ($P = 0.002$), 0.5 mg/kg/day ($P = 0.3136$), 2 mg/kg/day ($P = 0.0023$), 5 mg/kg/day ($P < 0.0001$) and 10 mg/kg/day ($P = 0.0059$) of BNTX-treated mice. **d** Vehicle (dash line, $n = 14$) and 5 mg/kg/day of BNTX (solid line, $n = 10$) treated mice were monitored for survival for a total of 5 weeks starting the 2 weeks of treatment. The survival rates of mice between two groups were plotted and compared ($P = 0.0442$) using log-rank (Mantel-Cox) test for statistical significance

upregulation of Fc γ RIIB levels was significantly impaired by inhibitors specific to either p38 MAPK (SB203580) or HO-1 (tin-protoporphyrin IX), but not by ERK inhibitor (U0126) in BJAB B cells. In concordance with these findings, BNTX induced expression of HO-1 levels in a

concentration-dependent manner (Fig. 5e). Moreover, results from western blotting showed that p38 MAPK inhibitor reduced the level of HO-1 proteins induced by BNTX (Fig. 5f). These results demonstrate that BNTX upregulates HO-1 via p38 MAPK.

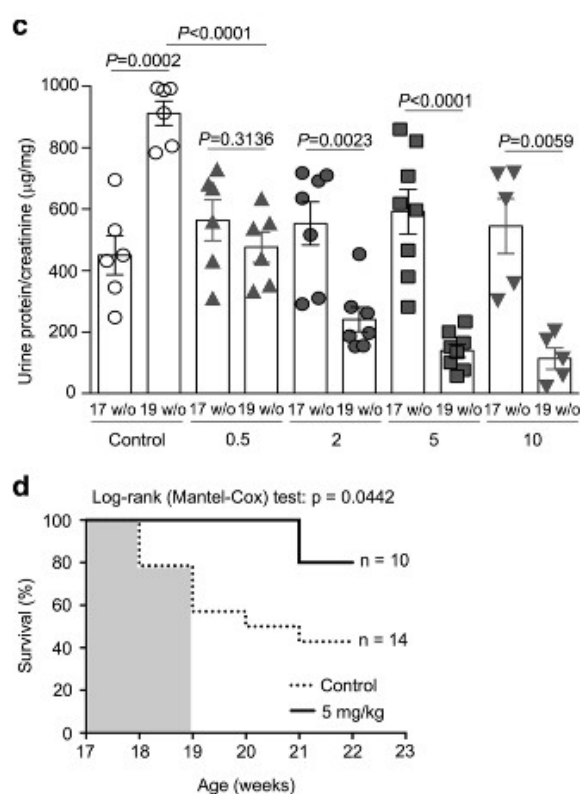


Fig. 6 (continued)

BNTX treatment effectively ameliorates lupus nephritis in MRL/lpr mice

As the autoantibody production significantly declined following the depletion of PCs by BNTX treatment (Fig. 3), we investigated glomerular IC accumulation, which can induce chronic inflammation and gradually results in destruction. Indeed, BNTX treatment at 2, 5 and 10 mg/kg/day, but not 0.5 mg/kg/day ($P = 0.4065$), significantly decreased deposition of IgM ICs in the glomerulus by ~20–40% (Fig. 6a). Except for the 0.5 mg/kg/day of BNTX treatment, the deposition of collagen fibers stained by Masson's trichrome was significantly reduced both in the glomeruli ($P = 0.0041$, < 0.0001 and < 0.0001 for 2, 5 and 10 mg/kg/day, respectively) and in the tubulo-interstitial space ($P = 0.0176$, 0.0009 and 0.01 for 2, 5 and 10 mg/kg/day, respectively) in diseased MRL/lpr mice (Fig. 6b). To determine if proteinuria was also improved by BNTX treatment, we collected 24-h urine samples from control and BNTX-treated MRL/lpr mice to measure their concentrations of protein and creatinine. The urinary protein/creatinine ratio was then used to report the severity of proteinuria resulting from glomerular destruction in MRL/lpr mice. As shown in Fig. 6c, BNTX treatment with 2, 5 and 10 mg/kg/day, respectively, all significantly improved

proteinuria in MRL/lpr mice ($P = 0.0076$, 0.0008 and 0.0059). In contrast, the proteinuria of control mice aggravated as the disease progressed ($P = 0.0002$). Because renal fibrosis was most significantly improved by 5 mg/kg/day of BNTX, we investigated the therapeutic durability 3 weeks after the cessation of treatment. As shown in Fig. 6d, the survival rate of BNTX-treated mice was significantly higher than that of control mice (80 vs. 50%).

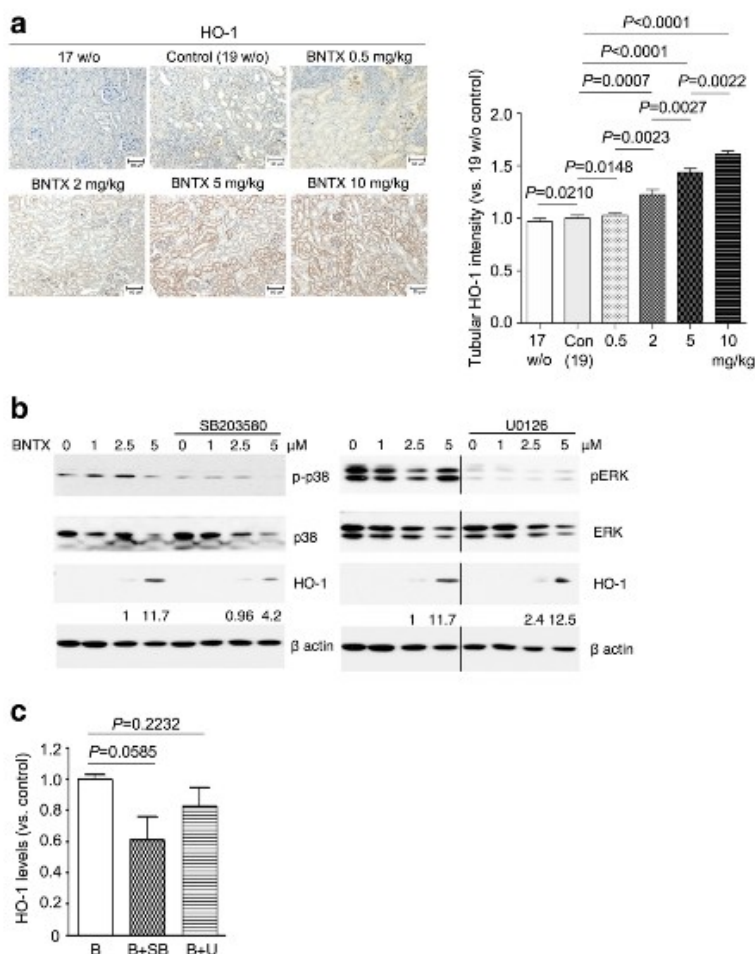
BNTX treatment induces HO-1 expression in proximal tubules of kidneys in MRL/lpr mice

Because deficiency of HO-1 in mice promotes renal fibrosis [17, 18], we examined if BNTX treatment induced HO-1 expression in the kidney to alleviate lupus nephritis. Indeed, in a dose-dependent manner, HO-1 expression was markedly up-regulated at the proximal tubules adjacent to the glomerulus by 2, 5 and 10 mg/kg/day of BNTX treatment ($P = 0.0007$, < 0.0001 and < 0.0001), respectively, in MRL/lpr mice (Fig. 7a). In contrast, HO-1 expression in proximal tubules remained low in vehicle-treated mice (Fig. 7a). We then used mouse NRK-52E cell line of proximal tubular origin to investigate the molecular basis of BNTX effects. Cells were treated with various concentrations (0, 1, 2.5, 5 μM) of BNTX for 24 h. We found that HO-1 expression was induced by BNTX in a concentration-dependent manner (Fig. 7b). Moreover, the expression level of HO-1 was reduced by p38 MAPK inhibitor SB203580 ($P = 0.0585$), but not by ERK inhibitor ($P = 0.2232$) (Fig. 7b, c). These results suggest that in renal tubular cells induction of HO-1 proteins by BNTX requires p38 MAPK.

Discussion

Lupus nephritis is a hallmark of SLE. About 20% of patients with lupus nephritis are refractory to immunosuppressive treatment, and 30 to 50% of these patients progress to end-stage renal failure even under intensive therapy [19]. To our knowledge, this is the first report of BNTX to alleviate lupus nephritis through a dual effect by reduction of autoreactive PCs via Fc γ RIIB and by induction of HO-1 expression to enhance renal tubular protection against glomerular proteinuria. Such a dual targeting of BNTX is of novelty and importance in that no current single agent or two independent drugs in clinical use exert a similar dual effect to BNTX for the treatment of any autoimmune diseases. Moreover, neither B cell depletion agents, e.g. rituximab, preferentially target PCs [20] nor are approved HO-1 activators available. Given that the DOR-deficient mice exhibit no spontaneous phenotype, the beneficial effects via the dual action of BNTX open an opportunity for the development of a new class of therapeutics to patients with lupus nephritis.

Fig. 7 BNTX treatment induced HO-1 expression in renal proximal tubules in MRL/lpr mice. **a** Immunohistochemical staining of HO-1 proteins in the kidneys. The bar graph (right panel) illustrated the quantification of HO-1 levels at renal tubules of control versus 2 mg/kg/day ($P = 0.0007$), 5 mg/kg/day ($P < 0.0001$) and 10 mg/kg/day ($P < 0.0001$) of BNTX-treated mice, respectively. **b** Mouse NRK-52E cells (2×10^6 /ml) were cultured in the absence or presence of various concentrations of BNTX (0, 1, 2.5 or 5 μM) with or without addition of 10 μM of SB203580 or U0126 for 24 h. Cells lysates were prepared for immunoblottings using mAbs specific to p38 MAPK, p-p38 MAPK, ERK, p-ERK, HO-1 and β actin, respectively. **c** Bar graph of quantification results of HO-1 levels from three independent experiments of (b)



Evidence from DOR knockout mice excludes the participation of DOR for the immunosuppressive effects of BNTX [8]. In addition, independent groups have reported no detectable expression of DORs in human PBMCs [21, 22]. Here, we show that BNTX can upregulate Fc γ RIIB expression in B cells to promote elimination of PCs via excess ICs in circulation (Fig. 2). The reduction of PC numbers eventually results in decreased formation of ICs and thereby diminished deposition of ICs in the glomerulus, dampening glomerulonephritis and ameliorating proteinuria (Fig. 6). Remarkably, the numbers of anti-dsDNA-secreting PCs in bone marrow were also reduced after treatment with BNTX at as low as 2 mg/kg/day (Fig. 2). Correspondingly, the serum concentrations of anti-dsDNA Abs significantly declined (Fig. 3). The elimination of bone marrow autoreactive PCs is of clinical importance because recent evidence indicates a necessity to eliminate these PCs for a complete cure of SLE [23–25]. Yet, none of the current therapeutic Abs is designed to directly target PCs for depletion [26].

Elimination of pathogenic B cells is crucial for the treatment of lupus in that B cell-deficient MRL/lpr mice fail to develop glomerulonephritis [27, 28]. A key finding of our study is that BNTX treatment up-regulates the expression level of Fc γ RIIB in B cells (Fig. 4a). Given that PCs express the highest level of Fc γ RIIB among populations of B cells and ICs can trigger apoptosis of B cells via Fc γ RIIB, PCs are therefore most sensitive to Fc γ RIIB-dependent apoptosis [13–16, 29]. Moreover, bone marrow long-lived PCs no longer express the B cell receptor on their surfaces [26]. Thus, BNTX-mediated upregulation of Fc γ RIIB can deliver apoptotic signals to decrease autoreactive PC numbers via an auto-regulatory feedback loop between Fc γ RIIB and excess ICs. In this study, we identified p38 MAPK and HO-1 as essential mediators for BNTX-induced upregulation of Fc γ RIIB in B cells (Fig. 5d). To the best of our knowledge, we are the first to report the inhibitory effect of HO-1 on B cells and the functional link between HO-1 and Fc γ RIIB. Of importance, the induction of HO-1 appears to be

specific to BNTX but not to other DOR antagonists, e.g. naltrindole and naloxone (Fig. 5a, b).

The most severe complication of SLE is lupus nephritis, which affects more than half of patients during the course of disease [10, 20]. Patients with lupus nephritis gradually develop glomerular proteinuria as a consequence of IC-associated chronic inflammation and impaired permeability and integrity of the glomerular structure. Plasma proteins are filtrated through the glomerulus and normally reabsorbed from the proximal tubules to prevent proteinuria. Excess urinary proteins therefore result in over-reabsorption by proximal tubular cells. Consequently, high tubular transport demands oxygen consumption, which is prone to produce excess reactive oxygen species to induce pro-inflammatory and pro-fibrotic processes [30]. HO-1 is an inducible molecule with anti-oxidant and anti-inflammatory properties [31]. The major physiological function of HO-1 is to convert heme to biliverdin, which is subsequently converted to bilirubin, and during the course carbon monoxide is produced and iron is released [31]. The crucial role of HO-1 as a renal protectant can be evidently demonstrated in a human patient with genetic deficiency of HO-1, who succumbed to proteinuria and renal tubular injury [32]. Conversely, HO-1 overexpression in mice protects against renal inflammation and fibrosis induced by ureter obstruction [33]. Moreover, HO-1 induction therapy has beneficial effects for renal diseases, including glomerulonephritis [34, 35]. Here, we showed that BNTX at 2 to 10 mg/kg/day significantly reduced renal fibrosis and improved proteinuria over 2 weeks of treatment (Fig. 6). Mechanistically, we showed that like B cells BNTX activated p38 MAPK to induce HO-1 expression in renal tubular cells (Fig. 7). The effective doses of BNTX range from 2 to 10 mg/kg/day to treat lupus nephritis indicating a considerable window for BNTX dose-finding and a good opportunity for safe use in clinical application. Along this line, a fivefold dose range of BNTX from 2 to 10 mg/kg/day appears to demonstrate comparable therapeutic efficacies. In support of this, mice treated with 2–10 mg/kg of BNTX showed no elevation of serum levels of alanine transaminase (ALT), indicative of no obvious hepatotoxicity (Supplemental Fig. 1). However, the ability of BNTX to cross blood-brain barrier can exert antagonistic actions on DORs prompts the use of a low, effective dose to avoid potential side effects from the central nervous system, e.g. antitussive and antinociception [36, 37]. Moreover, DOR agonists have recently been developed for the treatment of chronic pain [38, 39], e.g. neuropathic pain and inflammatory pain, both of which are aggravated in mice deficient in DOR1 gene [40, 41]. Therefore, for clinical application in lupus, it is essential to reduce the lipophilicity of BNTX and its derivatives to prevent the drugs from passing through the blood-brain barrier to result in adverse effects.

In conclusion, our studies reveal a dual effect of BNTX via FcγRIIB and HO-1 to confer therapeutic benefits to mice with lupus nephritis. Such a dual effect of BNTX to target both immune and renal systems is novel because neither PC-selective targeting drugs nor FDA-approved HO-1 activators are available at present. Although the absence of obvious phenotype of DOR1-deficient mice encourages the development of BNTX and its derivatives as a new class of immunosuppressive agents, it will be of importance to validate the DOR-independent effects of BNTX via FcγRIIB and HO-1 in respective gene deficient mice before consideration for clinical application [8, 42]. Importantly, the concept of dual immune and renal targeting could greatly contribute to the design of new therapeutics in particular for Ab-mediated autoimmune diseases, e.g. SLE.

Acknowledgements This study was supported by research grants from the Ministry of Science and Technology of Taiwan (NSC99-2320-B-002-011 and MOST-105-2321-B-002-040). We thank Dr. Wan-Wan Lin for critical reading and comment on the manuscript, and Ms. Yu-Syuan You for excellent technical supports. We also would like to acknowledge the services provided by the First Core Laboratory at College of Medicine, National Taiwan University and the RCF7 Laboratory of Department of Medical Research at National Taiwan University Hospital.

Compliance with ethical standards

Conflict of interest The authors declare no competing financial interests.

References

1. Al-Hashimi M, Scott SW, Thompson JP, Lambert DG (2013) Opioids and immune modulation: more questions than answers. *Br J Anaesth* 111:80–88
2. Bidlack JM, Khimich M, Parkhill AL, Sumagin S, Sun B, Tipton CM (2006) Opioid receptors and signaling on cells from the immune system. *J NeuroImmune Pharmacol* 1:260–269
3. Zaki PA, Bilsky EJ, Vanderah TW, Lai J, Evans CJ, Porreca F (1996) Opioid receptor types and subtypes: the delta receptor as a model. *Annu Rev Pharmacol Toxicol* 36:379–401
4. House RV, Thomas PT, Bhargava HN (1996) A comparative study of immunomodulation produced by in vitro exposure to delta opioid receptor agonist peptides. *Peptides* 17:75–81
5. House RV, Thomas PT, Kozak JT, Bhargava HN (1995) Suppression of immune function by non-peptidic delta opioid receptor antagonists. *Neurosci Lett* 198:119–122
6. Traynor JR, Elliott J (1993) Delta-opioid receptor subtypes and cross-talk with mu-receptors. *Trends Pharmacol Sci* 14:84–86
7. Portoghese PS, Sultana M, Nagase H, Takemori AE (1992) A highly selective delta 1-opioid receptor antagonist: 7-benzylidenenaltrexone. *Eur J Pharmacol* 218:195–196
8. Gavériaux-Ruff C, Filliol D, Simonin F, Matthes HW, Kieffer BL (2001) Immunosuppression by delta-opioid antagonist naltrindole: delta- and triple mu/delta/kappa-opioid receptor knockout mice reveal a nonopioid activity. *J Pharmacol Exp Ther* 298:1193–1198
9. Takahashi S, Fossati L, Iwamoto M, Merino R, Motta R, Kobayakawa T, Izui S (1996) Imbalance towards Th1

- predominance is associated with acceleration of lupus-like autoimmune syndrome in MRL mice. *J Clin Invest* 97:1597–1604
10. Bagavant H, Fu SM (2009) Pathogenesis of kidney disease in systemic lupus erythematosus. *Curr Opin Rheumatol* 21:489–494
 11. Tzeng SJ (2016) The isolation, differentiation, and quantification of human antibody-secreting B cells from blood: ELISpot as a functional readout of humoral immunity. *J Vis Exp* (118). <https://doi.org/10.3791/54582>
 12. Shinnakasu R, Kurosaki T (2017) Regulation of memory B and plasma cell differentiation. *Curr Opin Immunol* 45:126–131
 13. Fukuyama H, Nimmerjahn F, Ravetch JV (2005) The inhibitory Fcγ receptor modulates autoimmunity by limiting the accumulation of immunoglobulin G+ anti-DNA plasma cells. *Nat Immunol* 6:99–106
 14. Xiang Z, Cutler AJ, Brownlie RJ, Fairfax K, Lawlor KE, Severinson E, Walker EU, Manz RA, Tarlinton DM, Smith KG (2007) FcγRIIB controls bone marrow plasma cell persistence and apoptosis. *Nat Immunol* 8:419–429
 15. McGaha TL, Karlsson MC, Ravetch JV (2008) FcγRIIB deficiency leads to autoimmunity and a defective response to apoptosis in Mrl-MpJ mice. *J Immunol* 180:5670–5679
 16. Tzeng SJ, Li WY, Wang HY (2015) FcγRIIB mediates antigen-independent inhibition on human B lymphocytes through Btk and p38 MAPK. *J Biomed Sci* 22:87–98
 17. Kie JH, Kaptureczak MH, Traylor A, Agarwal A, Hill-Kaptureczak N (2008) Heme oxygenase-1 deficiency promotes epithelial-mesenchymal transition and renal fibrosis. *J Am Soc Nephrol* 19:1681–1691
 18. Morimoto K, Ohta K, Yachie A, Yang Y, Shimizu M, Goto C, Toma T, Kasahara Y, Yokoyama H, Miyata T, Seki H, Koizumi S (2001) Cytoprotective role of heme oxygenase (HO)-1 in human kidney with various renal diseases. *Kidney Int* 60:1858–1866
 19. Almaani S, Meara A, Rovin BH (2017) Update on lupus nephritis. *Clin J Am Soc Nephrol* 12:825–835
 20. Tsokos GC (2011) Systemic lupus erythematosus. *N Engl J Med* 365:2110–2121
 21. Williams JP, Thompson JP, McDonald J, Barnes TA, Cote T, Rowbotham DJ, Lambert DG (2007) Human peripheral blood mononuclear cells express nociceptin/orphanin FQ, but not mu, delta, or kappa opioid receptors. *Anesth Analg* 105:998–1005
 22. Al-Hashimi M, McDonald J, Thompson JP, Lambert DG (2016) Evidence for nociceptin/orphanin FQ (NOP) but not μ (MOP), δ (DOP) or κ (KOP) opioid receptor mRNA in whole human blood. *Br J Anaesth* 116:423–429
 23. Hiepe F, Dörner T, Hauser AE, Hoyer BF, Mei H, Radbruch A (2011) Long-lived autoreactive plasma cells drive persistent autoimmune inflammation. *Nat Rev Rheumatol* 7:170–178
 24. Mumtaz IM, Hoyer BF, Panne D, Moser K, Winter O, Cheng QY, Yoshida T, Burmester GR, Radbruch A, Manz RA, Hiepe F (2012) Bone marrow of NZB/W mice is the major site for plasma cells resistant to dexamethasone and cyclophosphamide: implications for the treatment of autoimmunity. *J Autoimmun* 39:180–188
 25. Hiepe F, Radbruch A (2016) Plasma cells as an innovative target in autoimmune disease with renal manifestations. *Nat Rev Nephrol* 12:232–240
 26. Mahévas M, Michel M, Weill JC, Reynaud CA (2013) Long-lived plasma cells in autoimmunity: lessons from B-cell depleting therapy. *Front Immunol* 4:494–498
 27. Chan O, Shlomchik MJ (1998) A new role for B cells in systemic autoimmunity: B cells promote spontaneous T cell activation in MRL-lpr/lpr mice. *J Immunol* 160:51–59
 28. Chan OT, Madaio MP, Shlomchik MJ (1999) B cells are required for lupus nephritis in the polygenic, Fas-intact MRL model of systemic autoimmunity. *J Immunol* 163:3592–3596
 29. Tzeng SJ, Bolland S, Inabe K, Kurosaki T, Pierce SK (2005) The B cell inhibitory Fc receptor triggers apoptosis by a novel c-Abl family kinase-dependent pathway. *J Biol Chem* 280:35247–35254
 30. Kitamura M, Fine LG (1999) The concept of glomerular self-defense. *Kidney Int* 55:1639–1671
 31. Jarmi T, Agarwal A (2009) Heme oxygenase and renal disease. *Curr Hypertens Rep* 11:56–62
 32. Ohta K, Yachie A, Fujimoto K, Kaneda H, Wada T, Toma T, Seno A, Kasahara Y, Yokoyama H, Seki H, Koizumi S (2000) Tubular injury as a cardinal pathologic feature in human heme oxygenase-1 deficiency. *Am J Kidney Dis* 35:863–870
 33. Chen X, Wei SY, Li JS, Zhang QF, Wang YX, Zhao SL, Yu J, Wang C, Qin Y, Wei QJ, Lv GX, Li B (2016) Overexpression of heme oxygenase-1 prevents renal interstitial inflammation and fibrosis induced by unilateral ureter obstruction. *PLoS One* 11:e0147084
 34. Takeda Y, Takeno M, Iwasaki M, Kobayashi H, Kirino Y, Ueda A, Nagahama K, Aoki I, Ishigatsubo Y (2004) Chemical induction of HO-1 suppresses lupus nephritis by reducing local iNOS expression and synthesis of anti-dsDNA antibody. *Clin Exp Immunol* 138:237–244
 35. Elmarakby AA, Faulkner J, Baban B, Saleh MA, Sullivan JC (2012) Induction of hemeoxygenase-1 reduces glomerular injury and apoptosis in diabetic spontaneously hypertensive rats. *Am J Physiol Renal Physiol* 302:F791–F800
 36. Kamei J, Iwamoto Y, Suzuki T, Misawa M, Nagase H, Kasuya Y (1994) Involvement of delta 1-opioid receptor antagonism in the antitussive effect of δ-opioid receptor antagonists. *Eur J Pharmacol* 251:291–294
 37. Abdallah K, Gendron L (2017, 2017 May 17) The delta opioid receptor in pain control. *Handb Exp Pharmacol*. https://doi.org/10.1007/164_2017_32
 38. Gavériaux-Ruff C, Kieffer BL (2001) Delta opioid receptor analgesia: recent contributions from pharmacology and molecular approaches. *Behav Pharmacol* 22:405–414
 39. Peppin JF, Raffa RB (2015) Delta opioid agonists: a concise update on potential therapeutic applications. *J Clin Pharm Ther* 40:155–166
 40. Nadal X, Baños JE, Kieffer BL, Maldonado R (2006) Neuropathic pain is enhanced in delta-opioid receptor knockout mice. *Eur J Neurosci* 23:830–834
 41. Gavériaux-Ruff C, Karchewski LA, Hever X, Matifas A, Kieffer BL (2008) Inflammatory pain is enhanced in delta opioid receptor-knockout mice. *Eur J Neurosci* 27:2558–2567
 42. Charbogne P, Kieffer BL, Befort K (2014) 15 years of genetic approaches *in vivo* for addiction research: opioid receptor and peptide gene knockout in mouse models of drug abuse. *Neuropharmacology* 76:204–217